# AN EXPERIMENTAL INVESTIGATION OF M-SUBSHELL FLUORESCENCE YIELDS AND OF THE $L_1$-$L_3$ RADIATIVE TRANSITION IN NEPTUNIUM AND CURIUM FROM THE RADIOACTIVE DECAYS OF $^{241}Am$ AND $^{249}Cf$

A THESIS

Presented to

The Faculty of the Division of Graduate

Studies and Research

by

Esko Ilmari Karttunen

In Partial Fulfillment

of the Requirements for the Degree

Doctor of Philosophy

in the School of Nuclear Engineering

Georgia Institute of Technology

February, 1971

In presenting the dissertation as a partial fulfillment of the requirements for an advanced degree from the Georgia Institute of Technology, I agree that the Library of the Institute shall make it available for inspection and circulation in accordance with its regulations governing materials of this type. I agree that permission to copy from, or to publish from, this dissertation may be granted by the professor under whose direction it was written, or, in his absence, by the Dean of the Graduate Division when such copying or publication is solely for scholarly purposes and does not involve potential financial gain. It is understood that any copying from, or publication of, this dissertation which involves potential financial gain will not be allowed without written permission.

_____

7/25/68

AN EXPERIMENTAL INVESTIGATION OF M-SUBSHELL FLUORESCENCE YIELDS AND OF THE $L_1$-$L_3$ RADIATIVE TRANSITION IN NEPTUNIUM AND CURIUM FROM THE RADIOACTIVE DECAYS OF $^{241}Am$ AND $^{249}Cf$

Approved:

Date approved by Chairman: Feb. 12, 1971

## ACKNOWLEDGMENTS

This research project was supported by AEC Contract AT(40-1)-3346 as part of a larger program in nuclear spectroscopy--nuclear chemistry. I am indebted to Prof. R. W. Fink for giving me an opportunity to participate in this program.

I am also grateful to the other reading committee members, Prof. G. G. Eichholz and Prof. D. S. Harmer for detailed and valuable critique of the content and style of the manuscript.

I wish to thank Prof. R. H. Fetner from the School of Biology for his kind permission to use the curve resolving computer and Dr. R. D. Baybarz and Dr. O. L. Keller, Jr., of Transuranium Research Laboratory, Oak Ridge National Laboratory, for preparation and loan of the $^{249}Cf$ source.

Good cooperation within the nuclear spectroscopy group made the work enjoyable. Especially my thanks belong to Dr. H. U. Freund, whose competent advice in the course of experimental work cannot be overemphasized.

I am thankful to Prof. J. K. Miettinen from the University of Helsinki for his encouragement and willing help. I am also grateful to the Finnish Atomic Energy Commission (Suomen Atomienergianeuvottelukunta) for a travel grant, and to Prof. C. J. Roberts for an assistantship in the first year of graduate studies.

Mrs. Lydia Geeslin deserves my best thanks for professional and

fast editing and typing of this thesis.

Finally, I want to express my appreciation to my wife, Marja, who was ready to interrupt her career and join me in this adventure which was not always easy for her.

TABLE OF CONTENTS

TABLE OF CONTENTS (Concluded)

# LIST OF TABLES

LIST OF TABLES (Continued)

LIST OF TABLES (Concluded)

## LIST OF ILLUSTRATIONS

LIST OF ILLUSTRATIONS (Concluded)

## SUMMARY

The construction and performance of a wall-less multiwire proportional counter (MWPC) is described. The measured and calculated efficiencies are compared, and possible reasons for observed discrepancies are discussed. The absolute emission rate of M x rays from an $^{241}Am$ source was measured with the MWPC and with a single-wire proportional counter and a value of $(6.35 \pm 0.60) \times 10^{-9}$ M x rays per decay, or $(0.470 \pm 0.045)$ M x rays per $L_\alpha$ x ray is obtained.

High resolution Ge(Li) and Si(Li) x-ray spectrometers and the multiwire proportional counter (MWPC) were used for measuring coincidences, respectively, between various L x rays and the M x rays of neptunium (Z=93) from a $^{241}Am$ source. In addition, M x rays of curium from a $^{249}Cf$ source were measured with a Si(Li) detector in coincidence with various K and L x rays detected with a Ge(Li) spectrometer. Coincidence rates were corrected both experimentally and on the basis of calculation for the effect of multiple M-shell vacancies. Expressions for quantitative calculation of this correction are derived. High resolution in the detection of L and K x-ray spectra permits determination of most of the mean M-subshell fluorescence yields of Np and Cm. The following results are obtained using the experimental correction for multiple vacancies due to cascading nuclear gamma transitions:

$$\nu_1^M \ (Z=93) = 0.065 \pm 0.014, \qquad \nu_2^M \ (Z = 93) = 0.080 \pm 0.029,$$

$\nu_4^M$ (Z=93) = 0.062 ± 0.005, $\nu_{4,5}^M$ (Z=93) ≈ $\omega_5^M$ = 0.065 ± 0.012

$\nu_1^M$ (Z=96) = 0.081 ± 0.016, $\nu_2^M$ (Z=96) = 0.068 ± 0.023,

$\nu_3^M$ (Z=96) = 0.062 ± 0.019, $\nu_4^M$ (Z=96) = 0.080 ± 0.006,

$\nu_{4,5}^M$ (Z=96) ≈ $\omega_5^M$ = 0.075 ± 0.012.

The experimental method of correcting for multiple vacancy cascades is more accurate than a method based on calculation. Owing to strong Coster-Kronig effect in the M shell, the values for the various mean subshell yields are essentially identical and of the order of that for the $M_5$ subshell.

The Auger width of the $M_5$ subshell was found to be essentially constant from Z=76 to 96, and it was found to increase considerably more than the x-ray width with increasing angular momentum from $s_{1/2}$ to $p_{3/2}$ while only slightly more (if any) from $p_{3/2}$ to $d_{5/2}$.

Measurements of M x rays with high resolution makes it possible to determine the magnitude of radiative filling of the two innermost M subshells and to estimate the strength of the Coster-Kronig process between the $M_{1,2}$ and $M_{3,4,5}$ subshells. The following values were obtained:

$\omega_1^M + f_{1;2}^M \omega_2^M = (2.0 \,^{+\,3.1}_{-\,2.0}) \times 10^{-3}$ at Z = 93 and $(7.5 \,^{+\,8.9}_{-\,7.5}) \times 10^{-3}$

at Z = 96, and $\omega_2^M = (4.6 \,^{+\,5.1}_{-\,4.6})$ at Z ≈ 96. About 97 percent of the $M_{1,2}$-subshell vacancies thus were found to shift to higher subshells before filling from higher major shells occurs

Observation of the radiative $L_1$-$L_3$ transition was made for the first

time in the high-Z region. Its intensity is compared to the total intensity of the $L_3$ and $L_1$ x rays, and reasonable agreement with the theoretical predictions is obtained. The radiative fraction $\omega_{13}^{L}$ in the Coster-Kronig yield $f_{13}^{L}$ is found to be about five percent in the region Z=93-96:

$$\omega_{13}^{L} = (0.030 \pm 0.014) \quad \text{at } Z = 93 \quad \text{and} \quad (0.028 \pm 0.020) \quad \text{at } Z = 96.$$

# CHAPTER I

# INTRODUCTION

## 1.1. Atomic Transitions and Their Yields

Experimental investigation of electronic transitions in excited atoms has been the main source of information on atomic structure ever since the discovery of characteristic x rays served as a guide in the construction of the central nucleus (Bohr) model of the atom with quantized electron orbits. It is conventional to distinguish three types of transitions through which an electron vacancy in one of the inner atomic subshells $X_i$ can be filled: radiative-, Auger-, and Coster-Kronig (CK) transitions. In a radiative transition, e.g. K-$L_3$, an electron from the $L_3$ subshell fills the vacancy in the K shell, and the energy and angular momentum are conserved through emission of a characteristic x ray, called K x ray in this case. In the Auger transition, K-$L_3M_5$, for example, the conservation laws in the electron transfer from the $L_3$ to the K shell are satisfied through the emission of another electron from the $M_5$ subshell. An example of the L-Auger process is the transition $L_1$-$M_4N_5$. It is characteristic that both the electron filling the original $L_1$ vacancy and the electron emitted in the process are from a shell above the L shell. The CK transition, e.g. $L_1$-$L_3M_5$ represents a vacancy shift within a major shell. The nonradiative CK process differs from the Auger effect only in that the original vacancy is filled from an orbital of the same principal quantum number n, whereas in the Auger effect it is filled from

an orbital of higher n. Of the radiative transitions the electric dipole (E1) transition is the most intense and is essentially the only one which can compete with nonradiative processes. Discussion of the selection rules governing the radiative transitions is given, for example, by Compton and Allison (1), and the possible final states in nonradiative processes in various coupling schemes have been considered by Burhop (2), Bergstrom and Nordling (3), and Mehlhorn (4), among others.

The relative competition among the three transition modes for the $X_i$ subshell is described by fluorescence-, Auger-, and CK-yields, $\omega_i^X$, $a_i^X$, and $f_{ij}^X$, respectively. These yields are defined as the probabilities of filling an $X_i$-subshell vacancy by a radiative, Auger, or CK transition, and therefore

$$\omega_i^X + a_i^X + \sum_{j>i} f_{ij}^X = 1 \qquad (1)$$

It has, however, been proposed by Bambynek et al. (5) that the small radiative component which only involves orbitals of the same principal quantum number n, should for practical reasons be included in the CK yield as its radiative component $\omega_{ij}$. According to this proposal the CK yield then is

$$f_{ij}^X = a_{ij}^X + \omega_{ij}^X \qquad (2)$$

and

$$\omega_i^X + a_i^X + \sum_{j>i} (a_{ij}^X + \omega_{ij}^X) = 1$$

where $a_{ij}^X$ is the ordinary, radiationless CK component.

## 1.2. Significance of the Fluorescence, Auger, and Coster-Kronig Yields

The relationship between the intensity of x-ray or electron emission and the number of atoms ionized in various shells, is determined by fluorescence, Auger, and CK yields. Accurate knowledge of this relationship proves to be important in a wide variety of applications. X-ray fluorescence analysis, experimental determination of ionization cross sections, standardization of radionuclides, efficiency calculations for photon detectors, and scanning electron microscopy are examples of these applications. Accurate photon transfer calculations for the purpose of shielding or medical therapy must consider the effect of x rays and electrons separately. Ionization multiplication due to radiationless atomic transitions plays an important role in radiation damage and hot atom chemical effects. Measurement of electron capture probabilities and internal conversion coefficients are nuclear applications where absolute x-ray counting combined with the knowledge of fluorescence yields is commonly employed. Information on electron wave functions close to the nuclear surface and on the multipolarities of nuclear gamma transitions, and hence on the level spins and parities, is obtained from such measurements.

The primary purpose of experimental studies of inner shell transitions, however, is to advance the fundamental understanding of atomic structure itself. Basically, the yields are the radiative, Auger, and CK fractions of the total, spontaneous decay rate of a one-vacancy initial state. Theoretical calculation involves computation of the absolute rates for individual transitions and summing over all final states of radiative,

Auger, or CK processes. Comprehensive discussions of these calculations are given by Powell (6) and Condon and Shortley (7), among others. It has been pointed out by Kostroun, Chen, and Crasemann (8) that the transition rates are more sensitive to the detailed nature of the electron wave functions than any other measurable quantities. Accurate experimental determination of the transition rates, therefore, is an effective means for testing the quality of the wave functions. This is one of the frontiers of present theoretical atomic studies.

It is obvious that, in the process of integration over the final states in the subshell yield calculations, some of the sensitivity characteristic to the transition rates is lost, e.g. the strength of the spin-orbit coupling does not affect the yields (8). However, the yields are often measurable even when the individual transition rates remain unattainable, due to experimental difficulties. Subshell yields give the best test for the calculated total, absolute, radiative, and nonradiative decay rates of a one-vacancy initial state.

## 1.3. Present Status of Knowledge of Subshell Yields

In addition to the increased interest in atomic transitions due to theoretical implications and important applications, two major factors have helped the remarkable progress in theoretical and experimental studies of various subshell yields within the last few years. Development of high-resolution, high-efficiency photon detectors — lithium-drifted germanium and silicon semiconductors — has facilitated the use of powerful coincidence methods. On the other hand, availability of fast computers has made possible theoretical calculations needing fewer approximations

and with computational accuracy comparable to the best experimental results.

Experimental studies have concentrated on determination of the K- and L-shell yields throughout the periodic table as can be seen from the general review articles by Fink et al. (9) and Bambynek et al. (5). At present $\omega_K$* and $a_K$ are experimentally known within a few percent for all elements. In contrast, the picture of the six independent L-subshell yields is still somewhat unclear, especially as regards the $L_1$ quantities. The bulk of the published results gives values for $\omega_2$,** $\omega_3$, and $f_{23}$ which are accessible in selective ionization experiments and coincidence methods. Current experimental activity is centered on the L subshells and the results obtained with modern methods are accurate generally to better than 10 percent. Comprehensive discussions of the experimental methods together with reviews of published results are given in Refs. (5,9).

Information on the M and higher shells is very scarce. Only a few mean M-shell fluorescence yield measurements have been reported and these will be discussed later in this chapter.

As mentioned above, theoretical calculation of the subshell yields requires a knowledge of decay rates for each of the radiative and non-radiative decay channels of the initial ionized state. Computation of these rates is laborious and time-consuming, and has been essentially completed with good accuracy only for a K-shell vacancy. Absolute radia-

*The K-shell yields and all average fluorescence yields carry designation of the major shell as a subscript.

**The super- or subscript L will be omitted in this text from the symbols of the L-subshell quantities where confusion is not likely to arise.

tive transition rates for all important K-L,M,N transitions and for the L-M,N transitions through the periodic table have recently been calculated by Scofield (10) and by Rosner and Bhalla (11) in a fully relativistic manner using Hartree-Fock-Slater (HFS) wave functions. Bhalla (12) has published similar calculations of the radiative M-N,O and some of the M-P, Q transition rates. Relativistic HFS calculation of the K-LL and some of the K-LM and L-MM Auger transition rates from Z=10 to Z=94 were presented by Ramsdale (13) in his thesis, and Bhalla, Rosner, and Ramsdale (14) have later completed this work as regards to the other transitions in the K-LM and K-MM groups. These relativistic calculations with self-consistent-field wave functions are the most accurate ones performed, especially in the high-Z region where jj-coupling is a good approximation. Certain approximations are still involved in the HFS-wave functions, as discussed by Hartree (15). They are one-electron wave functions and exclude the time-dependency of the electron-electron interactions. The Slater-exchange concept is probably the most serious approximation. A comparison of the HFS calculations with the experimental nonradiative rates has been made by Bhalla (16) and good agreement has been observed, in contrast to older work a comprehensive review of which is given in Ref. (4). On the other hand, some discrepancies between the calculated and experimental radiative rates have been pointed out (17,18,19). The calculations seem to underestimate the rates when levels of high angular momentum are involved.

The K-shell fluorescence yields can be calculated from the transition rate information from Refs. (10,11,13,14). Bhalla, Ramsdale, and Rosner (20) have performed this calculation and report an excellent agree-

ment within the limits of experimental accuracy. Similarly, excellent agreement with experimental K-shell fluorescence yields through the region Z=10-55 has been achieved by Kostroun, Chen, and Crasemann (8) by less rigorous calculation. They used Scofield's radiative rates but computed the nonradiative components from nonrelativistic, screened, hydrogenic wave functions. McGuire (21,22) has also made an independent nonrelativistic calculation of $\omega_K$ values from Z=10 to 54 using wave functions which are analytic solutions of the wave equation for an approximate self-consistent-field potential. This approach gave good agreement with experiments except at low Z, where the prediction was up to 10 percent too high.

The same approach as in his $\omega_K$ calculations was used by McGuire (23) for computation of all the L-subshell quantities from Z=12 to 90. These calculations are the most sophisticated ones presently available for the L shell and in the case of $\omega_2$ and $\omega_3$ show qualitative agreement with general trends observed from the rather inaccurate experimental information. For $f_{23}$ the prediction seems to be low. The scarcity of experimental information on the $L_1$ subshell makes it premature to comment on the validity of the calculation regarding the $L_1$ quantities. Kostroun, Chen, and Crasemann (24) have also calculated the $L_2$- and $L_3$-subshell quantities using the same method as in Ref. (8), but the results are not yet available. The lack of data on many significant radiationless transition probabilities precludes calculations based directly on relativistic, realistic wave functions. In addition to the L-MM rates given in ref. (13), the only relativistic calculations of nonradiative L-shell transition rates are those by Talukdar and Chattarji (25) for

the $L_1$-$L_2M_{4,5}$ CK rates in the region Z=32-41. In these calculations with hydrogenic wave functions, the inclusion of relativity effects almost doubles the nonrelativistic rates in this case. Bhalla (26) has made an attempt to combine the information on total K-level widths obtained from Refs. (11,13) with the radiative L-subshell widths from Ref. (11), in order to compute $\omega_2$, $\omega_3$, $f_{23}$. Experimental $K_\alpha$-line widths, together with theoretical K-level widths, were used to find the total widths of the $L_2$ and $L_3$ subshells. Due to inaccuracies in the experimental values, error limits in the results are wide (up to 50 percent) and "agreement" with experimental $L_2$- and $L_3$-subshell quantities can be claimed.

It is not surprising that no systematic theoretical study of M-subshell yields has been worked out. Calculations for the five subshells are lengthy even with the simplest approximations and the lack of experimental values is also discouraging. However, a good calculation of the M x-ray rates has already appeared (12). Only two calculations of nonradiative rates have been published. Rubenstein (27) has computed the $M_1$ transition rates for Z=36 and the $M_1$-$M_{2,3}X$ rates for Z=47 with Hartree self-consistent-field wave functions. Ramberg and Richtmeyer (28) determined both the radiative and nonradiative transition probabilities for gold (Z=79) with the aid of numerically-integrated nonrelativistic wave functions, calculated for electrons moving in a statistical Thomas-Fermi field of doubly-ionized thallium. The calculated total widths were found to be appreciably in excess of the observed widths, but of the same order of magnitude. These results enable one to estimate the M-subshell fluorescence yields of gold. The following results were obtained (5,9): $\omega_1^M = 0.005$, $\omega_2^M = 0.0084$, $\omega_3^M = 0.0045$, $\omega_4^M = 0.017$, and $\omega_5^M = 0.019$. The

calculation was very rough and restricted to a few dominant transitions.

## 1.4. Previous M-Shell Fluorescence Yield Measurements

No experimental measurements of any of the M-subshell quantities have been reported previously, but a mean M-fluorescence yield has been measured for a few elements. Mean yields are quantities which give the number of M x rays emitted by the atom per total number of vacancies in the M shell, distributed among the subshells in a particular way, which depends on the mode of M-shell excitation. The relationship to the subshell yields which are characteristic of the atom alone is rather complicated and will be explained in Chapter II.

The first measurement of a mean M-fluorescence yield $\bar{\omega}_M$ was performed by Lay (29) as early as 1934. He photoionized the M-shell of uranium and measured the M x-ray intensity with a photographic plate. It is surprising how close to the modern estimate his result is, as can be seen in Table 1 which shows all present experimental information on mean M-fluorescence yields.

Jaffe (30) calculated the M-shell ionization of bismuth atoms in the radioactive decay of RaD ($^{210}$Pb). Internal conversion of the single 46.5 keV M1 gamma transition creates vacancies in the M and L subshells. The latter partly shift to the M shell contributing to the total ionization of this shell. Estimation of this contribution is necessary and requires a knowledge of the L-subshell yields and transition rates. For absolute measurement of the M x-ray intensity, Jaffe used a gas proportional counter.

Konstantinov and Sazanova (31) also based their measurements of

Table 1. Previous Measurements of Mean M-Shell Fluorescence Yields

| Z | Element | $\bar{\omega}_M$ | $\omega_{LM}$ | Reference |
|---|---|---|---|---|
| 76 | Os | | 0.016 ± 0.003 | 32 |
| | | | 0.013 ± 0.0024 | 32* |
| 79 | Au | 0.023 ± 0.001 | | 31 |
| | | | 0.030 ± 0.006 | 32 |
| | | | 0.024 ± 0.005 | 32* |
| 82 | Pb | 0.029 ± 0.002 | | 31 |
| | | | 0.032 ± 0.006 | 32 |
| | | | 0.026 ± 0.005 | 32* |
| 83 | Bi | 0.037 ± 0.007 | | 30 |
| | | 0.035 ± 0.002 | | 31 |
| | | | 0.037 ± 0.007 | 32 |
| | | | 0.030 ± 0.006 | 32* |
| 92 | U | 0.06 | | 29 |

*Reference 32* means the value of 32 corrected for a 20 percent contribution of double M-shell vacancies (5).

mean M-fluorescence yields of gold, lead, and bismuth on direct calculation of the M-shell ionization. In this case, M-shell vacancies were selectively created by fluorescent excitation with 5.9 keV K x rays of cobalt from the decay of $^{55}Fe$. This energy is too low to ionize the L shell. The M-shell ionization was calculated from photoelectric cross sections, and the x rays were counted with a $2\pi$ proportional counter of known efficiency. Thin target foils were used and corrections for self-absorption of M x rays were applied. The reported error limits of about five percent seem to be optimistic, because uncertainty in the M-shell photoelectric cross sections may be as large as 50 percent. This uncertainty, together with strong self-absorption of x rays in sources of reasonable thickness, is the main factor limiting the usefulness of the selective M-shell fluorescence excitation method.

A completely different method was employed in the experiments of Jopson et al. (32). They ionized the L shell of osmium, gold, and lead by fluorescent excitation with low-energy photons from a $^{125}I$ source, and measured the M x rays in coincidence with the L x rays. In this way calculation of the M-shell ionization and the errors associated to the use of cross sections are avoided. The quantity measured is called a mean M-fluorescence yield in coincidence with L x rays and is denoted by $\omega_{LM}$. The L x-ray spectrum was detected with a thin NaI(Tl) scintillator and the M x rays, with a calibrated proportional counter. In order to get the fraction of L x rays which creates M-shell vacancies, the primary ionization of $L_1$, $L_2$, and $L_3$ subshells was assumed to be roughly in the ratio 1:2:3, and experimental L-subshell yields and x-ray rates were used. Creation of double vacancies in the M shell due to L shell CK transitions

was assumed to be negligible. According to a reevaluation in ref. (5), however, this effect seems to contribute up to 20 percent of all M-shell vacancies, and the measured results should be reduced by this amount. The corrected values are also given in Table 1.

### 1.5. Motivation for Further M-Shell Fluorescence Yield Measurements

It can be observed from sections 1.3. and 1.4. above that essentially no detailed experimental or theoretical work concerning the M-subshell quantities exists. On the other hand, the situation in the K shell is already satisfactory, except in the high-Z region, both regarding experimental accuracy and theoretical understanding. Knowledge of L-subshell quantities is rapidly improving, as indicated by the number of very recent experimental and theoretical publications. It is logical to expect that attention will next be shifted towards the M subshells. This can already be seen, since a relativistic Hartree-Fock-Slater calculation of radiative M-transition rates has been published. In fact, for many of the applications mentioned in Section 1.2. information on M-shell yields is as valuable as that on the K- or L-shell yields. For stimulation of further theoretical investigation of M-shell transitions, existence of accurate experimental values of fundamental subshell quantities as test points is essential. Subshell M-fluorescence yields and mean M-subshell fluorescence yields are such fundamental quantities. Knowledge of these yields may be helpful in construction of wave functions for outer shells with numerical methods.

The means for M-subshell fluorescence yield measurements have just become available. One purpose of this work is to probe such questions as:

to what extent can detailed information be extracted, what are the dominant experimental limitations, and what is the experimental accuracy which can be achieved with modern semiconductor and proportional counter methods?

# CHAPTER II

# BASIS FOR EXPERIMENTAL INVESTIGATION OF M SHELL FLUORESCENCE YIELDS

## 2.1. Notation and Basic Interrelations

Owing to the complicated process of electronic rearrangements in an ionized atom and to the imperfect detector resolution, experimental investigation is often unable to determine the values of individual L- and M-subshell yields, which of course is the primary goal. Consequently, values for various L- and M-mean yields are commonly reported, and the notation has been developed to correspond to the experimental techniques and the resolution obtained. It is necessary to set forth this notation and the relationship of the mean yields to fundamental subshell yields.

As was mentioned above, fluorescence and Auger yields are defined as the probabilities for one vacancy in the subshell $X_i$ to fill by means of radiative or Auger processes, respectively. In terms of macroscopic quantities, these probabilities can be expressed as the ratios of the x-ray and Auger electron intensities, $I_{xi}^X$, and $I_{Ai}^X$, respectively, filling the $X_i$-subshell vacancies, to the total number of vacancies in this subshell

$$\omega_i^X = \frac{I_{xi}^X}{V_i^X} \qquad a_i^X = \frac{I_{Ai}^X}{V_i^X} \tag{3}$$

The intensities of the CK electrons are generally not measured, owing to their low kinetic energies, and direct determination of the CK

yields is therefore not generally feasible.

As a result of photon- or charged-particle bombardment, or of electron capture, or internal conversion in a radioactive decay, a certain distribution of vacancies is created among the subshells of the major shell X. This directly-produced vacancy distribution $N'^{X}_{i}$, is often calculable from the cross sections, electron capture probabilities, or internal conversion coefficients. In addition to these directly-produced vacancies, those shifted from the major inner shells contribute to the so-called original vacancy distribution $N^{X}_{i}$ in the shell X. Before transitions from major higher shells have filled these vacancies, CK transitions will have rearranged the distribution from the original into the final vacancy distribution $V^{X}_{i}$. This final distribution, which can be calculated only with a knowledge of the CK yields, must be applied in eqs. (3), the use of which is considerably complicated by this fact.

The original vacancy distribution is related to the directly-produced distribution according to the general equation

$$N^{X}_{i} = N'^{X}_{i} + \sum_{Y_j} N'^{Y}_{j}\, n_{Y_j X_i} \tag{4}$$

where the sum is taken over all subshells of the inner major shells Y, and $n_{Y_j X_i}$ is the number of $X_i$-subshell vacancies created per initial vacancy in the $Y_j$ subshell (33,9). For example

$$N_K = N'_K \tag{5}$$

$$N^{L}_{i} = N'^{L}_{i} + N_K\, n_{KL_i}$$

$$N^{M}_{i} = N'^{M}_{i} + N_K\, n_{KM_i} + N'^{L}_{1}\, n_{L_1 M_i} + N'^{L}_{2}\, n_{L_2 M_i} + N'^{L}_{3}\, n_{L_3 M_i}$$

As a further example the quantity $n_{L_3M_5}$ is given by (34)

$$n_{L_3M_5} = \omega_3^L \frac{I(L_3\text{-}M_5)}{I(L_3\text{-}X)} + a_K \frac{I(L_3\text{-}M_5X)}{I(L_3\text{-}XY)} + a_K \frac{2\, I(L_3\text{-}M_5M_5)}{I(L_3\text{-}XY)} \tag{6}$$

where $I(L_3\text{-}X)$ and $I(L_3\text{-}XY)$ are the total intensities of the $L_3$ x rays and Auger transitions, respectively, and $I(L_3\text{-}M_5)$, $I(L_3\text{-}M_5X)$, and $I(L_3\text{-}M_5M_5)$ are the intensities of the transition indicated in parentheses.

The relationship between the original and final vacancy distributions in the K, L, and M shells is the following (5):

$$V_K = N_K \tag{7}$$

$$V_1^L = N_1^L$$

$$V_2^L = N_2^L + f_{12}^L N_2^L$$

$$V_3^L = N_3^L + f_{23}^L N_2^L + (f_{13}^L + f_{12}^L f_{23}^L) N_1^L$$

$$V_1^M = N_1^M$$

$$V_2^M = N_2^M + f_{12}^M N_1^M$$

$$V_3^M = N_3^M + f_{23}^M N_2^M + (f_{13}^M + f_{12}^M f_{23}^M) N_1^M$$

$$V_4^M = N_4^M + f_{34}^M N_3^M + (f_{24}^M + f_{23}^M f_{34}^M) N_2^M + (f_{14}^M + f_{13}^M f_{34}^M + f_{12}^M f_{24}^M + f_{12}^M f_{23}^M f_{34}^M) N_1^M$$

$$V_5^M = N_5^M + f_{45}^M N_4^M + (f_{35}^M + f_{34}^M f_{45}^M) N_3^M + (f_{25}^M + f_{24}^M f_{45}^M + f_{23}^M f_{35}^M + f_{23}^M f_{34}^M f_{45}^M) N_2^M + (f_{15}^M + f_{14}^M f_{45}^M + f_{13}^M f_{35}^M + f_{12}^M f_{25}^M$$

(Continued)

$$+ f_{13}^{M} f_{34}^{M} f_{45}^{M} + f_{12}^{M} f_{24}^{M} f_{45}^{M} + f_{12}^{M} f_{23}^{M} f_{35}^{M}$$
$$+ f_{12}^{M} f_{23}^{M} f_{34}^{M} f_{45}^{M}) N_{1}^{M}$$

In view of these equations it is clear that the calculation of the final vacancy distribution $V_i$ in the L shell, and especially in the M shell, starting from known ionization rates is, in general, a very complicated and inaccurate process. One has to look for an experimental arrangement, where the situation can be simplified.

Selective ionization of the shell of interest together with higher shells is often possible. In this case, which may arise both in radioactive decay proper and in external ionization by photons or particles of sufficiently low energy, $N_i^X$ is the same as $N'^X_i$. When only the highest subshell is ionized, the direct ionization gives the final distribution.

Another way for avoiding complications due to determination of $V_i^X$ is by the use of coincidence techniques. In this method the creation of a vacancy in a specific subshell is observed by detecting the process which creates it. The radiation due to the filling of this vacancy is measured in a coincidence arrangement during a period, short compared to the mean interval between random ionizations. The effective number of final vacancies equals the number of detected vacancy-creating events (gate counts).

The application of eq. (3) further requires that $I_{xi}^X$ or $I_{Ai}^X$ – the intensity of radiation filling $X_i$-vacancies – can be determined, i.e. this radiation must be resolved from that associated with adjacent subshells. Commonly the detector is unable to meet this requirement and

only separates the fillings of major shells. In such a low-resolution coincidence experiment with clean detection of the subshell vacancy creation by a well resolved gate transition, the quantity determined by the measured ratio $I^X/V_i^X$ is not $\omega_i^X$, but the probability that a vacancy created in the $X_i$-subshell is followed by emission of an X-shell photon. This quantity, denoted by $\nu_i^X$, and called a <u>mean subshell fluorescence yield</u>, is related to the subshell fluorescence yield $\omega_i^X$ according to the equation

$$\nu_i^X = \omega_i^X + f_{i,i+1}^X \omega_{i+1}^X + (f_{i,i+2}^X + f_{i,i+1}^X f_{i+1,i+2}^X) \omega_{i+2}^X + \cdots \quad (8)$$

Specifically, for L and M shells the following is valid

$$\begin{aligned}
\nu_1^L &= \omega_1^L + f_{12}^L \omega_2^L + (f_{13}^L + f_{12}^L f_{23}^L) \omega_3^L \qquad (9)\\
\nu_2^L &= \omega_2^L + f_{23}^L \omega_3^L\\
\nu_3^L &= \omega_3^L\\
\nu_1^M &= \omega_1^M + f_{12}^M \omega_2^M + (f_{13}^M + f_{12}^M f_{23}^M) \omega_3^M\\
&\quad + (f_{14}^M + f_{13}^M f_{34}^M + f_{12}^M f_{24}^M + f_{12} f_{23} f_{34}) \omega_4^M\\
&\quad + (f_{15}^M + f_{14}^M f_{45}^M + f_{13}^M f_{35}^M + f_{12}^M f_{25}^M + f_{13}^M f_{34}^M f_{45}^M\\
&\quad + f_{12}^M f_{24}^M f_{45}^M + f_{12}^M f_{23}^M f_{35}^M + f_{12}^M f_{23}^M f_{34}^M f_{45}^M) \omega_5^M\\
\nu_2^M &= \omega_2^M + f_{23}^M \omega_3^M + (f_{24}^M + f_{23}^M f_{34}^M) \omega_4^M\\
&\quad + (f_{25}^M + f_{24}^M f_{45}^M + f_{23}^M f_{35}^M + f_{23}^M f_{34}^M f_{45}^M) \omega_5^M\\
\nu_3^M &= \omega_3^M + f_{34}^M \omega_4^M + (f_{35}^M + f_{34}^M f_{45}^M) \omega_5^M
\end{aligned}$$

(Continued)

$$\nu_4^M = \omega_4^M + f_{45}^M \omega_5^M$$

$$\nu_5^M = \omega_5^M$$

It is to be noted that these quantities, being combinations of fluorescence and CK yields only, still are purely functions of the atomic properties.

It is not always possible to signal the creation of a vacancy in a specific subshell $X_i$, but rather just somewhere in a major shell X. The measurement gives in this case a linear combination of $\nu_i$'s weighted with the vacancy production rates in the subshells, as determined by the gating process. If Y-X x rays are used for gating, the quantity measured is denoted by $\omega_{YX}$ and called a mean X-shell fluorescence yield following (Y-X) x-ray emission. With such experiments Jopson (32) determined some values of $\omega_{LM}$.

The occurrence of CK transitions in the X shell does not affect the total number of vacancies, $N_X$, in this shell, and therefore

$$N_X = \sum N_i^X = \sum V_i^X \tag{10}$$

Because the absolute emission rate of X-shell x rays $I_x^X$ is the

$$I_x^X = \sum N_i^X \nu_i^X = \sum V_i^X \omega_i^X$$

probability for radiative filling of an X-shell vacancy, the mean X-shell fluorescence yield $\bar{\omega}_X$ is given by

$$\bar{\omega}_X = \frac{I_x^X}{N_X} = \frac{\Sigma\, N_i^X\, \nu_i^X}{N_X} = \frac{\Sigma\, v_i^X\, \omega_i^X}{N_X} \qquad (11)$$

This is the M-shell quantity measured by Jaffe (30), Lay (29), and Konstantinov (31). The value of $\bar{\omega}_X$, as well as that of $\omega_{YX}$, is dependent on the vacancy distribution, and these mean yields, therefore, are not fundamental subshell quantities. In principle however, the $\ell$ independent subshell yields can be determined, if the measurement of $\bar{\omega}_X$ can be repeated $(\ell-1)$ times with different, known vacancy distributions among the subshells.

The standard notation introduced above will be followed in this text with the exception that the super- or subscript L will be omitted from symbols of the L-shell quantities for the sake of simplicity.

## 2.2. Coincidence Method for M-Subshell Fluorescence Yield Measurements

The application of coincidence methods with K-$M_i$, or $L_j$-$M_i$ x-ray gating is, at present, the only practical choice for extraction of information on M-subshell fluorescence yields. Since $v_i^M$ in basic eq. (3) is measured by the gate counts multiplied by the number of $M_i$-subshell vacancies associated with one gate count and since the intensity of M x-rays is only partially observed, due to limited detection efficiency, the following equations in terms of measurable quantities are valid in the cases of high or poor resolution in the detection of M x rays, respectively

$$\omega_i^M = \frac{1}{\varepsilon_{Mi}(1+m_j^X)} \frac{C_{M_i}(X_j M_i)}{C_{X_j M_i}} \qquad (12)$$

$$\nu_i^M = \frac{1}{\bar{\epsilon}_M(1+m_j^X)} \frac{C_{M(X_jM_i)}}{C_{X_jM_i}} \tag{13}$$

The quantities $C_{M_i(X_jM_i)}$ and $C_{M(X_jM_i)}$ are the coincidence counting rates of the $M_i$ or M x rays observed with gate counting rate $C_{X_jM_i}$. The detection efficiency $\bar{\epsilon}_{Mi}$ or $\bar{\epsilon}_M$ is the ratio of the detection rate in coincidence geometry, of $M_i$ or M x rays, respectively, to the emission rate of these x rays by the source. The factor $(1+m_j^X)$ is a correction for multiple M-shell vacancies associated with one gate pulse. In an ideal case this factor is unity, but generally it is different in each of the eqs. (12) and (13). The origin and calculation of this factor for K-M x-ray and L-M x-ray coincidence measurements with unresolved M x-ray spectrum is discussed in Appendix I.

The existence of multiple M-shell vacancies at the moment of K-M or L-M x-ray emission may have two basically different origins: i.e., electronic, starting from one original K- or L-shell vacancy, followed by nonradiative transitions from the M shell; or nuclear, arising from two or more original vacancies created simultaneously in cascading nuclear processes in a radioactive decay. The quantity $m_j^X$ is, therefore, the sum of the electronic and nuclear contributions, $m_{ej}^X$ and $m_{nj}^X$, respectively

$$m_j^X = m_{ej}^X + m_{nj}^X \tag{14}$$

In the high-Z region, the electronic multiplication term arises from CK transitions $L_1$-$L_3M_{3,4,5}$ and $L_2$-$L_3M_{4,5}$ and from certain K-Auger

transitions. If, for example, a vacancy is originally created in the $L_1$ subshell and then shifted to the $L_3$ subshell through one of these CK processes, there are two M-shell vacancies coincident with the $L_3$ x-ray, which arises from the filling of this particular $L_3$-subshell vacancy. The probability of a coincidence is thus approximately doubled for this gate. Owing to the smallness of the K-shell Auger yield $a_K$ ($\approx$ 0.025 at Z=96), the multiplication arising from Auger transitions can be generally neglected when high-Z sources are measured. It is shown in Appendix I that the electronic vacancy multiplication term $m_{ej}^X$ for the K and L shells is given by

$$m_e^K = m_{e1} = m_{e2} = 0 \tag{15}$$

$$m_{e3} = \frac{1}{V_3}\left\{\left[\frac{I(L_1\text{-}L_3M)}{I(L_1\text{-}L_3X)}\, f_{13} + \frac{I(L_2\text{-}L_3M)}{I(L_2\text{-}L_3X)}\, f_{12}\, f_{23}\right] \times N_1 + \frac{I(L_2\text{-}L_3M)}{I(L_2\text{-}L_3X)}\, f_{23}\, N_2\right\}$$

where $I(L_i\text{-}L_jM)$ is the intensity of the transition indicated and $I(L_i\text{-}L_jX)$ is the total intensity of all $L_i\text{-}L_jX$ transitions, with X meaning any possible subshell.

Calculation of the nuclear cascading term $m_{nj}^X$ is more difficult. In a simple cascade of two gamma rays (1) and (2), the conversion of one may result in emission of the gating K-M, or L-M x ray, while the other is free to create M-shell vacancies through M-shell conversion or through conversion in an inner shell with consequent shift of the vacancy to the M shell. The following equation for calculation of the nuclear cascading multiplication term in a cascade of two gamma rays is derived in Appendix I:

$$m^{X}_{nj} = \frac{V^{X}_{j}(1)\cdot b_2 + V^{X}_{j}(2)\cdot b_1}{V^{X}_{j}\cdot A} \tag{16}$$

where

$$b_s = N'_M(s) + N'_K(s)\ n_{KM} + N'_1(s)\ n_{L_1M} + n'_2(s)\ n_{L_2M} + N'_3(s)\ n_{L_3M}$$

The quantities $N'^{X}_{j}(s)$ and $V^{X}_{j}(s)$ are the directly-produced and final-vacancy distributions arising from conversion of gamma (s) (s=1,2), respectively. The quantity $n_{X_jM}$ is the number of M-shell vacancies arising from one initial $X_j$-subshell vacancy (33,5,34), and A is the feeding per decay of the intermediate level in the cascade (e.g., $\alpha$-branching to this level + deexcitation from higher energy levels).

The correction term $m^{X}_{nj}$ is the same, consistent with the notation, for any K, $L_1$, $L_2$, or $L_3$ x-ray gate pulse, but different for gates containing x rays filling different subshells. Therefore, the nuclear cascading corrections can be experimentally determined from coincidence rates measured with K-N,O.. and $L_j$-N,O.. gating.

Owing to the existence of multiple M-shell vacancies, the results obtained in coincidence measurements are not completely pure values of the quantities $\nu^{M}_{i}$, because a certain fraction of the original vacancies may lie outside of the subshell indicated by the gate pulse.

## 2.3. Choice of Detectors for Measurements of K-M X-Ray and L-M X-Ray Coincidences

For detection of K and L x rays from high-Z elements in the energy region above four keV, cooled (77°K) Ge(Li) and Si(Li) semiconductors are

superior to other detectors for coincidence measurements, where simultaneous high resolving power and good efficiency are required. Ge(Li) detectors were employed in this work for this purpose. However, in order to make use of such detectors for intensity measurements, a careful experimental study is necessary to determine for each detector a precise efficiency at various photon energies. This is particularly important for Ge(Li) detectors, since their efficiency curve is complicated by a discontinuity due to the germanium K edge at 11.1 keV. At low energies ($< 10$ keV), the detection efficiency of a standard-type x-ray spectrometer (see Section 3.2) is restricted by absorption in the beryllium window, in the dead surface layer, and in the dead annular ring around the edge of the detector. Variations in the properties of individual detectors give an unpredictable feature to every efficiency curve and thus preclude attempts to calculate a theoretical efficiency curve. An extensive study of the efficiencies of the Si(Li) and Ge(Li) spectrometers used in this work has been performed and reported by Freund et al. (35), Hansen, Freund, and Fink (17), and Nix, McGeorge, and Fink (36).

Modern semiconductors, especially Si(Li) spectrometers with very thin beryllium windows, are useful for x-ray measurements down to about two keV; i.e. in the energy region of M x rays from high-Z elements. The germanium escape peaks tend to disturb Ge(Li) spectra in this energy region below five keV. Therefore, a Si(Li) spectrometer was used in this work to detect the M x rays. Accurate determination of the efficiency at these energies becomes difficult, owing to the rapid change with energy and to the lack of intensity-calibrated standard x-ray sources. Such a source ($^{241}$Am) was calibrated for the present work as explained below

(Section 3.4.).

Below about four keV, the gas proportional counter begins to compete favorably with semiconductors, in spite of its inferior resolution. Having high gas amplification, proportional counters do not suffer from preamplifier noise limitations; e.g. single electrons can be detected down to essentially zero energy (37). The possibility of windowless operation with detection efficiencies up to unity is an important factor in low-energy photon detection from radioactive sources, because the photon intensities tend to be low due to the high nonradiative transition probabilities in atomic and nuclear deexcitation. A major advantage is the freedom of choice regarding the optimization of the efficiency for a particular energy by varying the type of gas and its pressure. Moreover, the proportional counter does not suffer from many of the non-reproducible effects on efficiency which afflict semiconductor spectrometers, e.g. uneven dead layer and gold layer on the surface, dead and possibly asymmetric annulus, internal collimators, and carrier trapping (35). The efficiency of a proportional counter below five keV can be calculated theoretically on the basis of photoelectric gas absorption, if care is taken to avoid wall effects.

Below a few keV, the background in a proportional counter increases rapidly with decreasing energy due to electrons from nonradiative transitions and wall effects. This background is drastically reduced in a multiwire proportional counter (MWPC), where a wall-less center counter is operated in anticoincidence with ring counters surrounding it. Such a MWPC was designed and constructed for this study (see Figure 5) and was used for detection of the M x rays alternatively with a Si(Li) spectrometer,

after its detection characteristics had been carefully examined (see Section 3.4.).

## 2.4. Choice of Radioactive Sources for Measurements of K-M X-Ray and L-M X-Ray Coincidences

Inner shell ionization can be produced either by fluorescent excitation or in radioactive decay. In order to avoid large corrections for self-absorption of M x rays in the source, from which the fluorescent excitation method suffers considerably, radioactive sources of high specific activity were used in this study.

Since the structure in K, L, and M x-ray spectra becomes better resolved with increasing atomic number Z, the selection of high-Z sources is necessary. Creation of multiple vacancies by fluorescent self-excitation with x rays and gamma rays is avoided by the use of a thin source of high specific activity mounted on a thin, low-Z backing. The availability of carrier-free samples of the nuclides $^{241}Am$ ($T_{\frac{1}{2}}$ 458 y) and $^{249}Cf$ ($T_{\frac{1}{2}}$ 352 y) permitted a study of M-subshell fluorescence yields of neptunium (Z=93) and curium (Z=96) to be carried out with these sources. In respect to cascading nuclear transitions, these nuclides with rather complex decay schemes are not ideal, resulting in sizeable creation of multiple M-shell vacancies due to simultaneous internal conversions.

The essential features of the decay schemes of $^{241}Am$ and $^{249}Cf$ are shown in Figure 1, simplified from schemes shown in Tables of Isotopes (38). The alpha and gamma branching in decay of $^{241}Am$ is well established on the basis of extensive studies by Baranov, Kulakov, and Shatinskii (39), Lederer et al. (40), Michaelis (41), and Günther and Parsignault (42),

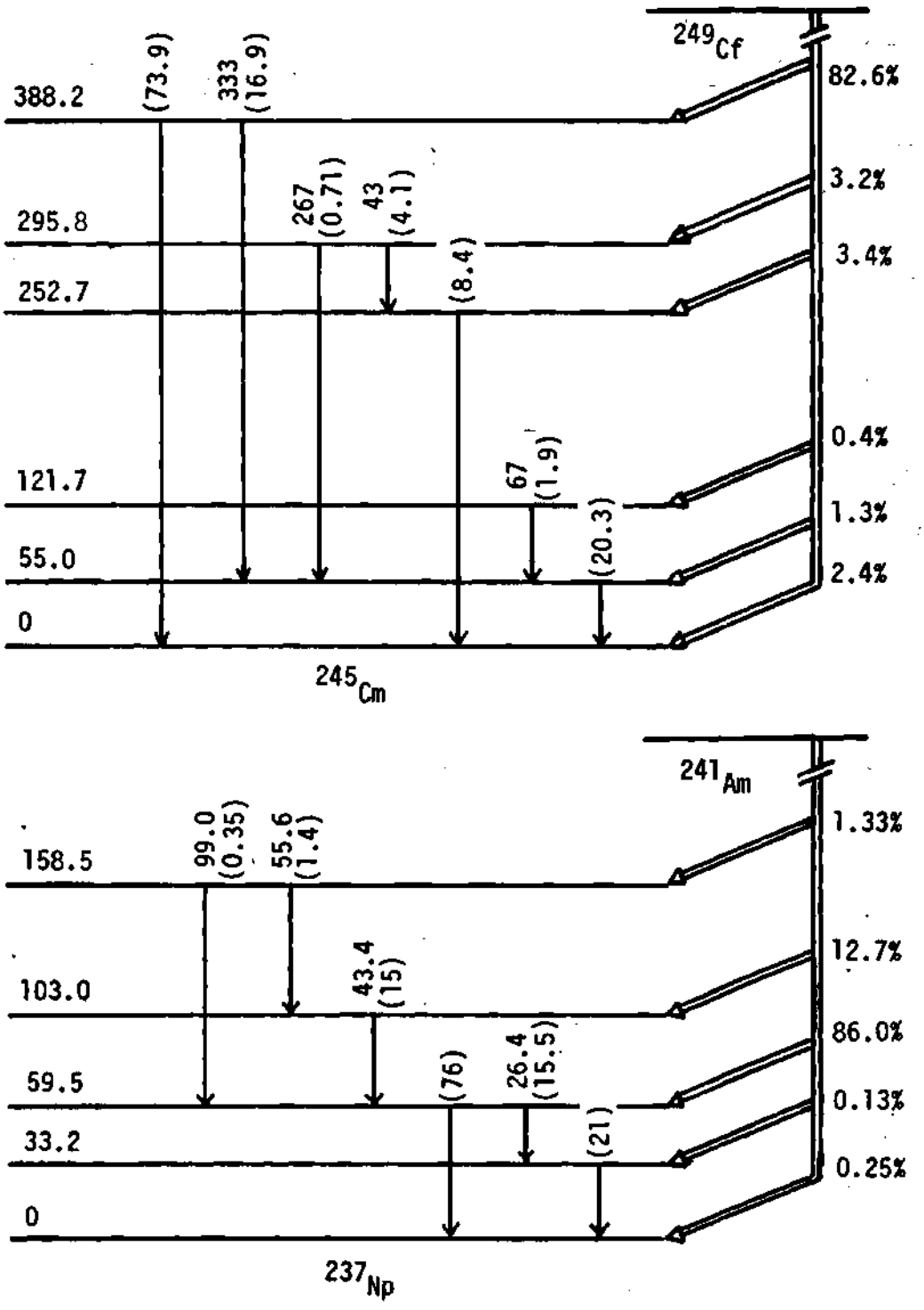


Figure 1. Decay Schemes of $^{241}Am$ and $^{249}Cf$. (Simplified from Ref. (38). In parentheses is the number of transitions per 100 decays and bare numbers give energies in keV.)

among others. Internal conversion coefficients have been examined by Yamazaki and Hollander (43) and Wolfson and Park (44), by means of high resolution electron spectroscopy. The data permit calculation of the original vacancy distribution in the L subshells and in the M shell, for evaluation of multiple vacancies within 10 percent accuracy. Information concerning the decay of $^{249}$Cf is less comprehensive.* Alpha feeding is well known from the work of Baranov, Shatinskii, and Kulakov (45), of Kooi and Wapstra (46), and of Ahmad (47), but minor uncertainties in gamma deexcitation still remain after the recent studies (46,47). Experimental internal conversion coefficients are available only for transitions over 200 keV in energy from a measurement with a Si(Li) detector (47). Calculation of the vacancy distribution is thus less certain ($\mp$ 20 percent) than from the decay of $^{241}$Am and must largely be based on theoretical conversion coefficients. In contrast to the decay of $^{241}$Am, an appreciable number of K-shell vacancies is created in the conversion of energetic gamma rays in the decay of $^{249}$Cf. This opens new channels for creation of multiple M-shell vacancies, but on the other hand permits measurements of such quantities as $\omega_2^M$, $\nu_2^M$, and $\nu_3^M$ by $K_\beta$ x-ray gating, which cannot be obtained by gating on the L x rays.

The details of the calculation of inner shell vacancy creation are shown in Appendix I.

---

*Extensive work on $\gamma$- and $\gamma\gamma$-coincidence measurements in $^{249}$Cf decay is currently in progress by W. D. Schmidt-Ott (48) in this laboratory.

# CHAPTER III

# EXPERIMENTAL MEASUREMENTS AND EVALUATION OF THE DATA

## 3.1. Radioactive Sources

The $^{241}Am$ sources for these experiments were made by droplet evaporation from a carrier- and solids-free $Am(NO_3)_3$-solution. High specific activity is required in order to minimize the possibility of ionization of the electron shells by the x rays and alpha particles. The sources were evaporated on a thin (0.9 mg/cm$^2$) aluminized Mylar foil which makes possible essentially absorption-free transmission of the L x rays through the backing. The sources were two to three millimeters in diameter and barely visible. They were covered with a Krylon-spray coating of 150-300 μg/cm$^2$ to prevent loss of activity due to alpha recoil effects. Comparison of $M_\alpha$ and $L_\alpha$ x-ray intensity ratios from several sources did not show any deviations outside the counting statistics, indicating that negligible self-absorption of the M x rays was present. The source used in the MWPC experiment had an activity of 0.451 μCi and that used in the Ge(Li)-gated experiment 1.53 μCi, as deduced from comparison of the 59.5 keV gamma-ray intensity to that from an IAEA-standard $^{241}Am$ source (IAEA standard set 31, 1969).

The $^{249}Cf$ source which was received as a loan from the Trans-Uranium Laboratory at Oak Ridge National Laboratory had been made by electro deposition on a 0.13 mm thick beryllium disk. The diameter of the circular source was 0.94 cm, and its activity 16 μCi. The source also

produces a few neutrons due to the $Be^{9}(\alpha,n)C^{12}$ reaction, but their presence was not disturbing.

## 3.2. Detectors

Two different coincidence systems were used in the course of the work: a Ge(Li)-Si(Li) system and a MWPC-Ge(Li) system. Four different detectors, therefore, were involved in the measurements.

A dipstick type Ge(Li) spectrometer, Ortec Model 8113-08, was used as the gate detector in the $^{249}Cf$ measurements and in the L x-ray-gated $^{241}Am$ measurements. This detector is eight mm in active diameter and five mm deep and gives a resolution of 436 eV FWHM at 14.4 keV. The spectrometer is provided with a 0.25 mm thick beryllium window which gives an essentially absorption-free entrance for the L x rays.

The coincidence spectra of M x rays in the experiments mentioned above, were measured with a Kevex Model 3000/SN 196 Si(Li) spectrometer which has a detector diameter of six mm and nominal depth of three mm. Its resolution is 260 eV FWHM at 6.4 keV and the beryllium window is 0.05 mm thick. Window absorption begins to affect the efficiency below about six keV, but the gold layer on the surface of the detector, together with a dead silicon surface layer, results in a rather rapid decrease in efficiency below nine keV, as is seen in Figure 2. The two detectors in coincidence arrangement are shown in Figure 3.

The second Ge(Li) spectrometer, Ortec Model 8013-08, which was used for detection of L x rays in coincidence with MWPC gate pulses, is eight mm in diameter, and its sensitive depth is 5.5 mm. The thickness of the beryllium window is 0.13 mm, and the spectrometer gives a resolution of 343 eV FWHM at 6.4 keV.

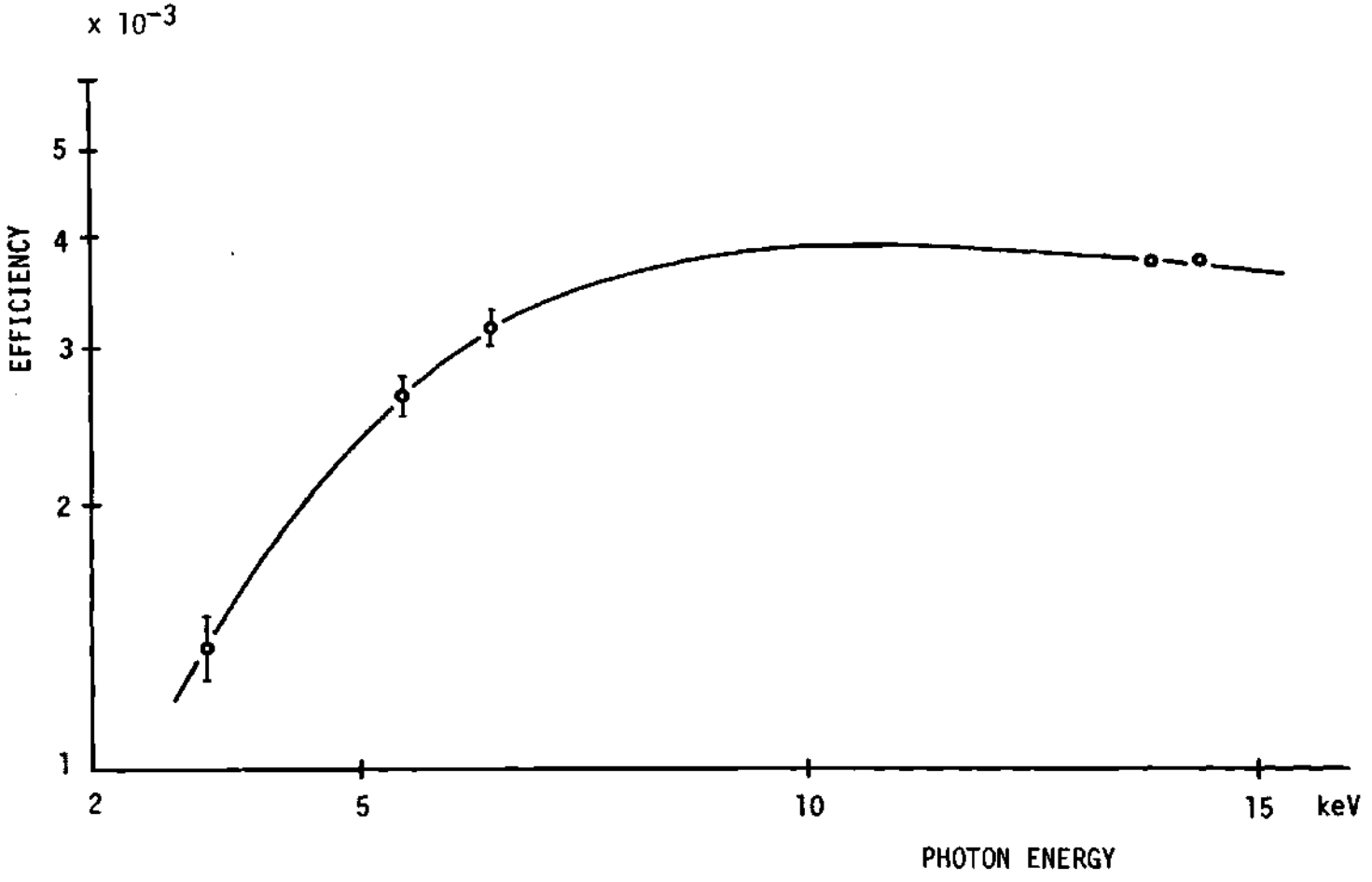


Figure 2. Detection Efficiency of the Si(Li) Spectrometer for Low-Energy Photons. (The numerical values are for the coincidence geometry used in measurements with a $^{249}$Cf source. Points at 3.3 and 13.9 keV are from $^{241}$Am decay, at 6.5 and 14.4 keV from $^{57}$Co decay and at 5.5 keV from $^{54}$Mn decay.)

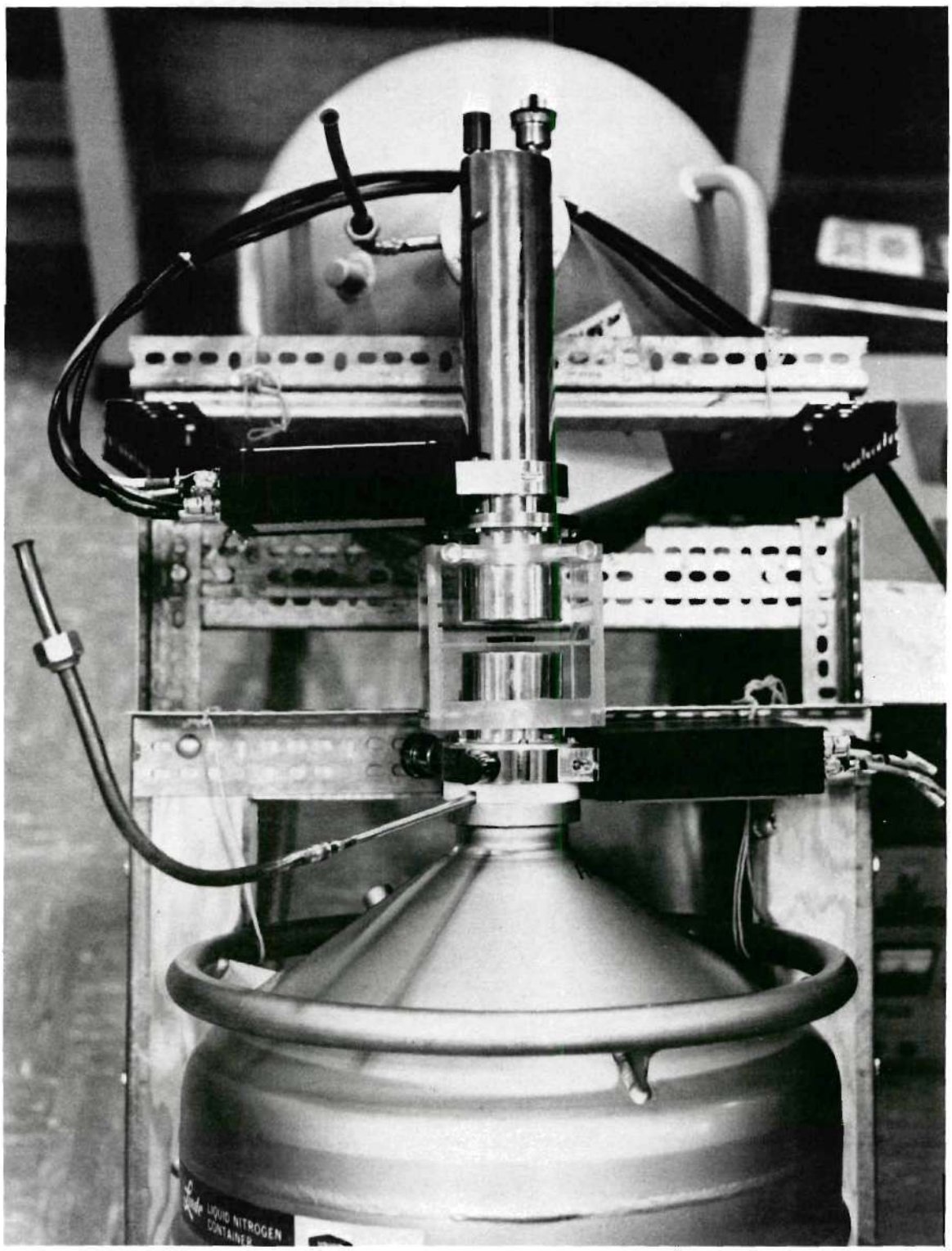


Figure 3. The Ge(Li) (upper) and Si(Li) (lower) Detectors in Coincidence Arrangement

The multiwire proportional counter (MWPC) which was specifically constructed for this work is shown in Figure 4, with its wire system exposed. The center-counter diameter 6.35 cm, is defined by a ring of 24 cathode wires. The 1.27 cm thick annulus is shared among 12 identical ring counters, each defined by five cathode wires and by the aluminum body of the counter. The stainless steel wires--0.2 mm thick cathode wires and 0.05 mm thick counting wires--are stretched between two Teflon disks and are held in slight tension by means of small springs. A detachable assembly in the body provides the means for mounting a solid source at the level of the inner surface of the body, while a 0.25 mm thick beryllium window serves as a low absorption exit for external detection of photons from this source and also makes possible the use of an external source. Figure 5 shows a cross section diagram of the MWPC and the method of fitting it into a coincidence arrangement with the Ge(Li) detector. The ring counters are all operated as one unit and form a thin anticoincidence layer surrounding the center counter. This anticoincidence layer is thin, in order to transmit most of the low-energy photons into the center counter, yet it is thick enough to detect all the ionizing particles from the source and from wall effects and thus to reject them by anticoincidence.

## 3.3 Electronic Circuits

The electronic circuits were designed to facilitate counting of those x-ray pulses from the "coincidence detector," which are time-related with pulses from the "gate detector," with maximum coincidence efficiency and minimum contribution by chance coincidences. In one assembly, de-

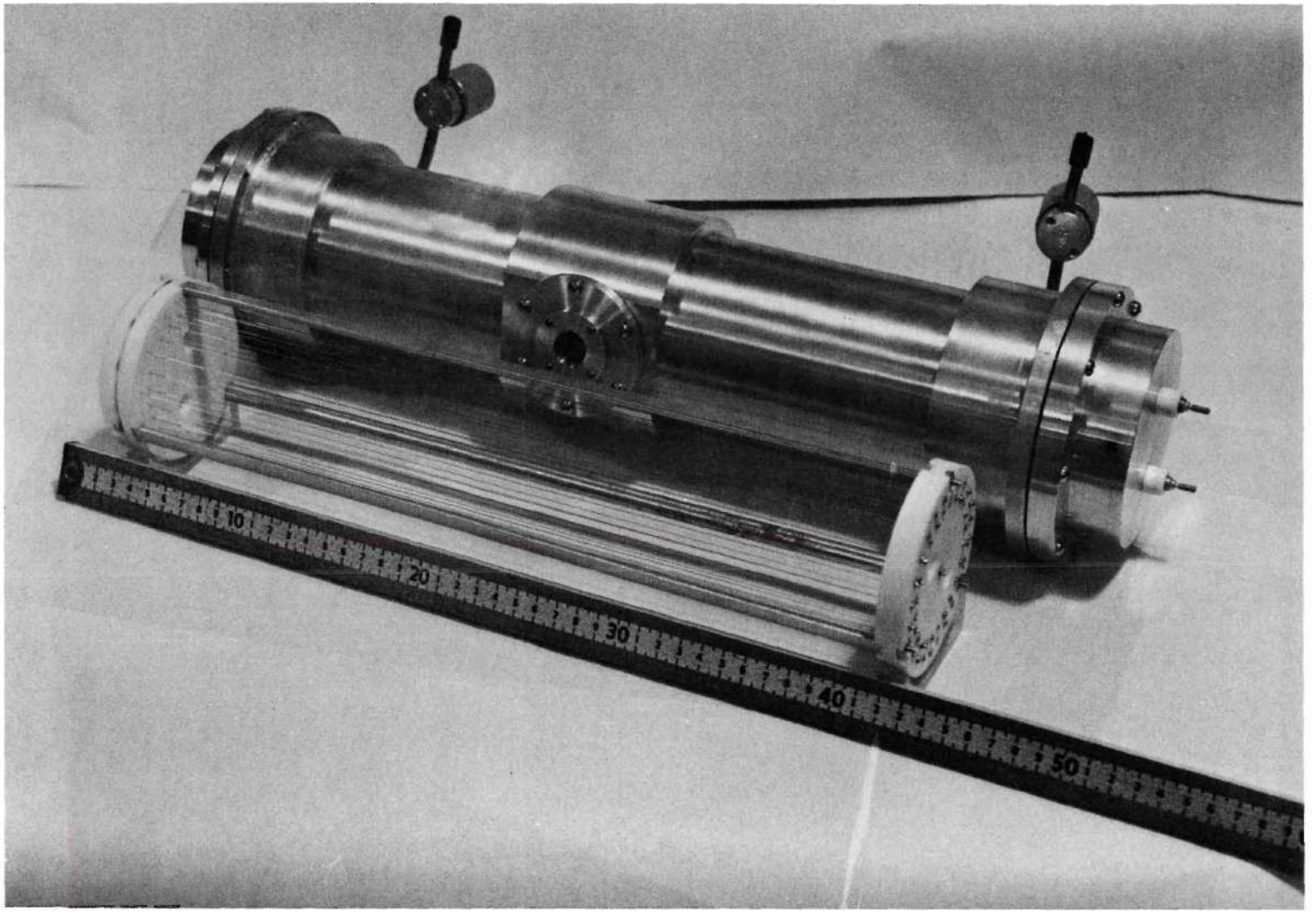


Figure 4. The Multiwire Proportional Counter (MWPC) with Its Wire System Exposed.

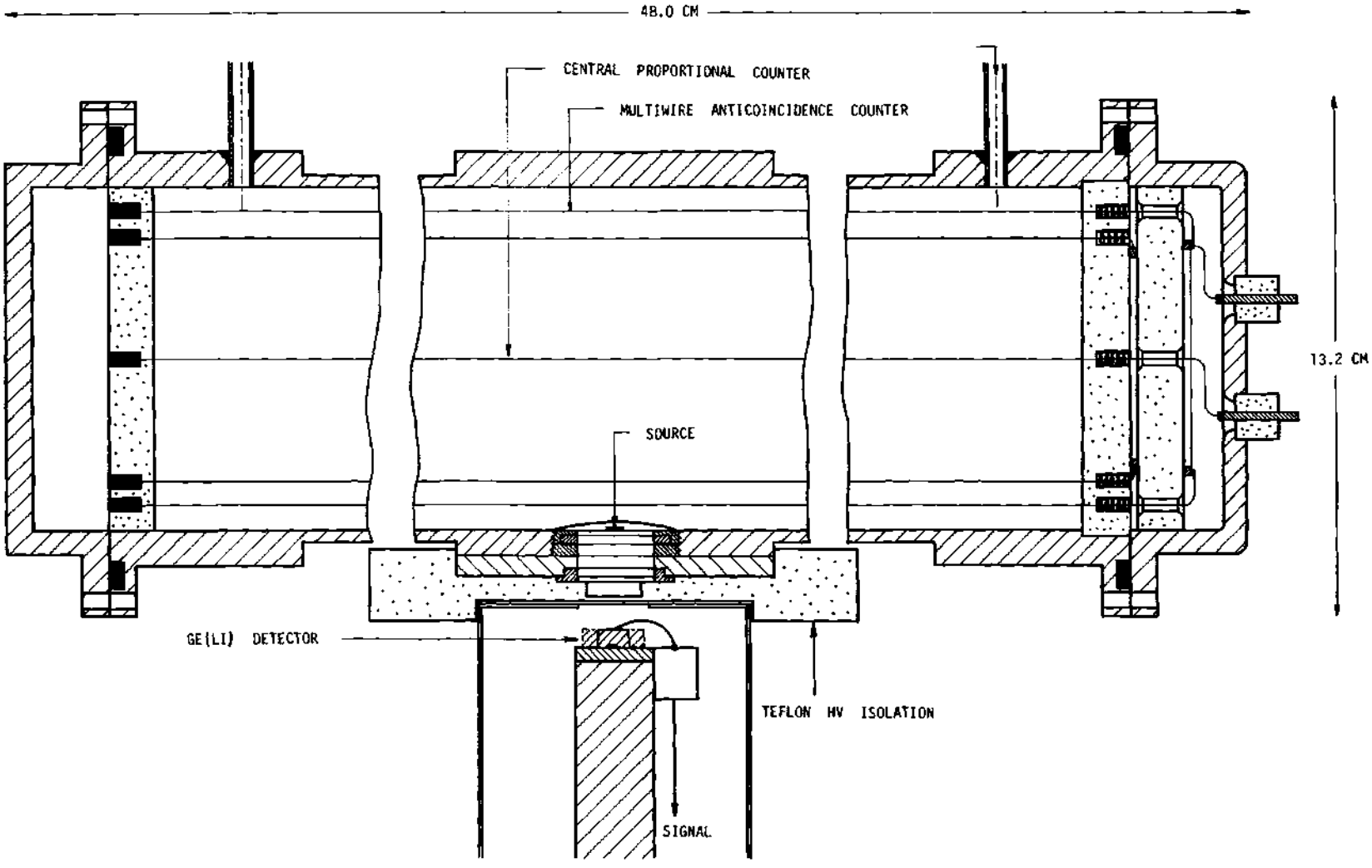


Figure 5. Cross Section Diagram of the MWPC and Coincidence Arrangement with the Ge(Li) Detector. (Details are explained in text.)

scribed in Figure 6, the MWPC was used as the "gate detector" and a Ge(Li) as the "gate detector." In the second system, shown in Figure 7, a Si(Li) detector was the coincidence detector and a Ge(Li) detector the gate detector. In order to save measurement time, several coincidence spectra were recorded simultaneously, which requires use of parallel, identical circuits and many-fold routing of the multichannel analyzer. Furthermore, in the MWPC-gated measurements of M-L x-ray coincidences, the M x-ray pulses had to be sorted out electronically from the background of energetic pulses due to charged particles in the center counter, in order to avoid detection of unwanted coincidences, e.g. $\alpha$-particle M x-ray coincidences. This was accomplished with the aid of an anticoincidence circuit triggered with ring-counter pulses.

Negative high voltage was connected to the shell and to the thick cathode wires of the MWPC and adjusted to give the required gas amplification for the center-counter pulses. The center wire was DC-connected to a charge-sensitive preamplifier (TC 133) while a voltage-sensitive preamplifier (TC 100B) was used in the ring-counter circuit. The gas amplification of the ring counter was independently adjustable by means of negative bias voltage on the thin ring-counter anode wires.

The circuit diagram for the MWPC-gated coincidence measurements is shown in Figure 6.* The use of an internal $^{241}$Am source in the MWPC results in a background of five to six MeV alpha pulses, which are huge compared to the 3.3 keV M x-ray pulses to be counted. In the anticoincidence

---

*The bare numbers in Figures 6 and 7 and in the text refer to Ortec module numbers and the letters in front of the other unit numbers identify other manufacturers.

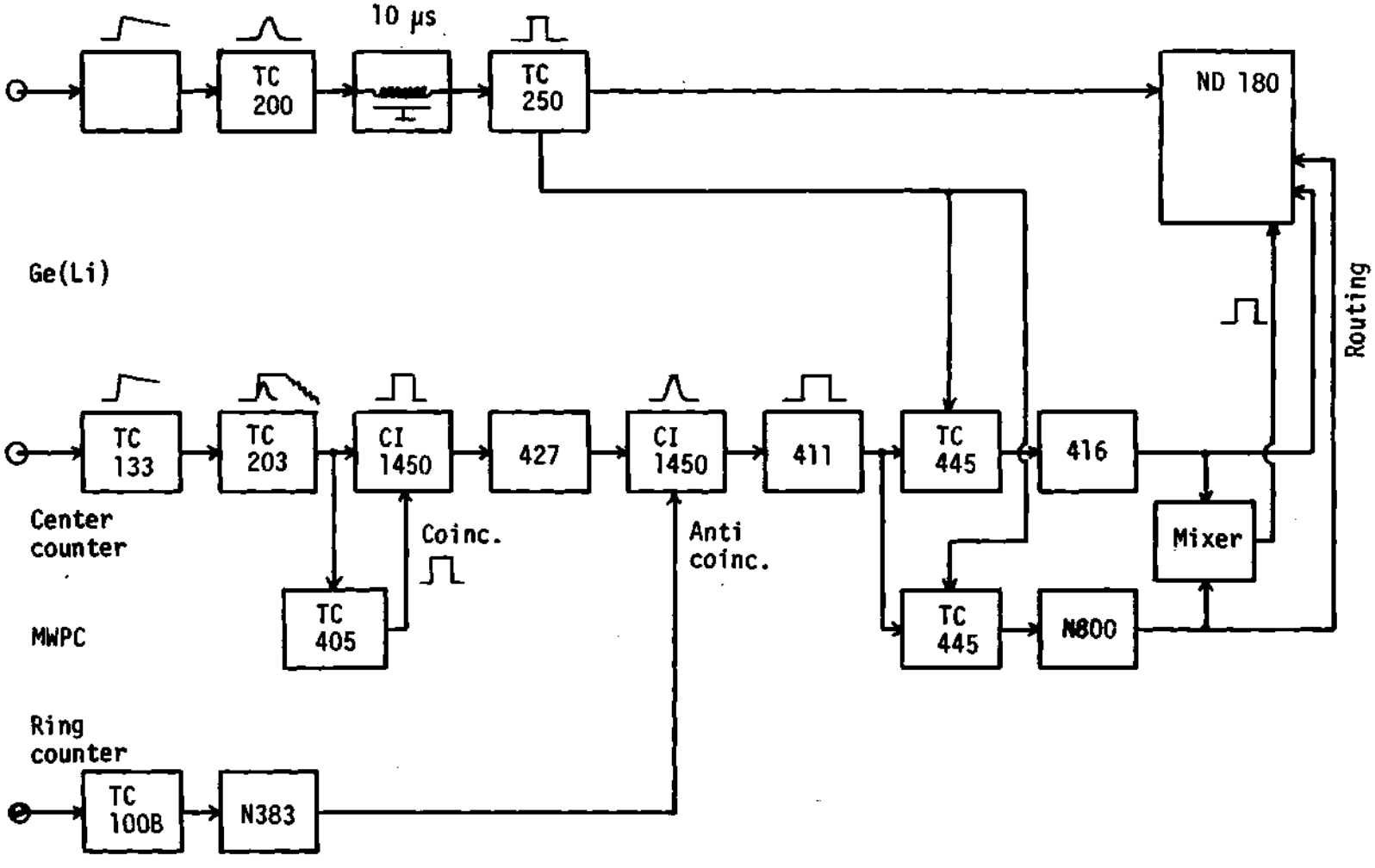


Figure 6. Diagram of the Electronic Circuits Used in the MWPC-Ge(Li) Coincidence Measurements with Two-Fold Routing. (Center-counter pulses which are not in anticoincidence with ring-counter pulses are used for gating.)

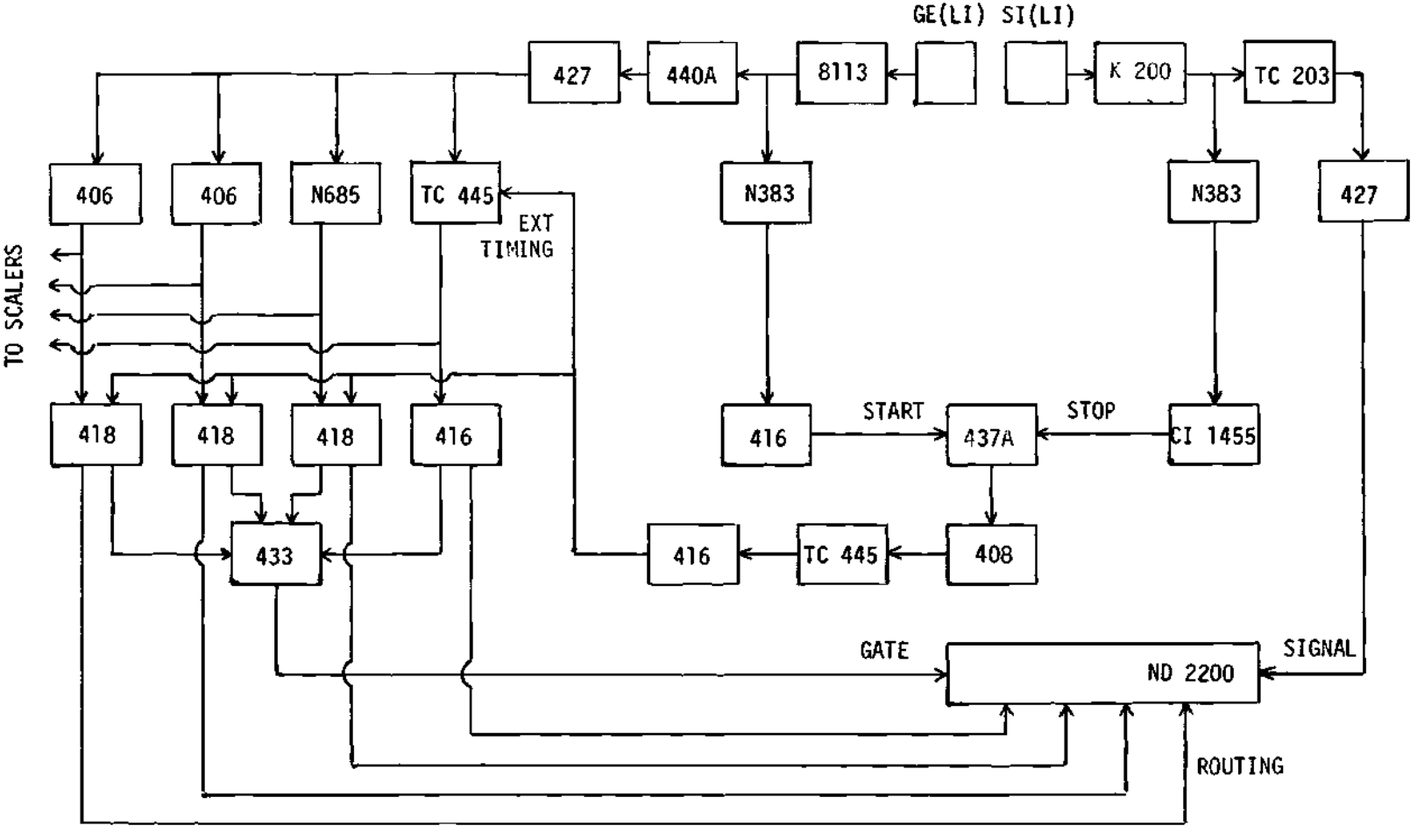


Figure 7. Diagram of the Electronic Circuits Used in the Ge(Li)-Si(Li) Coincidence Measurements with Four-Fold Routing. (Time and Energy Information is Treated Separately in Order to Minimize the Resolving Time.)

operation the afterpulses following these alpha pulses must be rejected. For this reason the pulses from the center counter were clipped to a maximum length of 4.5 μs by self-gating in the coincidence mode in the first linear gate (CI 1450). Anticoincidence was then required between this output pulse and a ring-counter pulse in order to get an output from the second linear gate. The gates were selected in two "timing-single-channel analyzers" (SCA's) (TC 445) in which the coincidences with Ge(Li) pulses were also made. The two coincidence spectra were stored simultaneously in a ND-180 multichannel analyzer by using two-fold routing. The resolving time was 11 μs, in order to allow for the rather broad time distribution (about two μs FWHM) of the MWPC pulses. For measurement of chance coincidences, the 10 μs delay line was removed from the Ge(Li) branch.

Figure 7 gives the circuit diagram for the Ge(Li)-Si(Li) coincidence setup with four-fold routing. Special attention was paid in order to maximize the true-to-chance coincidence ratio, which tends to be low owing to low detection efficiencies in both detectors. Fast coincidences between all output pulses of the detectors were, therefore, selected with short resolving time and the accurate time information thus obtained was combined with energy information analysed in a separate branch. Preamplifier output pulses from each detector were fed to fast Hamner N383 main amplifiers and then into the TH 200 A/M time-to-amplitude converter (TAC) which served as a fast-coincidence unit. The peak of the time distribution was selected with a SCA (TC 445) and its extended (416) output pulses carried the time information for the four coincidence units (418, TC 445). In these units, slow coincidences were taken with gate pulses from the Ge(Li) detector selected with SCA's (406, N685), or internally selected

in the timing SCA (TC 445). The extended (416) coincidence pulses from the timing SCA were mixed with output pulses from the other coincidence units in a sum-amplifier (433), and its output pulses triggered the gate of the ND-2200 multichannel analyzer. The gate information was carried by routing pulses from the coincidence units to the analyzer. A variable delay amplifier (427) makes it possible to match the timing of the linearly amplified (TC 203) signal from the Si(Li) detector to its associated gate in the analyzer. In chance coincidence measurements, the delay was reduced by two μs from its normal value. A resolving time of 340 ns was generally used, and the time distribution spectrum in Figure 8 proves that this is adequate. A test run with a doubled time window in TC 445 showed no timing losses of true coincidences in normal runs. The gate counting rates from the SCA's were continuously monitored with scalers (except from TC 445, in which this possibility does not exist). This gate, as well as the time gate, was monitored regularly by interrupting the run.

For the $^{249}$Cf measurements, the TAC unit was not available, but both the fast and slow coincidences were made with Ortec coincidence modules (418), where triple coincidence was required for an output. A resolving time of 500 ns was used in this case.

## 3.4. Detection Characteristics of the MWPC and Determination of the M X-Ray Emission Rate in Decay of $^{241}$Am

The detection characteristics of the MWPC, especially its efficiency, were examined in detail, both with internal $^{241}$Am and $^{57}$Co sources, and with collimated beams from several external low-energy x-ray sources.

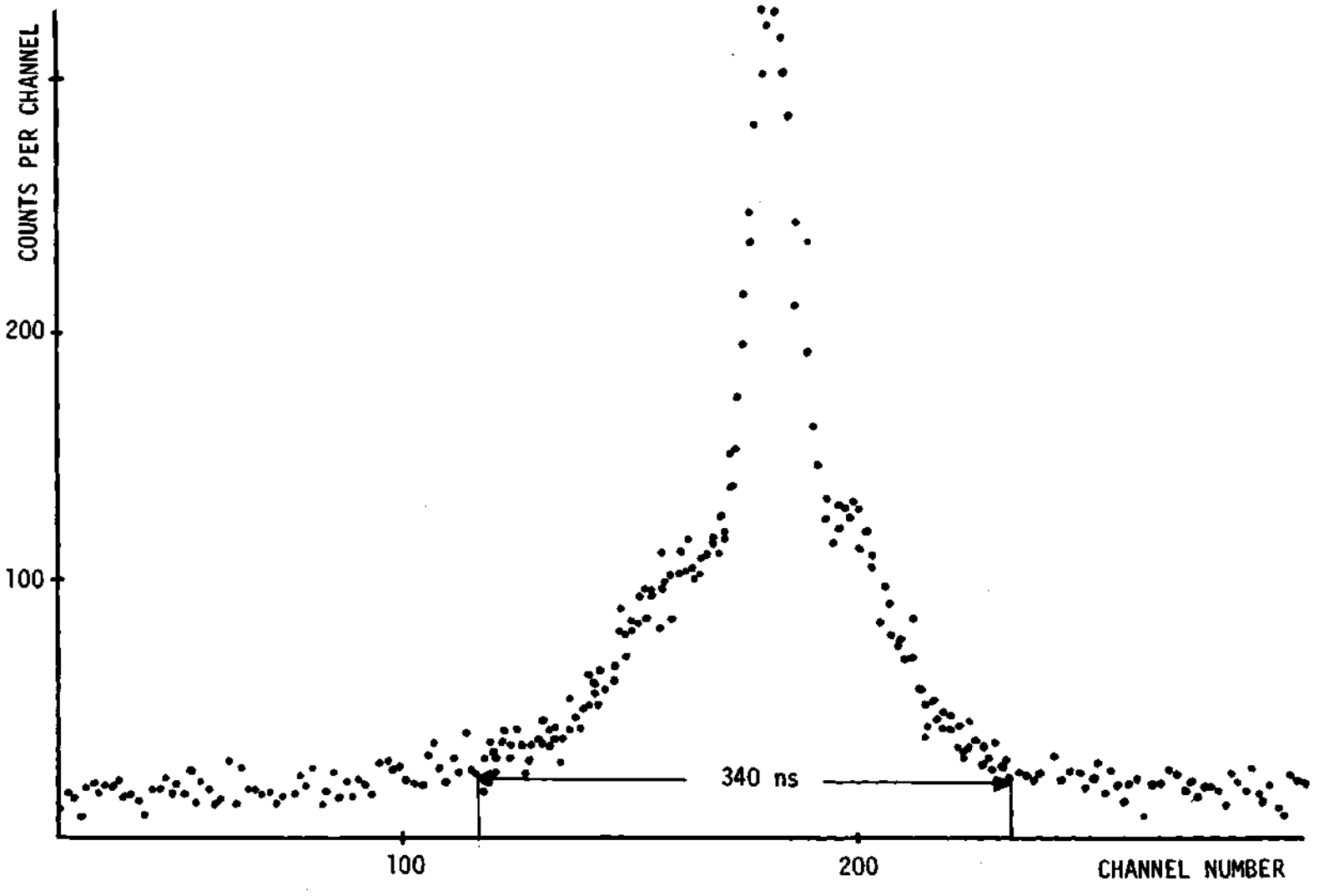


Figure 8. Time Distribution in the Ge(Li)-Si(Li) Measurements of L-M X-Ray Coincidences and the Time-Window Setting. (It can be seen that 340 ns is a sufficient resolving time.)

Figure 9 illustrates the effect of anticoincidence operation on the M x-ray spectrum from an internal $^{241}Am$ source. The counter was filled with propane to 380 torr. A two-fold reduction in the Np M x-ray intensity is observed due to anticoincidence operation, but the background reduction is ten-fold. A small peak at 6.4 keV appears only in the anticoincidence spectrum, probably arising due to fluorescent excitation of iron in the stainless steel wires. A resolution of 18 percent FWHM at 6.4 keV was obtained in measurements with a $^{57}Co$ source.

The efficiency of a proportional counter can be calculated on the basis of photoelectric absorption (Section 2.3.). For a narrow, collimated beam of radiation, entering perpendicularly to the axis of the MWPC, the following formula is valid

$$\varepsilon = \exp(-\mu d_r)\,[1 - \exp(-\mu d_c)] \qquad (17)$$

where $d_r$ is the thickness of the ring counter zone; $d_c$, the diameter of the center counter; and $\mu$, the linear absorption coefficient of the counting gas at a given photon energy. This equation presumes that, with zero thickness of the ring counter, the efficiency of the center counter is unity at sufficiently high gas pressure (large $\mu d_c$). The boundary between the center and ring counter is determined by field lines connecting the ring of cathode wires and need not coincide with the cylindrical, geometrical surface of the center counter. In fact, the true boundary will vary, depending on the ratio of the high voltages on the center and ring counter. This means that $d_r$ and $d_c$ and thus $\varepsilon$ also vary with this ratio. Figure 10 shows this effect measured with a collimated beam of 6.4 keV

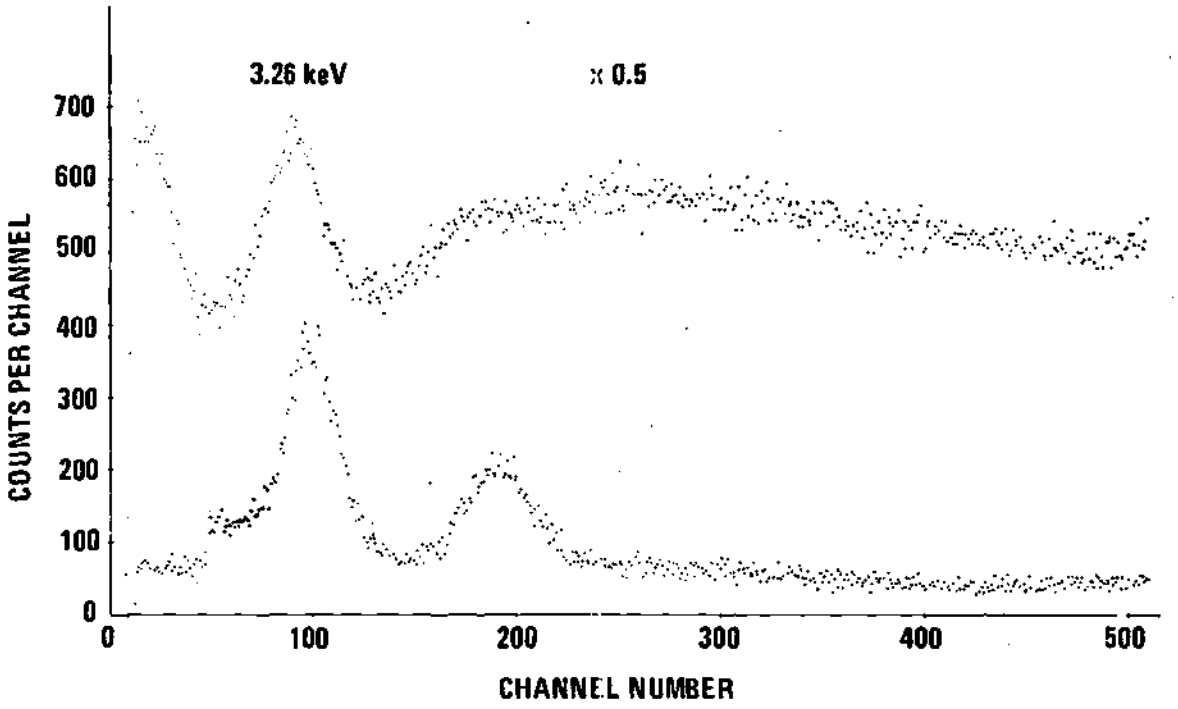


Figure 9. Effect of Anticoincidence Operation on the MWPC Spectrum of Np M X Rays. (Background in the free run spectrum (upper, notice the scale factor) is at least ten times higher than in the anticoincidence spectrum (lower).)

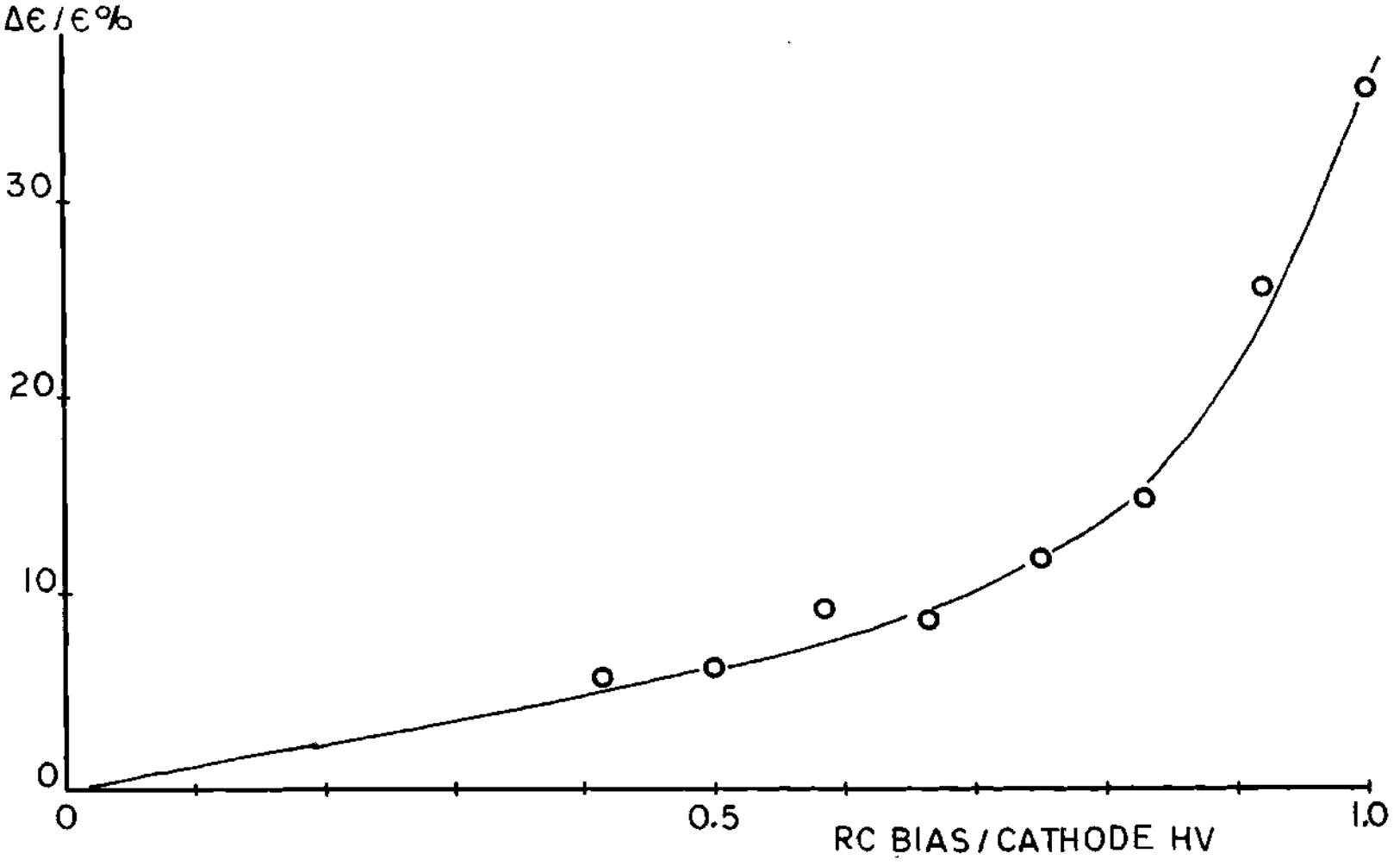


Figure 10. Effect of Ring Counter Bias Voltage on Detection Efficiency of the Center Counter. (Collimated beam of K x rays from a $^{57}$Co source was used. An increase in the efficiency by about 35 percent is seen when the negative bias is increased from zero to the value of the cathode high voltage.)

x rays from $^{57}Co$. Obviously, when both counters have the same high voltage, the field lines are bulged into the geometrical center counter volume due to higher field gradient in the smaller ring counter, thus reducing the center counter efficiency. With increasing ring counter bias, the field lines shift towards the geometrical boundary and result in a sizeable increase in the efficiency. Care was taken in the following measurements to maintain the high voltage to bias ratio constant, in order to avoid complications due to this effect.

The efficiency versus gas pressure curves measured without ring counter bias for a collimated beam of 5.5 keV and 6.5 keV x rays from $^{54}Mn$ and $^{57}Co$, respectively, and with 90 percent Ar + 10 percent $CH_4$ (P-10) filling gas, are shown in Figure 11 in comparison with the theoretical curves (eq. 17). Geometrical dimensions were used in calculation and the photoelectric cross sections were taken from Veigele et al. (49). The measurements were made with IAEA standard sources and the values (0.251 ± 0.002) and (0.558 ± 0.0067) K x-ray emissions per decay were used for conversion from counting rates to efficiencies for $^{54}Mn$ and $^{57}Co$, respectively. These numbers are obtained from well known values of $P_K\omega_K$ (5) ($P_K$ is the K-capture probability) and from conversion data listed by Freund and McGeorge (50). Corrections were made for absorption in the source disk, air, and beryllium window.* The calculated efficiencies (Figure 11) are

*The K x-ray intensity measurement with the IAEA standard $^{54}Mn$ showed nine percent more absorption on one side of the source disk than on the other. The absorption correction was determined experimentally by comparing the K x-ray and 835 keV gamma intensities from the IAEA source and from an open source. The absorption was eight percent higher than expected theoretically and measured for identical disks. Similar, but minor problems were met with the $^{57}Co$ source and one must conclude that the IAEA standards must be used as low energy x-ray standards only with great care.

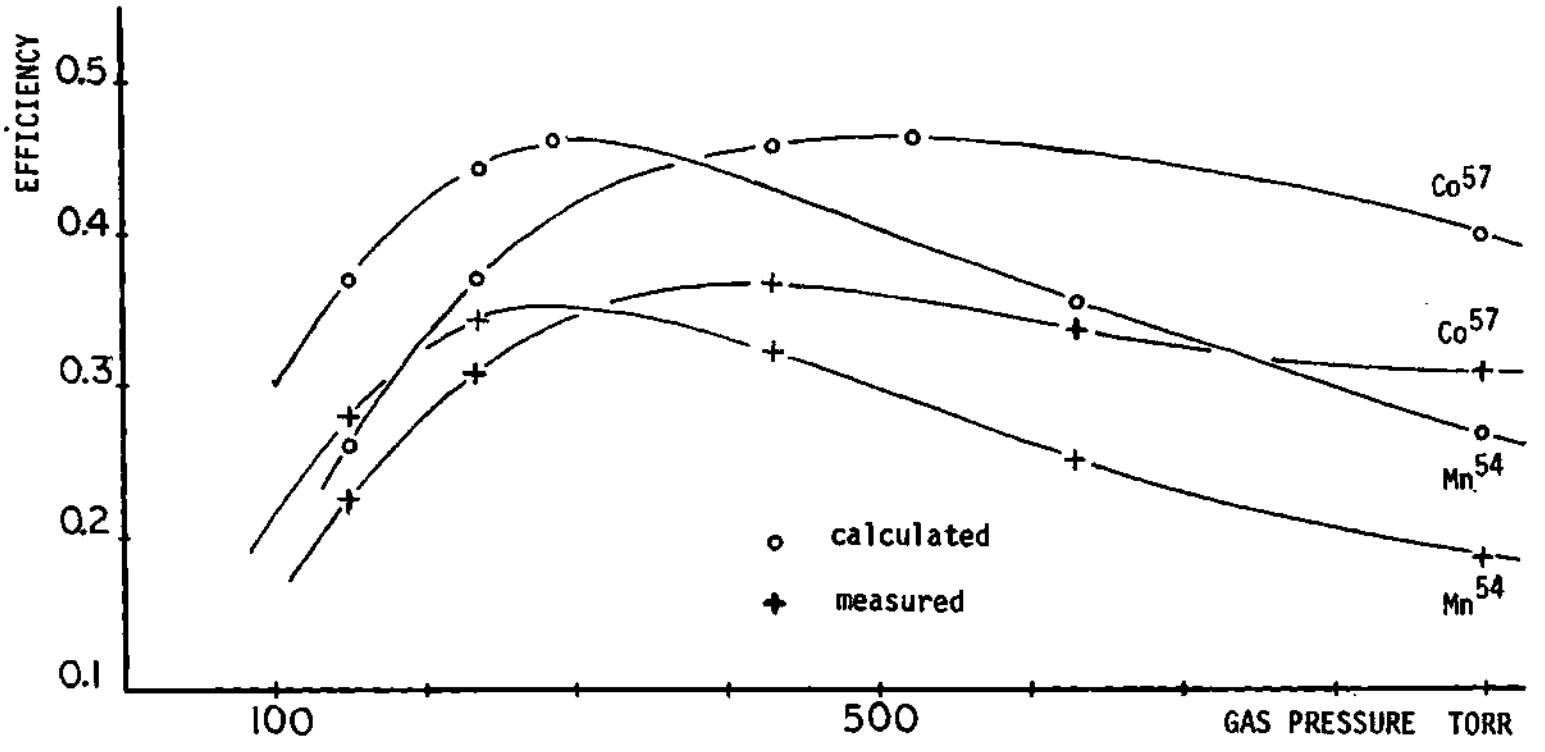


Figure 11. Calculated and Measured Efficiency Curves for Collimated Beams of K X Rays from External $^{57}Co$ and $^{54}Mn$ Sources with Argon (90 percent) Methane (10 percent) Filling Gas. (No ring-counter bias was applied. Large discrepancy between experiment and calculation is explained by reduced center counter diameter.)

about 30 percent higher than was measured. According to Figure 10, agreement could be obtained with a negative bias on the ring counter anode wires of about 95 percent of the cathode high voltage. At this value, which also is approximately predicted from the dimensions, the effective boundary seems to coincide with the geometrical boundary between the counters. On the other hand, if the theoretical calculation is performed by using effective dimensions of $d_c$ = 5.3 cm and $d_r$ = 1.29 cm, good agreement with the measurement is obtained. Thus, it appears that the effective sensitive dimaeter of the center counter was smaller than the geometrical diameter for this particular beam direction by 16 percent, when no bias was applied to the ring counter. The experimental curves, when plotted as a function of linear absorption coefficient, overlap within ± 3 percent at every point,* proving the consistency of the results.

For efficiency studies with an internal source, a carrier-free $^{57}Co$ source was made on an aluminized Mylar foil by drop evaporation, followed by Krylon spraying. The efficiencies were again measured in the MWPC at several different pressures of P-10 gas and the results are shown in Figure 12. The theoretical curve was calculated from the following equation

$$\int_{\Omega} \exp(-\mu x)\,[1 - \exp(-\mu y)]\,d\Omega \qquad (18)$$

where $\Omega$ is the solid angle at which the center counter is seen from the

---

*In all measurements with the MWPC and with a single-wire proportional counter, the maximum efficiency for K x rays from a $^{57}Co$ source seemed to be higher by five to seven percent than for K x rays from a $^{54}Mn$ source. The same phenomenon was later observed in Si(Li) measurements (36) and may indicate that the emission rate of K x rays in decay of $^{57}Co$ is higher than presently believed.

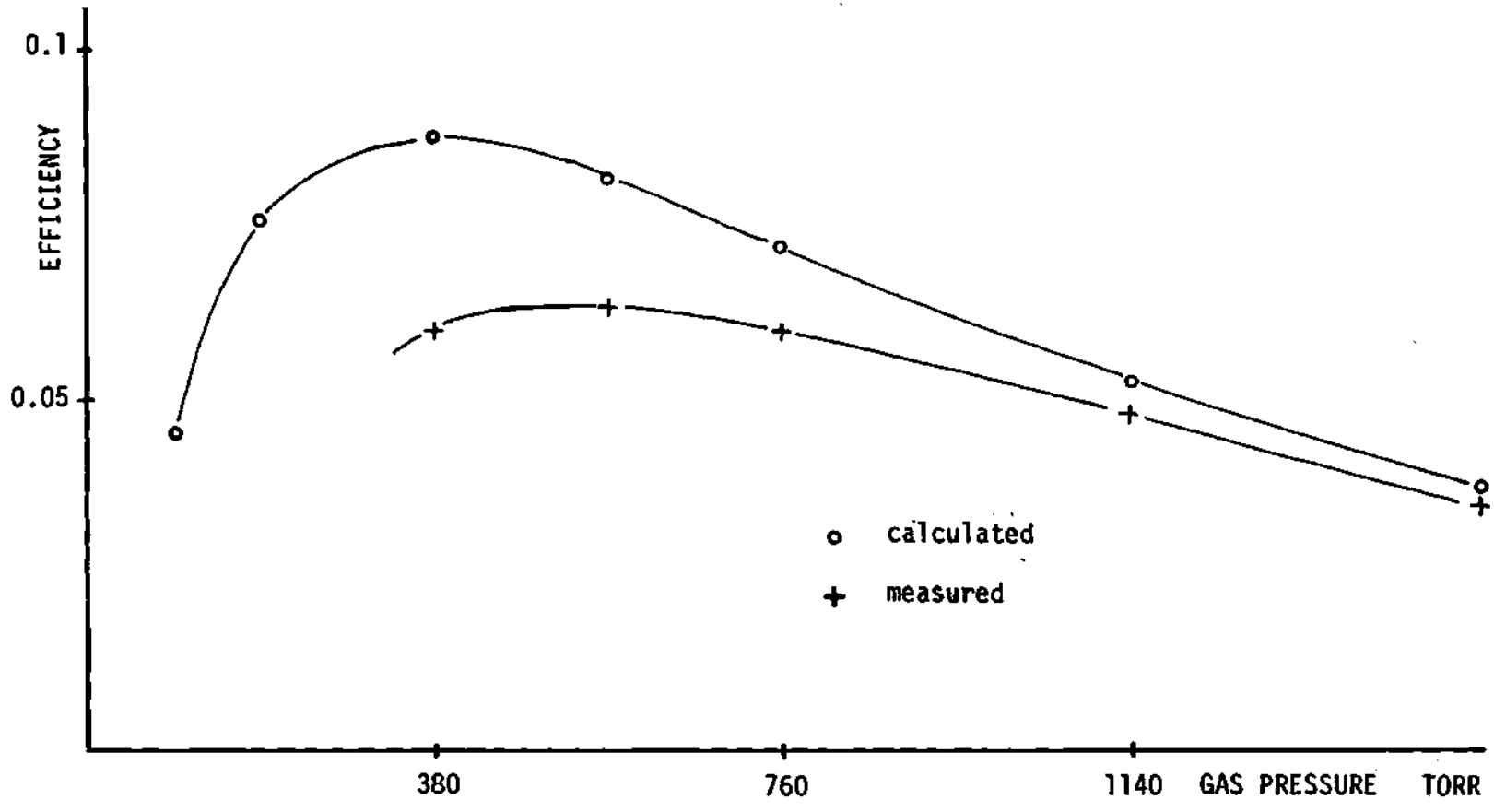


Figure 12. Calculated and Measured Efficiency Curves for K X Rays from an Internal $^{57}Co$ Source with Argon (90 percent) Methane (10 percent) Filling Gas. (No ring-counter bias was applied and a large discrepancy especially at low pressures is observed between experiment and calculation.)

source and x and y are the angular-dependent distances that a beam in direction $d\Omega$ travels in the ring and center counters, respectively. The integral was solved using the Runge-Kutta method (see e.g. 51) programmed into a PDP-8 computer. A large difference, which cannot now be explained with a model of a reduced cylindrical center counter, was observed between experiment and calculation especially at low gas pressures. Finite source thickness which affects results at low pressures when the whole length of the counter is active, may contribute to this behavior.

These comparisons suggest that large errors can be introduced in MWPC measurements with solid sources by use of a calculated efficiency without an accurate knowledge of the effective sensitive volume of the counter that may considerably differ from the geometrical volume. Since the single-wire proportional counter has uniquely defined dimensions, it is preferable for absolute intensity determinations with solid sources, in spite of its higher background. In the present work an experimentally determined efficiency was used for MWPC measurements; a single-wire proportional counter was also used to confirm the efficiency measurements.

As described above, good consistency was achieved in the collimated beam measurements between the $^{54}Mn$ and $^{57}Co$ sources. For this reason, these results were used to deduce the absolute emission rate of M x rays from the $^{241}Am$ source. The M x-ray spectrum was measured with the MWPC, filled with propane to 760 torr, using a collimated beam from an external source. According to information from Ref. (49) the linear absorption coefficient of propane at 760 torr pressure at 3.3 keV (energy of the strongly dominant Np M x-ray peak; see Figure 15) is the same as that of P-10 gas at pressures of 237 torr and 150 torr at the energy of K x rays

from $^{57}Co$ and $^{54}Mn$ sources, respectively. Therefore, an efficiency of 0.296 for Np M x rays in this geometry can be obtained from Figure 10. The emission rate of the M x rays can, however, be obtained independent of the solid angle, from the relationship

$$\frac{C^M(Am)}{I^M(Am)} = \frac{C^K(Co)}{I^K(Co)} = \frac{C^K(Mn)}{I^K(Mn)}$$

where $I^K$ and $I^M$ are the emission rates of K and M x rays from the indicated sources, respectively, and $C^K$ and $C^M$ are the counting rates measured at equivalent pressures for the same $\mu$. The following value of $I^M(Am)$ was obtained as an average of several measurements

$$I^M(Am) = 2.03 \pm 0.20 \quad M \text{ x rays/min}$$

In order to confirm this value, an identical set of measurements was performed with a single-wire proportional counter described by Genz et al. (52). The result was

$$I^M(Am) = 2.28 \pm 0.18 \quad M \text{ x rays/min}$$

Knowing the activity of the $^{241}Am$ source (1.53 $\mu$Ci) from comparison of L x ray and gamma lines with those from the IAEA standard source, the following value for the absolute emission rate of Np M x rays in decay of $^{241}Am$ was obtained as an average of all measurements

$$R = (6.35 \pm 0.60)\ 10^{-2} \text{ M x rays per decay of } ^{241}Am$$

All the efficiency values for M x rays in the coincidence experiments were based on this result, e.g. the 3.3 keV point in Figure 2. From the IAEA L x-ray intensities, the ratio of $M/L_\alpha$ x-ray emission in $^{241}Am$ decay then is

$$\frac{M}{L_\alpha} = 0.470 \pm 0.045$$

which ratio is very valuable for determining detector efficiencies in the region of 3.3 keV.

## 3.5. Determination of the K-Fluorescence Yield of Te from $^{125}I$ Decay

As a preliminary investigation using the coincidence method for fluorescence yield measurements, a precision measurement of the K-shell fluorescence yield of $_{52}Te$ from decay of 60-day $^{125}I$ was performed. The K-shell vacancies are created by K capture to the 35.5 keV level of tellurium, and in the internal conversion of the 35.5 keV gamma. Since the K-capture probability $P_K$ is accurately known, the selection of K-shell vacancies due to capture, by gating on the gamma peak, gives an accurate determination of $\omega_K$. The number of K-shell vacancies due to K capture is given by the product $P_K\omega_K$, and application of eq. (2) gives

$$\omega_K = \frac{1}{P_K \epsilon_K} \frac{C_{K(\gamma)}}{C_\gamma} \tag{19}$$

The number of K x-ray - K x-ray coincidences is related to the total number of K-shell vacancies per decay, created both by K capture and K conversion, and therefore depends on the K-conversion coefficient

$\alpha_K$. It can be shown that, by combining the results from gamma-gated and K x-ray-gated measurements, $\alpha_K$ can be determined from the equation

$$\alpha_K \omega_K = \frac{1}{2} \left( \frac{\epsilon_\gamma}{\epsilon_K} \right) \frac{C_{K(K)}}{C_{\gamma(K)}} \tag{20}$$

Furthermore, analysis of the K x-ray and gamma intensities in a singles spectrum, combined with the knowledge of $\omega_K$ and $\alpha_K$ from the coincidence experiments, gives the total conversion coefficient $\alpha_T$ for the 35.5 keV transition. The results obtained from these measurements are given in Table 2. They are in agreement with previous measurements but are considerably more accurate. The details of the experiments have been published and are contained in the reprint in Appendix II.

Table 2. Values of $\omega_K$(Te), and $\alpha_K$ and $\alpha_T$ for the 35.5 keV Transition

| | This Work | Previous Result | Reference |
|---|---|---|---|
| $\omega_K$ | 0.859 $\mp$ 0.002 | 0.872 | (53) |
| $\alpha_K$ | 12.01 $\mp$ 0.36 | 11.4 $\mp$ 2.5 | (54) |
| | | 12.0 | Theor. pure M1 (55) |
| $\alpha_T$ | 13.65 $\mp$ 0.55 | | |

## 3.6. Determination of Some M-Subshell Quantities and the Radiative $L_1$-$L_3$ CK Yield at Z=93 and Z=96 from Decays of $^{241}Am$ and $^{249}Cf$

### 3.6.1. MWPC-Ge(Li) Coincidence Measurement of Neptunium L X Rays Gated with M X Rays

The logical procedure in the application of the coincidence method for measurement of mean M-subshell fluorescence yields would be to signal the creation of an $M_i$-subshell vacancy by gating on an $L_j$-$M_i$ x-ray line and to measure the spectrum of coincident M x rays emitted. This procedure was employed in the Ge(Li)-Si(Li) coincidence experiments discussed below. When the MWPC was used for M x-ray detection, however, the procedure was reversed, and the gating was done on the M x rays. This approach allows one to take better advantage of the resolving power of the semiconductor without appreciable loss of M-spectral information, because the latter remains unresolved by the MWPC. For this procedure eq. (13) must be modified to give

$$\nu_i^M = \frac{1}{\bar{\varepsilon}_M(1+m_j^X)} \frac{C_{L_jM_i}(M)}{C_{L_jM_i}} \qquad (21)$$

The counting rates of the $L_j$-$M_i$ x rays must, therefore, be determined both in singles ("free run") ($C_{L_jM_i}$) and in coincidence [$C_{L_jM_i}(M)$] modes.

Four groups of neptunium L x rays are cleanly separated in the Ge(Li) spectrum as shown in Figure 13: $L_\ell(L_3$-$M_1)$, $L_\alpha(L_3$-$M_{4,5})$, $L_\beta$, and $L_\gamma$. The $L_\gamma$ group is composed of transitions L-N,O... only while the $L_\beta$ group contains most of the L-M lines. These lines, with the exception of the strong $L_2$-$M_4$, have a comparable low intensity and strongly overlap (see Table 3). Hence, their use for gating is not feasible. However, it is

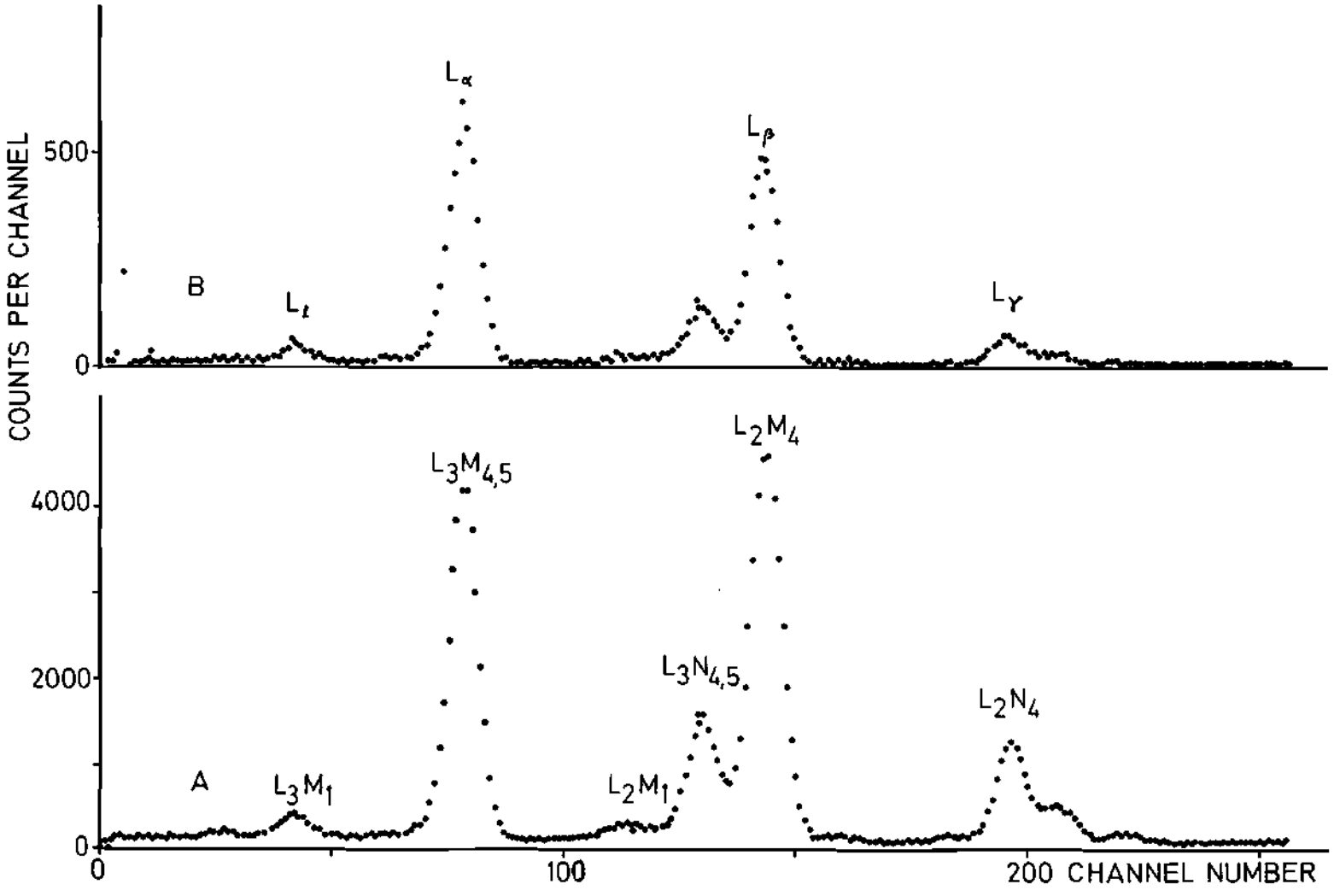


Figure 13. A Free Run (A) and an M X-Ray-Gated Coincidence Spectrum (B) of Np L X Rays.

possible to strip the complex L x-ray spectra by Gaussian fitting and thus obtain information on the nonresolved line intensities. This is the advantage of the M x-ray gating procedure.

A 0.451 μCi $^{241}Am$ source was mounted inside the window of the MWPC for coincidence measurements. Figure 14 shows the gate spectrum and the positioning of the gates. The first gate is set on the M x-ray peak, covering approximately the energy region from 2.2 to 4.4 keV. In order to determine the coincidence rate resulting from degraded high-energy pulses in the background within the M x-ray gate, another gate was set on the pure continuum from 5.6 to 8.5 keV. The shape of the continuum under the M x-ray peak was measured by absorbing the M x rays with 10 mg/cm$^2$ of aluminum which gives an attenuation of $3 \times 10^{-3}$.

The count ratio of the continuum contained in the M x-ray gate ($B_1$) to that in the pure continuum gate ($B_2$) was found to be

$$\frac{B_1}{B_2} = 0.969 \pm 0.030$$

The counting rate of M x rays within the gate ($C_M$) was

$$C_M = (943.0 \pm 5.0) \text{ cpm}$$

which together with the M x-ray emission rate of the source

$$I_M = (6.50 \pm 0.6) \times 10^4 \text{ M x rays/min}$$

gives the detection efficiency

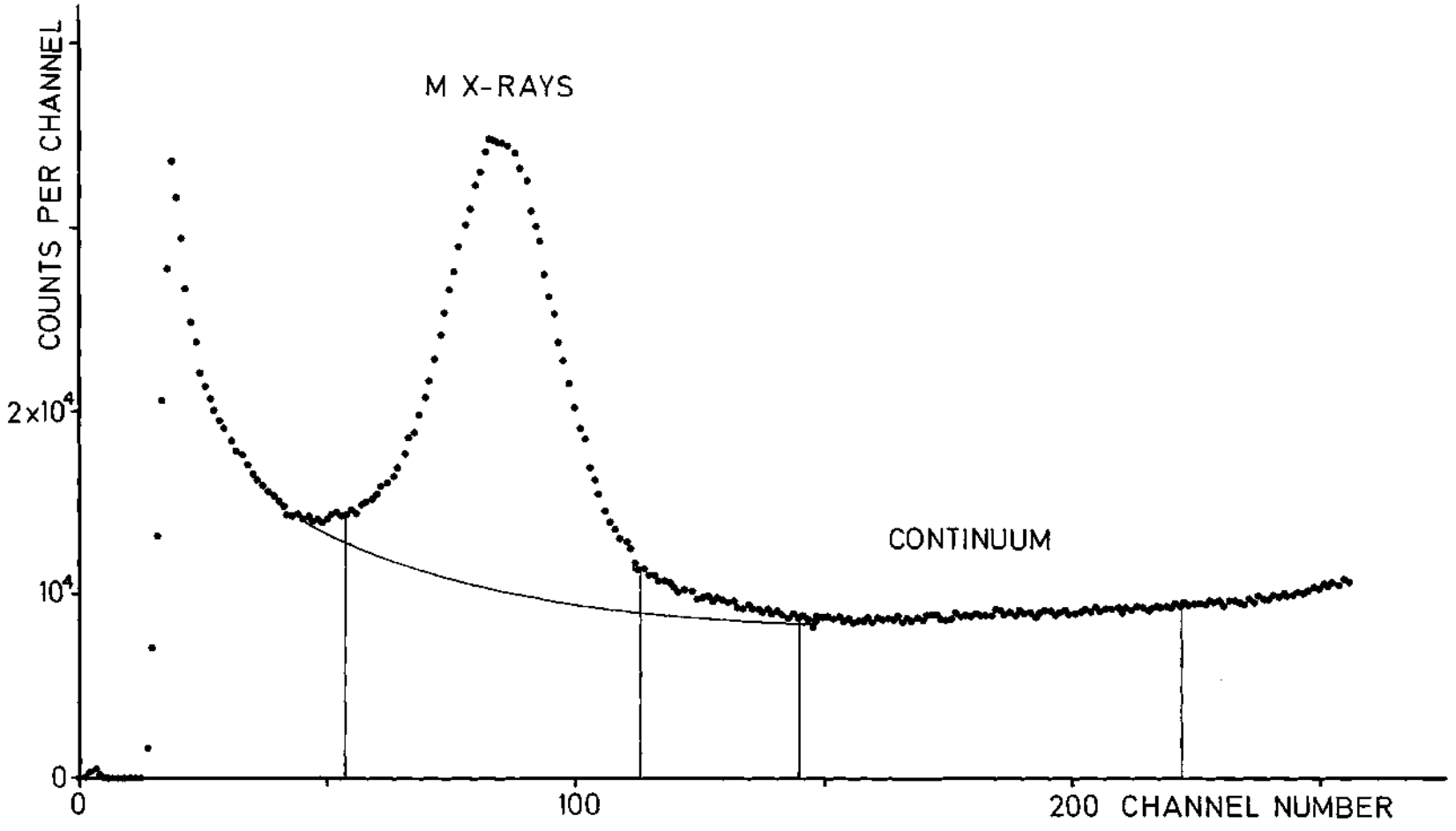


Figure 14. Gate Settings in the MWPC-Gated Measurements of M-L X-Ray Coincidences with a $^{241}Am$ Source. (Energy of the M X-Ray Peak is 3.3 keV. The Solid Line gives the Continuum Level.)

$$\bar{\epsilon}_M = (1.45 \pm 0.14) \times 10^{-2}$$

The gate counting rates were checked daily from the output of the TC 445 timing SCA's by operating them temporarily in "internal strobe" mode. The rates were constant within two percent. There was no shift in the peak position and no detectable deterioration in the resolution of the MWPC during the period of the measurements (about two weeks). The same gas filling, 685 torr of propane, was therefore used in all runs.

Figure 13 shows the M x-ray gated coincidence spectrum, together with a singles L x-ray spectrum, measured with the Ge(Li) detector. The continuum-gated spectrum was found to be a chance spectrum with only about 10 percent of true coincidences. The $L_\ell$, $L_\alpha$-, $L_\beta$-, and $L_\gamma$-group count rates were determined by computer integration following subtraction of the continuum under identical conditions from the M x-ray gated and the L x-ray singles spectra. The complex L x-ray groups were then analyzed for the relative intensities of individual lines with a Du Pont Model 310 curve-resolving analog computer, taking advantage of the good knowledge of transition energies available (38,56). The line shape for fitting was taken from the $L_\ell$ single line, and the line width was adjusted separately for the analysis of the $L_\beta$ and $L_\gamma$ groups. The width of the $L_3$-$M_5$ line, as deduced from the slope of the high-energy side of the $L_\alpha$ peak, was used in analysis of the $L_\beta$ group. Similarly, the slope of the low-energy side of the $L_2$-$N_4$ x-ray line was used to adjust the line width for analysis of the $L_\gamma$ group. These slopes are regarded as rather undisturbed single-line slopes in their respective energy regions. Because the width is somewhat energy-dependent, it is difficult to determine the lowest intensities from

complex groups with high accuracy. Furthermore, it is difficult to estimate the accuracy achieved in the procedure. Therefore, the stripping was repeated three times, each time with independently-adjusted line widths. The average values are given in Table 3 for the singles spectrum and in the "gross counting rate" column of Table 4 for the M x-ray gated coincidence spectrum. The precision, as deduced from the reproducibility, is about 2.5 percent for $L_2$-$M_4$, five percent for $L_2$-$N_4$, and from seven to 100 percent for the other lines depending on their strength compared to the neighboring lines. Relative intensities were normalized to the total group counting rates.

For comparison, the counting rates in a singles spectrum, calculated on the basis of the vacancy distribution and the fluorescence yields given in Appendix I and using theoretical radiative transition probabilities (10), are also given in Table 3, after normalizing to the total counting rate measured for the $L_\alpha$ group. Although the group counting rates are in reasonable agreement, it is observed that the calculated $L_2$ x-ray lines tend to be too strong and the $L_1$ x-ray lines, too weak. This may indicate an error in selection of the value for $\omega_1$ and/or $\omega_2$, or in the conversion coefficients used to calculate the vacancy distribution. This error might be responsible for the discrepancy found between the calculated and experimental correction for the effect of nuclear cascading on coincidence rates, as is observed below.

The counting rates of single lines, obtained from the M x-ray-gated spectrum, were corrected for chance coincidences and for coincidences arising from the continuum (gate correction) as shown in Table 4. From the net counting rate $C'_{L_jM_i}(M)$ and from the calculated vacancy multiplica-

Table 3. A Curve Resolver Analysis of the Ge(Li) Singles Spectrum of Np L X Rays from Decay of $^{241}Am$, and a Comparison with Calculated[a]. Line Intensities

| X Ray $L_i$-$X_j$ | Group Name | Energy keV | $C_{L_iX_j}$ Calc. counts/min | $C_{L_iX_j}$ Meas. counts/min |
|---|---|---|---|---|
| $L_3$-$M_1$ | $L_\ell$ | 11.89 | 46.5 | 41.8 ± 0.5 |
| $L_3$-$M_{4,5}$ | $L_\alpha$ | 13.9 | 735[b] | 735.3 ± 1.0 |
| $L_2$-$M_1$ | | 15.88 | 25.6 | 28.4 |
| $L_3$-$N_1$ | | 16.11 | 12.0 | 14.4 |
| $L_3$-$N_{4,5}$ | $L_\beta$ | 16.8 | 157 | 201 |
| $L_1$-$M_2$ | | 17.05 | 60 | 130 |
| $L_3$-$O_{4,5}$ | | 17.5 | 29.4 | 35.8 |
| $L_2$-$M_4$ | | 17.75 | 905 | 787 |
| $L_1$-$M_{4,5}$ | | 18.7 | 7.7 | 13.1 |
| $L_2$-$N_1$ | | 20.10 | 7.0 | 10.2 |
| $L_2$-$N_4$ | | 20.78 | 206 | 183 |
| $L_1$-$N_2$ | $L_\gamma$ | 21.09 | 16 | 44.4 |
| $L_1$-$N_3$ | | 21.33 | 16 | 27.7 |
| $L_1$-$O_{2,3}$ | | 22.2 | 8.2 | 21.0 |

[a] Ref. (10) and Appendix I.

[b] Normalized to the measured value.

Table 4. Evaluation of Net Coincidence Counting Rates of L X Rays in the MWPC-Ge(Li) Measurements of M-L Coincidences with a $^{241}Am$ Source

| L X Ray | Gross Counting Rate counts/min | Chance Coincidences | Gate Correction | $C'_{L_jM_i}(M)$ [a] | Experimental Nuclear Cascading | $C_{L_jM_i}(M)$ [b] |
|---|---|---|---|---|---|---|
| $L_2$-$N_4$ | 0.2390 ± 0.0120 | 0.0786 ± 0.0012 | 0.0163 ± 0.0033 | 0.1391 ± 0.0125 | | |
| $L_2$-$M_4$ | 1.6810 ± 0.0420 | 0.3241 ± 0.0049 | 0.0369 ± 0.0074 | 1.3200 ± 0.0430 | 0.6042 ± 0.0543 | 0.7158 ± 0.0691 |
| $L_3$-$M_1$ | 0.1229 ± 0.0048 | 0.0172 ± 0.0026 | 0.0017 ± 0.0021 | 0.1040 ± 0.0059 | 0.0320 ± 0.0029 | 0.0720 ± 0.0065 |
| $L_3$-$M_{4,5}$ | 1.9809 ± 0.0113 | 0.3028 ± 0.0055 | 0.0429 ± 0.0185 | 1.6352 ± 0.0222 | 0.5648 ± 0.0507 | 1.0704 ± 0.0555 |
| $L_1$-$M_2$ | 0.3075 ± 0.0215 | 0.0537 ± 0.0008 | | 0.2510 ± 0.0218 | 0.1000 ± 0.0090 | 0.1510 ± 0.0236 |
| $L_2$-$M_1$ | 0.0574 ± 0.0057 | 0.0117 ± 0.0018 | 0.0010 ± 0.0010 | 0.0447 ± 0.0061 | 0.0218 ± 0.0020 | 0.0229 ± 0.0066 |

[a] Net rate without nuclear cascading correction.

[b] Net rate with experimental nuclear cascading correction.

tion correction (Table 23 in Appendix I) the following values are obtained for the mean M-subshell fluorescence yields of neptunium (Z=93)

$$\nu_1^M = \frac{1}{\bar{\epsilon}_M(1+m_3)} \frac{C'_{L_3M_1}(M)}{C_{L_3M_1}} = 0.089 \pm 0.016 \qquad \text{(from } L_\ell \text{ peak)}$$

$$\nu_1^M = \frac{1}{\bar{\epsilon}_M(1+m_2)} \frac{C'_{L_2M_1}(M)}{C_{L_2M_1}} = 0.077 \pm 0.030 \qquad \text{(from } L_2\text{-}M_1 \text{ peak)}$$

$$\nu_2^M = \frac{1}{\bar{\epsilon}_M(1+m_1)} \frac{C'_{L_1M_2}(M)}{C_{L_1M_2}} = 0.095 \pm 0.027$$

$$\nu_4^M = \frac{1}{\bar{\epsilon}_M(1+m_2)} \frac{C'_{L_2M_4}(M)}{C_{L_2M_4}} = 0.080 \pm 0.009$$

$$\nu_{4,5}^M = \frac{1}{\bar{\epsilon}_M(1+m_3)} \frac{C'_{L_3M_{4,5}}(M)}{C_{L_3M_{4,5}}} = 0.080 \pm 0.011 \ ^*$$

The M x rays in coincidence with $L_2$-$N_4$ x rays arise from multiple ionization due to nuclear cascades. Therefore, the coincidence rate measured with $L_2$-$N_4$ x-ray gating is a measure of the strength of this effect and gives an experimental correction for the number of M-shell vacancies in coincidence with $L_2$ x rays. The same correction for the $L_1$ and $L_3$ x rays is obtained by adjusting the $L_2$-$N_4$ x-ray-gated coincidence rate (per gate pulse) with the difference expected from calculation; i.e. by multiplying by the ratio $m_{n1}/m_{n2}$ or $m_{n3}/m_{n2}$, respectively. This experimental nuclear

---

$^*\nu_{4,5}^M = 0.89\ \omega_5^M + 0.11\ (\omega_4^M + f_{45}^M \cdot \omega_5^M) \approx \omega_5^M$

cascading correction is given in Table 4, as well as the corrected coincidence rate $C_{L_jM_i}(M)$. The following values for the mean M-subshell fluorescence yields of neptunium are obtained with experimental correction for nuclear cascading

$$\nu_1^M = \frac{1}{\bar{\epsilon}_M(1+m_{e3})} \frac{C_{L_3M_1}(M)}{C_{L_3M_1}} = 0.082 \pm 0.018 \qquad \text{(from } L_\ell \text{ peak)}$$

$$\nu_1^M = \frac{1}{\bar{\epsilon}_M} \frac{C_{L_2M_1}(M)}{C_{L_2M_1}} = 0.056 \pm 0.034 \qquad \text{(from } L_2\text{-}M_1 \text{ peak)}$$

$$\nu_2^M = \frac{1}{\bar{\epsilon}_M} \frac{C_{L_1M_2}(M)}{C_{L_1M_2}} = 0.080 \pm 0.029$$

$$\nu_4^M = \frac{1}{\bar{\epsilon}_M} \frac{C_{L_2M_4}(M)}{C_{L_2M_4}} = 0.063 \pm 0.012$$

$$\nu_{4,5}^M = \frac{1}{\bar{\epsilon}_M(1+m_{e3})} \frac{C_{L_3M_{4,5}}(M)}{C_{L_3M_{4,5}}} = 0.069 \pm 0.012$$

It is observed that the calculated nuclear cascading correction is smaller than the measured one. The results, however, agree within the error limits. These indicated error limits are obtained from the uncertainties of the count rates and of the vacancy multiplication factors by taking the square root of the sum of the squared relative errors and by multiplying this by two. This corresponds to the statistical criterion of twice the standard deviation ($2\sigma$). The possible systematic error ($\leq$ 9 percent) in the value of the efficiency is not included in the error.

### 3.6.2. Ge(Li)-Si(Li) Coincidence Measurements of Neptunium M X Rays Gated with L X Rays

A high resolution singles spectrum of the neptunium M x-ray region is shown in Figure 15 with the energies of allowed transitions (38,56) marked. This spectrum was taken with a six millimeter diameter by three millimeter deep Kevex Si(Li) x-ray spectrometer having a resolution of 180 eV FWHM at 6.4 keV. The most intense peak is composed mainly of transitions filling the $M_{4,5}$ subshells. All of the x rays which arise from $M_{1,2}$-subshell fillings are outside of this peak on the high-energy side, with the exception of the $M_2$-$N_1$ line. On the other hand, the $M_3$-O,P... group and the line identified as the radiative $L_1$-$L_3$ transition on the basis of the transition energy which accurately corresponds the difference in binding energy between the $L_1$ and $L_3$ subshells, contain the only x rays in this higher-energy region (from four to six keV) that do not belong to $M_{1,2}$ fillings. This gives an opportunity to observe, in a coincidence experiment, the direct radiative filling of the two lowest M subshells and thus to estimate the quantity $\omega_1^M + f_{12}^M \omega_2^M$ and the magnitude of the CK process from $M_{1,2}$ to $M_{3,4,5}$ subshells.

The gates in the Ge(Li)-Si(Li) coincidence experiments with a $^{241}Am$ source were set as shown in Figure 16. The only single line available for gating, $L_\ell$ ($L_3$-$M_1$), is unfortunately of rather low intensity as compared to the continuum, which is composed of degraded high-energy pulses from gamma rays and L x rays. In order to be able to correct for the coincidence rate due to this continuum within the $L_\ell$ gate, another gate was set on the flat spectral region between the germanium $K_\alpha$ x-ray energy

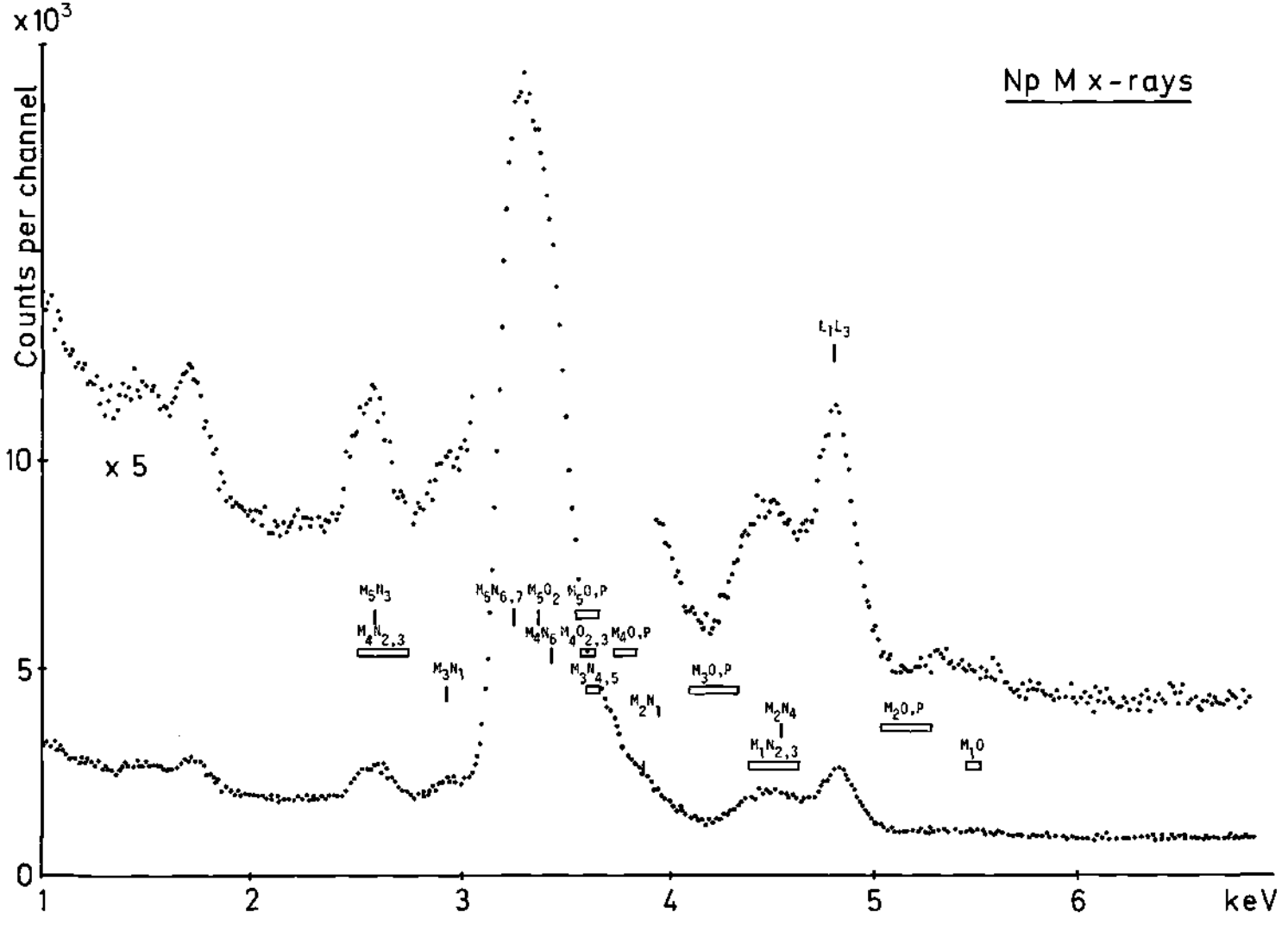


Figure 15. A Singles Spectrum of Np M X-Ray Region Measured with a Si(Li) Spectrometer (180 eV FWHM at 6.4 keV). (Separation of the $M_{1,2}$ X-Rays from the Main Peak is Observed, as well as the Radiative $L_1$-$L_3$ Transition).

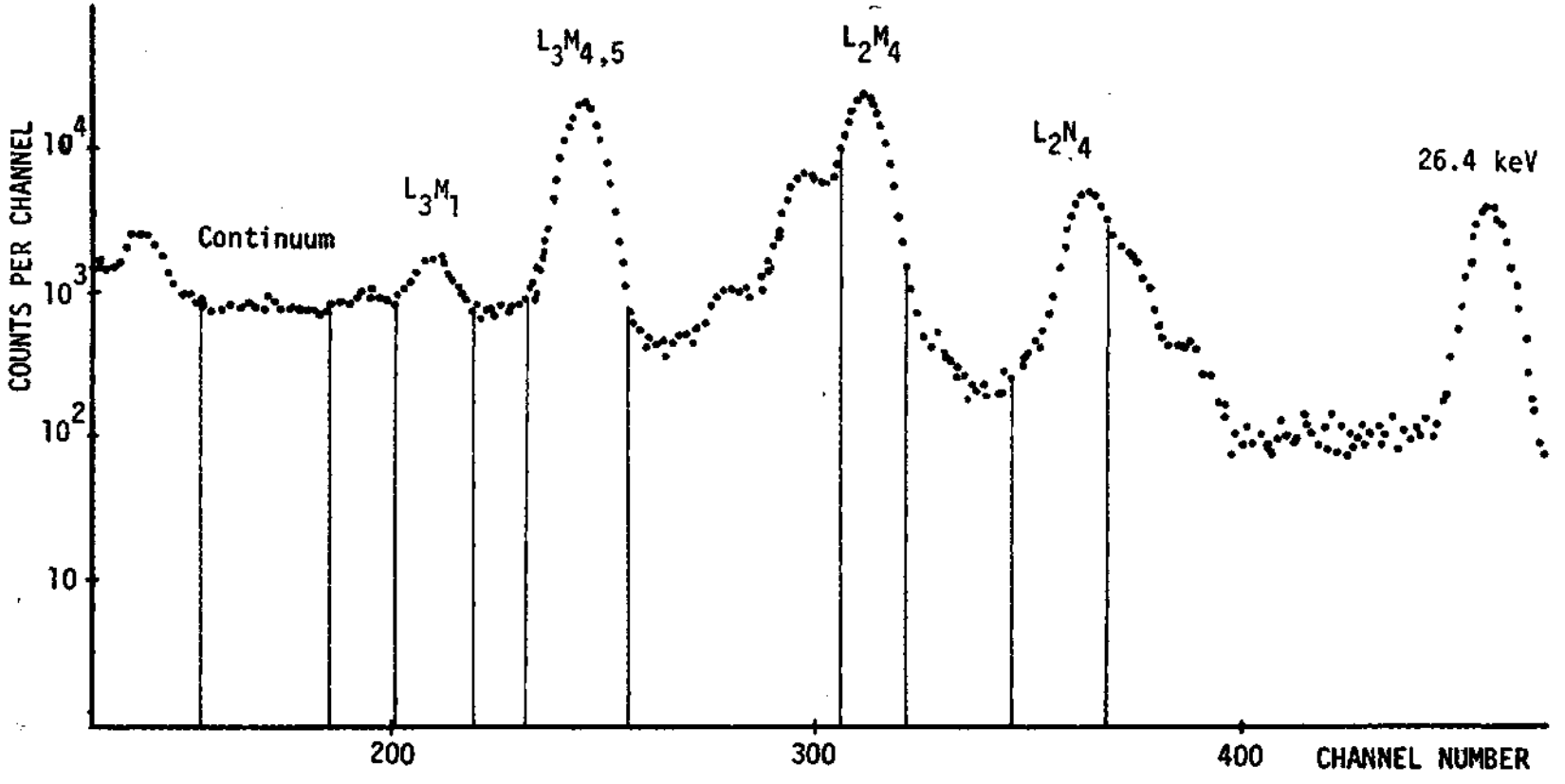


Figure 16. Gate Settings in the Ge(Li)-Gated Measurements of L-M X-Ray Coincidences with $^{241}Am$ Source.

(9.9 keV) and the $L_\ell$ gate. The contribution of degraded $L_\ell$ pulses in this gate is small (< 2 percent), and the coincidence rate gives a good correction, assuming that the composition of the continuum in both gates is otherwise the same. Unfortunately, the Compton edge of the 59.5 keV gamma at 11.2 keV falls into the continuum gate, giving rise to a possible slight difference in the continuum in the two gates. Because no sign of the Compton edge was actually observed in the spectrum, this difference appears to be negligible.

The $L_\alpha$ gate contains, in addition to the $L_3$-$M_{4,5}$ lines, a contribution from the continuum of five percent. In this continuum, the contribution arising from degraded gamma pulses (together with the small natural background) from $L_\ell$ x rays and from $L_\beta$ x rays must be estimated, because they all have coincident M x rays with different probabilities; i.e. gamma, and $L_\gamma$ pulses due to nuclear cascading and $L_\beta$ pulses due to L-M x rays in this group. The gamma contribution was determined by extrapolation from the channels above the x-ray region, and other contributions were determined using the assumption that the amount of degraded pulses per channel is proportional to the intensity of the full-energy peak and inversely proportional to its channel number. Because of the strength of the $L_\alpha$ line, the final results are insensitive to this assumption.

A third gate was set on the $L_2$-$M_4$ line which dominates the $L_\beta$ x-ray group. In addition to the continuum fraction, this gate partially contains the small unresolved $L_1$-$M_3$ and $L_3O_{4,5}$ lines. These contributions, five and four percent, respectively, were deduced from curve-resolver analysis of the $L_\beta$ group. The $L_1$-$M_3$ pulses were, however, accepted as good gate pulses, since their coincidence rate can not be separately

measured. Since this $L_1$-$M_3$ fraction is small compared to the true $L_2$-$M_4$ contribution in the gate and since the M x-ray coincidence rates per gate pulse of either type are not very different (as can be seen from the MWPC gated experiment), the error introduced is negligible.

The purpose of gating on the $L_\gamma$ group is to obtain an experimental correction for the nuclear cascading effect. In order to get a representative correction for the $L_2$ x rays, the gate was set to cover mainly the $L_2$-$N_4$ line. According to a curve-resolver analysis, the $L_1$ x rays do not contribute more than 13 percent to the total $L_\gamma$ pulses in the gate.

In summary, the composition of the five gates, determined as described above, is shown in Table 5.

One chance coincidence run and four separate coincidence runs were performed, each lasting three to four days. For one of the coincidence runs the resolving time was doubled (Section 3.3.). In each run, four spectra were registered simultaneously using four-fold routing (see Figure 7). Three of the gates, continuum, $L_\ell$, and $L_\alpha$ gates, were maintained in all runs but the fourth gate was set on the $L_2$-$M_4$ line in three runs and on the $L_2$-$N_4$ line in the fourth run. Both the energy- and time-gate positions were checked before and after each run by measuring the gate detector spectrum in coincidence with the SCA output pulses. A coincidence efficiency of unity was confirmed in these test measurements.

A set of four coincidence spectra is shown in Figure 17. These spectra, which are representative to the gates indicated, are displaced by shifting the base line in order to ease the comparison. The logarithmic scale, shown only for the lowest spectrum, is common to all spectra. The small difference in the shape of the M x-ray spectrum, regardless of

Table 5. Composition of the Five Coincidence Gates in the Ge(Li)-Si(Li) L-M X-Ray Coincidence Runs with the $^{241}Am$ Source

| Gate | Contribution | Counting Rate counts/min |
|---|---|---|
| Continuum | total | 3,046 ± 15 |
| | $L_3$-$M_1$ | 48 ± 6 |
| | net continuum | 2,998 ± 16 |
| $L_3$-$M_1$ | total | 2,316 ± 11 |
| | continuum | 1,489 ± 32 |
| | net $L_3$-$M_1$ | 827 ± 34 |
| $L_3$-$M_{4,5}$ | total | 15,215 ± 63 |
| | $L_\gamma$ + $\gamma$ | 830 ± 20 |
| | $L_2$-$M_4$ | 672 ± 45 |
| | net $L_3$-$M_{4,5}$ | 13,713 ± 80 |
| $L_2$-$M_4$ | total | 14,004 ± 129 |
| | $L_\gamma$ + $\gamma$ + $L_3$-$O_{4,5}$ | 1,070 ± 45 |
| | net $L_2$-$M_4$ | 12,934 ± 137[a] |
| $L_2$-$N_4$ | total | 4,525 ± 35 |
| | gamma | 348 ± 20 |
| | net $L_2$-$N_4$ | 4,177 ± 40 [b] |

[a] Contains about five percent of $L_1$-$M_3$.

[b] Contains about 13 percent of $L_1$ x rays.

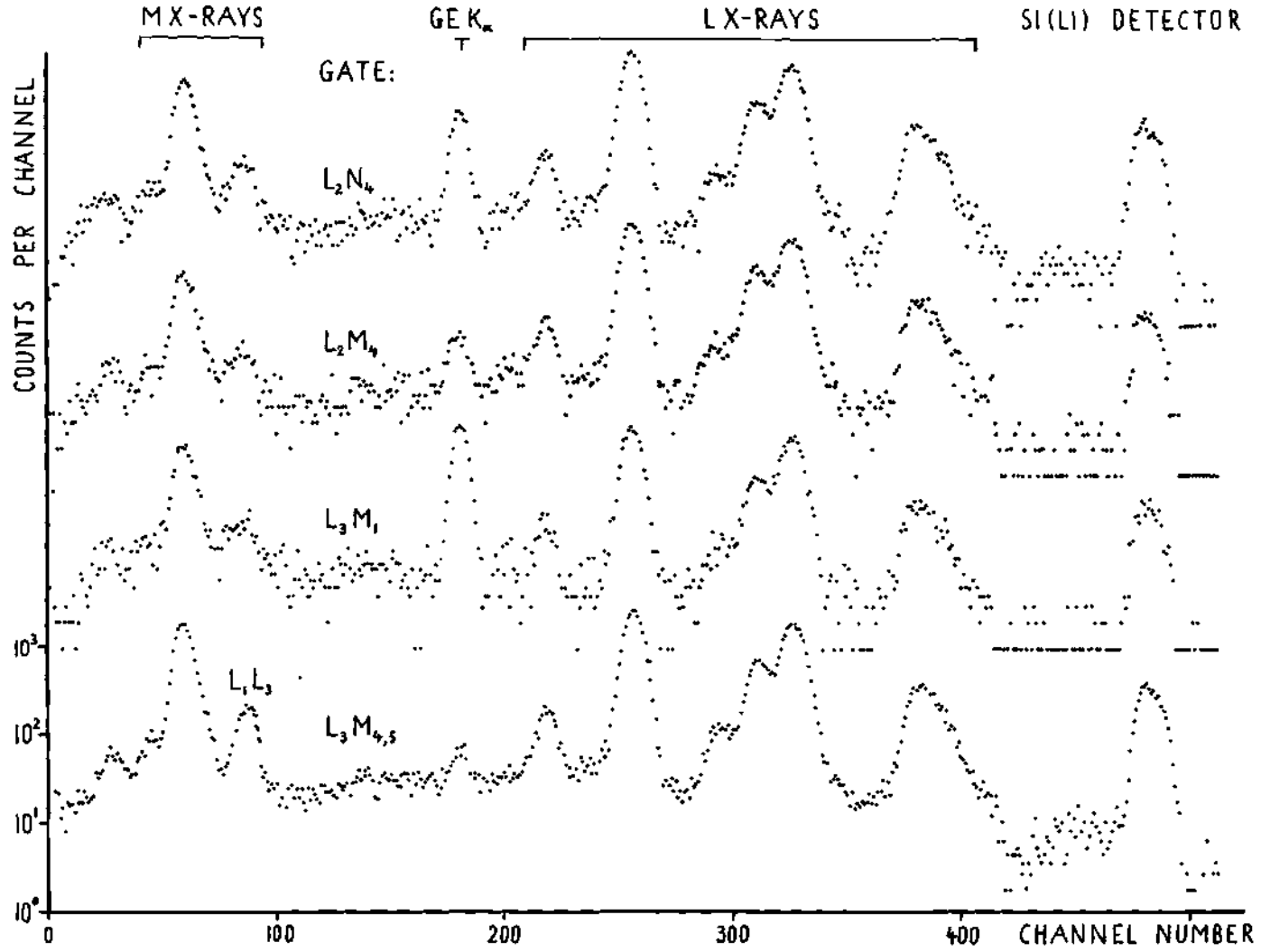


Figure 17. L X-Ray-Gated Coincidence Spectra of Np X Rays. (The Spectra have Different Base Lines. The $L_1$-$L_3$ CK X Ray is in Coincidence with $L_3$ X Rays which Confirms its Identification.)

whether the filling of a vacancy created in the $M_1$- or $M_5$-subshell is followed, indicates the importance of CK transitions in the M shell. The line, identified as an $L_1$-$L_3$ Coster-Kronig x ray in the singles spectrum on the basis of the transition energy, is seen to be in coincidence with the $L_3$ x rays, particularly with the $L_3$-$M_{4,5}$ x rays. This confirms the identification by showing that the line is not due to x rays arising from the filling of $M_{1,2}$-subshell vacancies, which lie in the same energy region.

The M x-ray counting rates, evaluated from the coincidence spectra, must be corrected for chance coincidences and for coincidences due to unwanted contributions in the gates (gate correction). Table 6 gives the evaluation of corrected coincidence rates corresponding to the net $L_2$-$N_4$-, $L_2$-$M_4$-, $L_3$-$M_{4,5}$-, continuum-, and $L_3$-$M_1$-gate counting rates given in Table 5. In the case of the $L_2$-$N_4$ gate, the gate correction arises from degraded gamma pulses alone. In order to determine this correction, the result of the MWPC-gated experiment was used. The coincidence rate in the channels above the $L_\gamma$ group, when corrected for the efficiency difference between the two setups, gives a value for the M(Y) coincidence rate in the Ge(Li)-Si(Li) experiment of

$$C_{M(\gamma)} = (1.5 \pm 0.5)\ 10^{-6}$$

coincidences per gate, which number was used in the evaluation. No correction for the $L_1$ x-ray contribution in the gate was made, because of the small calculated difference in the coincidence rate, compared to the $L_2$-N gate pulses (see Appendix I).

The gate correction for the $L_2$-$M_4$ gated spectra arises from gamma

Table 6. Evaluation of Net Coincidence Counting Rates of M X Rays and $L_1$-$L_3$ Radiative Transitions in the Ge(Li)-Si(Li) Coincidence Measurements with a $^{241}Am$ Source

| Gate | M or $L_1L_3$ | Gross Counting Rate counts/min | Chance Correction | Gate Correction | $C'_{M(Gate)}$ [a] | Experimental Nuclear Cascading Correction | $C_{M(Gate)}$ [b] / $C_{L_1L_3(Gate)}$ |
|---|---|---|---|---|---|---|---|
| $L_2$-$N_4$ | M | 1.626 ± 0.036 | 0.058 ± 0.006 | 0.046 ± 0.005 | 1.522 ± 0.037 | | |
| Continuum | M | 1.561 ± 0.082 | 0.033 ± 0.004 | 0.035 ± 0.004 | 1.493 ± 0.083 | | |
| $L_2$-$M_4$ | M | 11.825 ± 0.272 | 0.168 ± 0.020 | 0.042 ± 0.004 | 11.615 ± 0.273 | 4.550 ± 0.111 | 7.065 ± 0.295 |
| $L_3$-$M_1$ | M | 1.793 ± 0.036 | 0.031 ± 0.004 | 0.735 ± 0.039 | 1.026 ± 0.054 | 0.333 ± 0.008 | 0.693 ± 0.055 |
| $L_3$-$M_{4,5}$ | M | 16.797 ± 0.536 | 0.132 ± 0.015 | 0.294 ± 0.016 | 16.371 ± 0.540 | 4.915 ± 0.121 | 11.456 ± 0.555 |
| $L_3$-$M_{4,5}$ | $L_1L_3$ | 1.529 ± 0.092 | 0.008 ± 0.002 | | | 0.296 ± 0.050 | 1.225 ± 0.105 |

[a] Net rate without nuclear cascading correction.

[b] Net rate with experimental nuclear cascading correction.

and $L_\gamma$ pulses in the gate. The evaluation of the latter contribution was based on the corrected $L_2$-$N_4$ coincidence rate. The $L_\alpha$-gated spectra need an additional correction due to the $L_\beta$ contribution in the gate. This was calculated using the corrected $L_2$-$M_4$ coincidence rate obtained above. No appreciable error is introduced in the final rate by use of this approximation, since the total correction is small and since about 70 percent of the $L_\beta$ tail arises from $L_2$-$M_4$ pulses.

The last two columns in Table 6 give the experimental correction for the nuclear cascading effect and the coincidence rate after this correction has been applied, respectively. The correction was evaluated from the $L_2$-$N_4$-gated coincidence rate in an identical way as in the MWPC-gated case.

The gross coincidences are averages of the values obtained in the separate runs, except the $L_2$-$N_4$-gated rate, which is a result of one measurement. The error limits are one-sigma standard deviations in the rates evaluated for the four (or three) runs, except in the case of the $L_2$-$N_4$-gated and chance rates, where a one-sigma error is derived from the counting statistics.

The efficiency of the coincidence detector for the M x rays was obtained from the counting rate in a singles spectrum and from the absolute emission rate of the M x rays (Section 3.4.) and was

$$\bar{\epsilon}_M = (8.86 \pm 0.80) \times 10^{-3}$$

With this efficiency, with data on counting rates from Tables 5 and 6, and with the calculated vacancy-multiplication factor $(1+m_j)$ from Table 23 of Appendix I, the following mean M-subshell fluorescence yields for

neptunium (Z=93) were obtained:

$$\nu_1^M = 0.072 \pm 0.013$$

$$\nu_2^M = 0.070 \pm 0.011$$

$$\nu_{4,5}^M = 0.070 \pm 0.012$$

The same results, but with the experimental correction for nuclear cascading, are:

$$\nu_1^M = 0.065 \pm 0.014$$

$$\nu_4^M = 0.062 \pm 0.005$$

$$\nu_{4,5}^M = 0.065 \pm 0.012$$

Error limits are the two-sigma standard deviations derived from the uncertainties of the individual factors without inclusion of the possible systematic error of about nine percent in efficiency.

It can again be noticed that the experimental nuclear cascading correction is higher by about 13 percent than the calculated value, although the results agree within the error limits. As explained below (Section 4.1.), the results based on the experimental correction are probably the most reliable.

In order to determine the magnitude of the direct radiative filling of the $M_{1,2}$ subshells, pulses in the channels corresponding to the energy region from 4.2 to 5.7 keV (above the main M peak) were separately

integrated. An assumption is made that the loss of the $M_2$-$N_1$ line outside the integrated region is approximately balanced by the unavoidable inclusion of the $M_3$-O,P group. This assumption is reasonable, because the theoretical transition probability (12) for $M_2$-$N_1$ ($6.96 \times 10^{-3}$ eV/ħ) is essentially equal to the total probability for $M_3$-O,P x-ray emission ($7.04 \times 10^{-3}$ eV/ħ), and the subshell fluorescence yields $\omega_2^M$ and $\omega_3^M$ obviously do not differ radically. Furthermore, due to the high CK yields, the vacancy distribution in the $M_2$ and $M_3$ subshells followed in these coincidence experiments is essentially the same.

The counting rate in the $L_\ell$ gated spectrum was first corrected for the continuum contribution in the normal way with the aid of the continuum-gated spectrum. The remaining rate is partly due to the x rays filling the $M_{1,2}$ subshells and partly due to $L_1$-$L_3$ x rays. The latter contribution was subtracted with the aid of the $L_\alpha$-gated spectrum, where $M_{1,2}$ x rays arise only due to the nuclear cascading. By use of the gross $L_1$-$L_3$ counting rate from Table 6, corrections for chance coincidences and for nuclear cascading are automatically accomplished in this subtraction. Table 7 gives the results of the numerical evaluations.

Table 7. Evaluation of Net Coincidence Counting Rates of $M_{1,2}$ X Rays in the Ge(Li)-Si(Li) Measurements of L-M Coincidence with a $^{241}$Am Source

| Gate | Gross Counting Rate counts/min | Continuum Correction | $L_1$-$L_3$ Correction | $C_{M_{1,2}(L_3M_1)}$ |
|---|---|---|---|---|
| $L_3$-$M_1$ | 0.161 ± 0.010 | 0.052 ± 0.008 | 0.092 ± 0.005 | 0.018 ± 0.014 |

For calculation of the quantity $\omega_1^M + f_{12}^M \omega_2^M$, one must take into account the fact that the detection efficiency for $M_{1,2}$ x rays is higher than the average efficiency for the M x rays. A value

$$\epsilon_{M_{1,2}} = (1.1 \pm 0.1) \times 10^{-2} \text{ at } 4.5 \text{ keV}$$

is obtained from the efficiency curve for the coincidence geometry (similar to that in Figure 2) by interpolation between 3.3 and 5.5 keV points. With this value the following result is obtained

$$\omega_1^M + f_{12}^M \omega_2^M = \frac{1}{\epsilon_{M_{1,2}}} \frac{C_{M_{1,2}}(L_3M_1)}{C_{L_3M_1}} = (2.0 \begin{smallmatrix} + 3.1 \\ - 2.0 \end{smallmatrix}) \times 10^{-3}$$

Application of the two-sigma criterion, therefore, only leaves an upper limit for the quantity, due to poor counting statistics in the $M_{1,2}$ x-ray peak and due to subtraction of the large $L_1$-$L_3$ x-ray contribution.

According to Bhalla (12), the radiative widths of the M subshells are essentially the same ($3.3 \times 10^{-2}$ eV/$\hbar$ for $M_1$ and $2.3 \times 10^{-2}$ eV/$\hbar$ for $M_5$). Assuming that this is true for the Auger widths as well, one can estimate the CK transition probability from the $M_{1,2}$ subshells to the higher subshells. In the $M_5$ subshell, the ratio of $a_5/\omega_5$ is approximately

$$\frac{a_5^M}{\omega_5^M} = \frac{0.94}{0.06} = 15.7$$

where $a_5^M$ is the Auger yield of the $M_5$ subshell. Therefore

$$a_1^M + f_{12}^M a_2^M = 15.7 \times 2.0 \times 10^{-3} = 0.03$$

and

$$\sum_{j=3-5} f_{1,2j}^M = 0.97 \begin{matrix} + 0.03 \\ - 0.05 \end{matrix}$$

This means that 97 percent of the $M_{1,2}$ vacancies shift to higher subshells before the filling from higher major shells occurs and explains the similarity of all the coincidence spectra.

The net counting rate of $L_1$-$L_3$ Coster-Kronig x rays in the $L_\alpha$-gated coincidence spectrum, $C_{L_1L_3(L_3M_{4,5})}$, is also evaluated in Table 6. Since obviously the fraction $N_1(f_{13} + f_{12}f_{23})/V_3$ of the $L_3$ x rays originates from $L_1$-subshell vacancies, one can obtain the radiative component $\omega_{13}$ of the L-shell CK yield $f_{13}$ (eq. 2) from

$$\omega_{13}^L = \frac{1}{\epsilon_{L_1L_3}} \frac{V_3}{N_1(f_{13} + f_{12}f_{23})} \times \frac{C_{L_1L_3(L_3M_{4,5})}}{C_{L_3M_{4,5}}} \qquad (22)$$

which, with the numerical values for vacancies and CK yields as given in Appendix I, gives

$$\omega_{13}^L \text{ (Np)} = 0.030 \pm 0.014$$

A value

$$\epsilon_{L_1L_3} = (1.12 \pm 0.06) \times 10^{-2} \text{ at } 4.81 \text{ keV}$$

was used for the detection efficiency according to the calibration curve. This value is essentially independent of the Np M x-ray point at 3.3 keV

and is as accurate as the nearby $^{54}Mn$ point at 5.5 keV (± 5 percent).

3.6.3. Ge(Li)-Si(Li) Coincidence Measurements of Curium M X Rays Gated with L X Rays

Owing to the higher atomic number, the L and M x-ray spectra of curium (Z=96) are better resolved than the respective spectra of neptunium and some additional structure can be seen, especially in the Si(Li) spectrum of the M x rays, shown in Figure 18. The improvement, however, is not decisive for the present purpose. The procedure in these coincidence experiments for the M-subshell yields of curium was identical to that in the L x-ray gated measurements of the M x rays of neptunium from $^{241}Am$ decay, as discussed above.

A singles spectrum of the L x rays, measured with the Ge(Li) gate detector is shown in Figure 19, with gate positions indicated. The analysis of the gate composition is given in Table 8.

As in the neptunium case, one chance coincidence run and four separate coincidence runs, one with doubled resolving time, were made. However, only three-fold routing could be used at the time of these runs owing to equipment limitations, resulting in fewer measurements with unchanged gates. The $L_\ell$ and continuum gates were maintained in all four runs, while the third gate was set twice on the $L_2$-$N_4$ x-ray peak and once on each of the $L_2$-$M_4$ and $L_\alpha$ x-ray peaks. Each run lasted four to five days. A set of representative coincidence spectra is in Figure 20. The corrections for the coincidence rates were evaluated by accurately following the procedure explained above for the neptunium case, and this evaluation is given in Table 9.

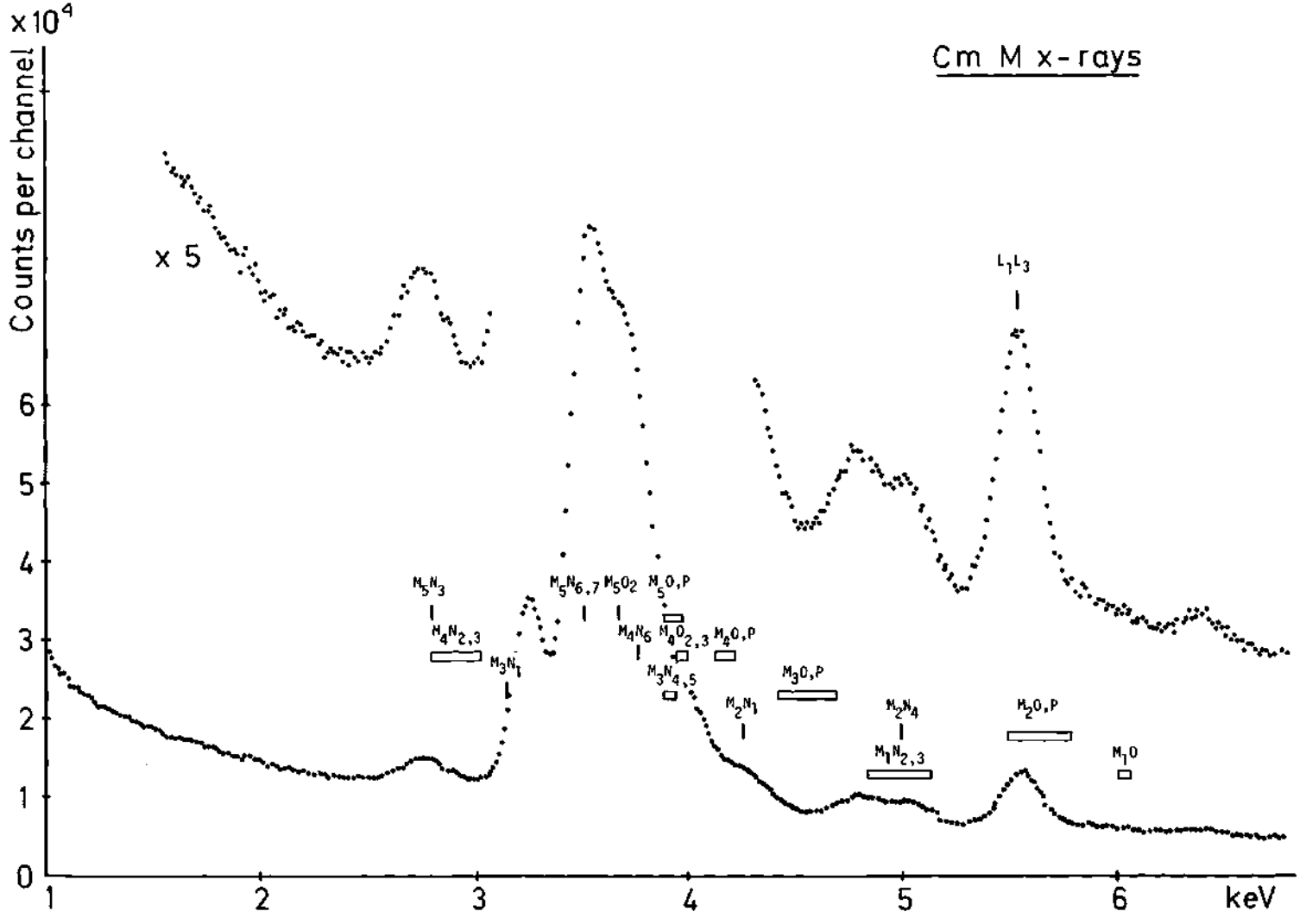


Figure 18. A Singles Spectrum of Cm M X-Ray Region Measured with a Si(Li) Spectrometer (180 eV FWHM at 6.4 keV). (Some additional Structure Compared to Figure 15 is Observed.)

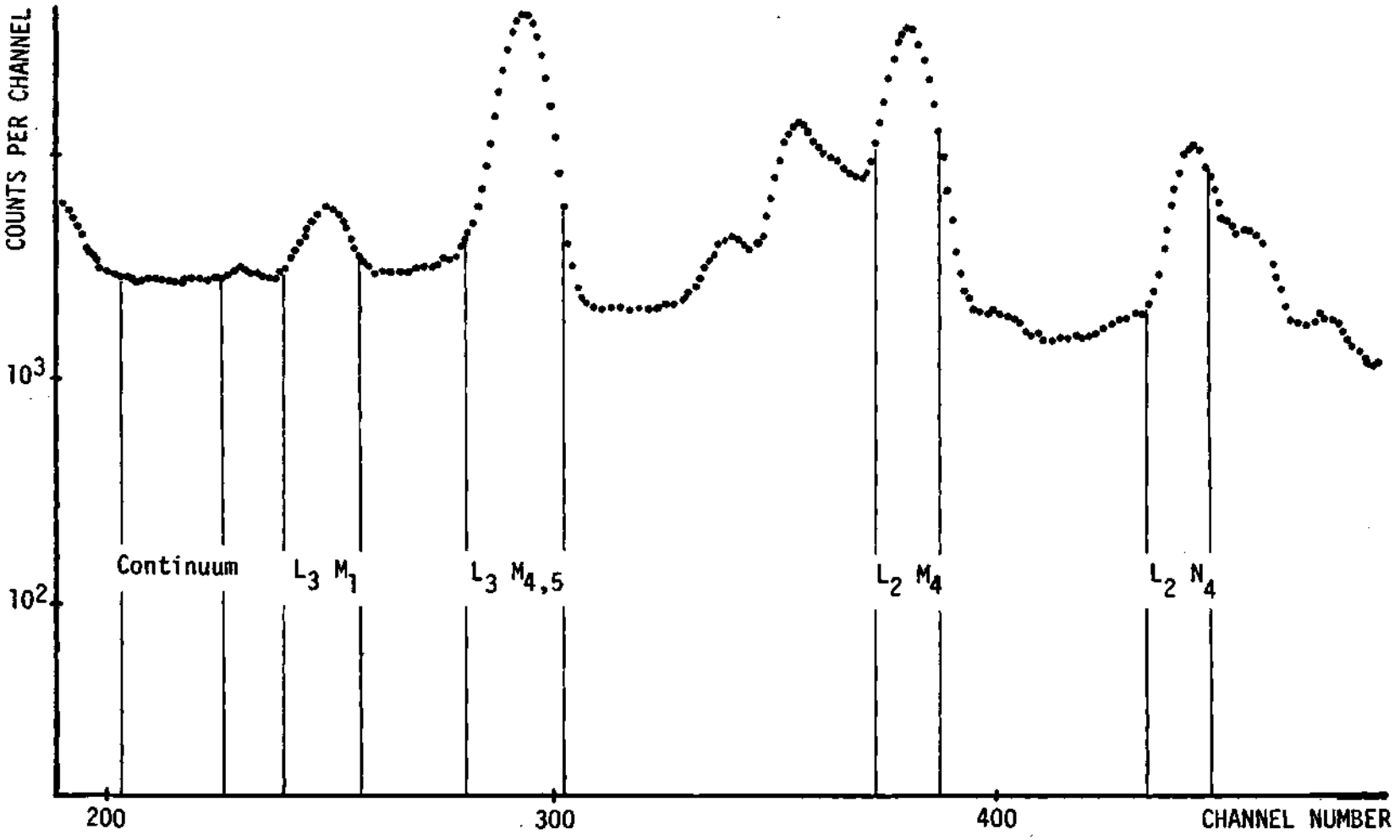


Figure 19. Gate Settings in the Ge(Li)-Gated Measurements of L-M X-Ray Coincidences with $^{249}$Cf Source.

Table 8. Composition of the Five Coincidence Gates in the Ge(Li)-Si(Li) L-M X-Ray Coincidence Measurements with the $^{249}Cf$ Source

| Gate | Contribution | Counting Rate counts/min |
|---|---|---|
| Continuum | total | 3,487 ± 14 |
| | $L_3$-$M_1$ | 81 ± 8 |
| | net continuum | 3,406 ± 16 |
| $L_3$-$M_1$ | total | 4,101 ± 10 |
| | continuum | 2,453 ± 65 |
| | net $L_3$-$M_1$ | 1,708 ± 66 |
| $L_3$-$M_{4,5}$ | total | 29,181 ± 68 |
| | $L_\gamma$ + $\gamma$ + K x ray | 1,743 ± 591 |
| | $L_2$-$M_4$ | 1,198 ± 120 |
| | net $L_3$-$M_{4,5}$ | 26,240 ± 150 |
| $L_2$-$M_4$ | total | 17,649 ± 52 |
| | $L_\gamma$ + $\gamma$ + $L_3$-$O_{4,5}$ | 852 ± 60 |
| | net $L_2$-$M_4$ | 16,797 ± 80 |
| $L_2$-$N_4$ | total | 6,661 ± 34 |
| | $\gamma$ + K x ray | 614 ± 28 |
| | net $L_2$-$N_4$ | 6,047 ± 44[a] |

[a] Contains about 10 percent of $L_1$ x rays.

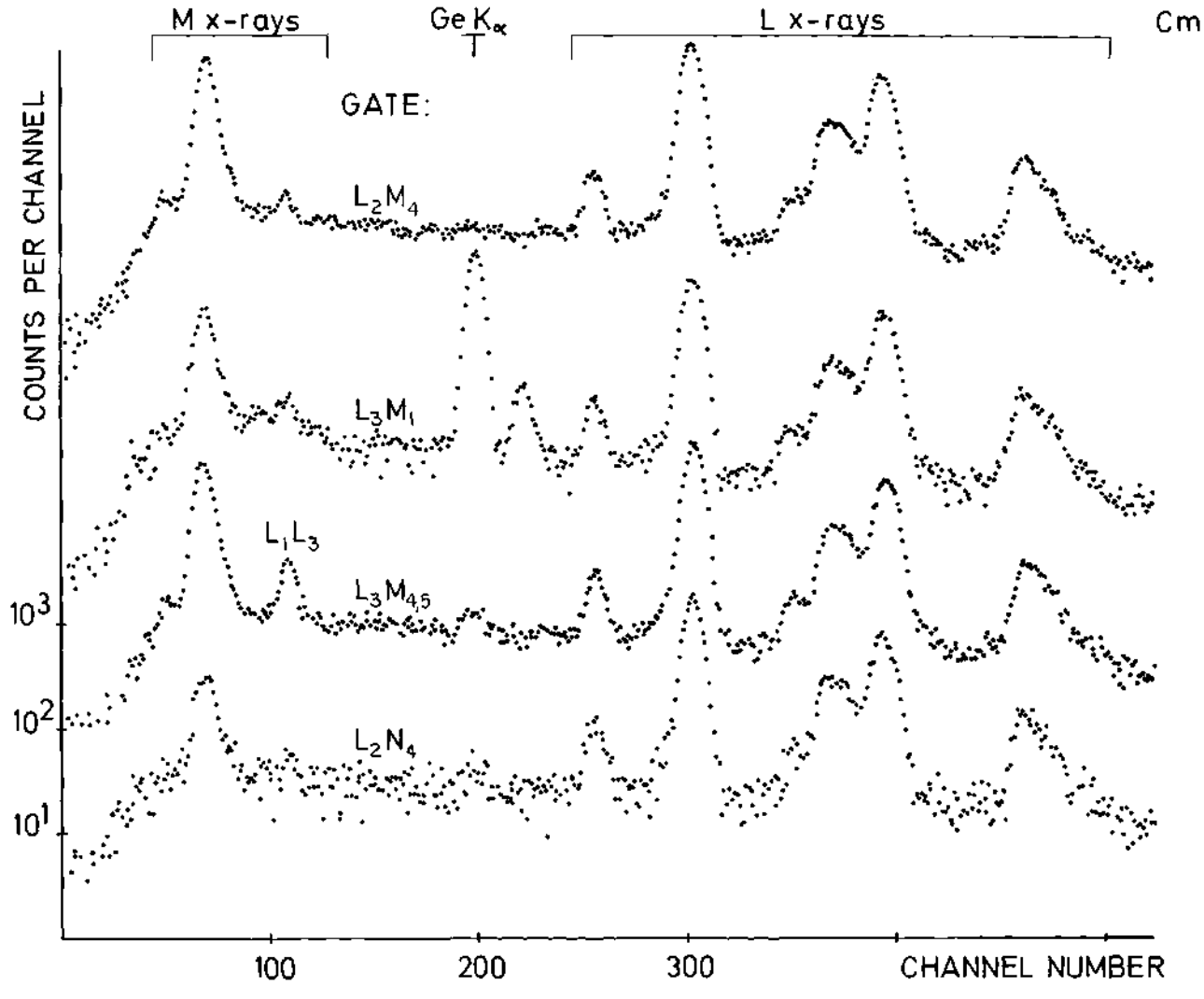


Figure 20. L X-Ray Gated Coincidence Spectra of Cm X Rays. (See Text for Figure 17.)

Table 9. Evaluation of Net Coincidence Counting Rates of M X Rays, $M_{1,2}$ X Rays, and $L_1$-$L_3$ Radiative Transitions in the Ge(Li)-Si(Li) Measurements of L-M Coincidences with a $^{249}Cf$ Source

| Gate | M $M_{1,2}$ or $L_1L_3$ | Gross Counting Rate counts/min | Chance Correction | Gate Correction | $C_{M(Gate)}$ [a] | Experimental Nuclear Cascading Correction | $C_{M(Gate)}$ [b] $C_{M_{1,2}(Gate)}$ $C_{L_1L_3(Gate)}$ |
|---|---|---|---|---|---|---|---|
| $L_2$-$N_4$ | M | 0.6131 ± 0.0226 | 0.1625 ± 0.0088 | | 0.4506 ± 0.0242 | | |
| Continuum | M | 0.3523 ± 0.0204 | 0.0851 ± 0.0046 | 0.0121 ± 0.0015 | 0.2551 ± 0.0210 | | |
| $L_2$-$M_4$ | M | 3.751 ± 0.034 | 0.418 ± 0.016 | | 3.333 ± 0.037 | 1.181 ± 0.064 | 2.152 ± 0.075 |
| $L_3$-$M_1$ | M | 0.6660 ± 0.0120 | 0.0845 ± 0.0047 | 0.1792 ± 0.0147 | 0.4023 ± 0.0195 | 0.1152 ± 0.0062 | 0.2871 ± 0.0205 |
| $L_3$-$M_1$ | $M_{1,2}$ | 0.0529 ± 0.0143 | 0.0008 ± 0.0005 | 0.0186 ± 0.0051 | 0.0335 ± 0.0147 | 0.0090 ± 0.0035 | 0.0245 ± 0.0147 |
| $L_3$-$M_{4,5}$ | M | 6.910 ± 0.069 | 0.697 ± 0.026 | 0.147 ± 0.015 | 6.066 ± 0.075 | 1.970 ± 0.106 | 4.096 ± 0.129 |
| $L_3$-$M_{4,5}$ | $L_1L_3$ | 0.670 ± 0.022 | 0.008 ± 0.006 | | 0.662 ± 0.023 | 0.162 ± 0.033 | 0.500 ± 0.041 |

[a] Net rate without nuclear cascading correction.

[b] Net rate with experimental nuclear cascading correction.

The efficiency curve plotted in Figure 2 is applicable in these $^{249}Cf$ measurements. A value

$$\bar{\epsilon}_M \ (1.61 \pm 0.55) \times 10^{-3}$$

is read at the main M x-ray line energy 3.6 keV. Thus, the following values are obtained for the mean M-subshell fluorescence yields of curium (Z=96) by using the calculated nuclear cascading corrections from Table 23 of Appendix I.

$$\nu_1^M = 0.091 \pm 0.016$$

$$\nu_4^M = 0.096 \pm 0.014$$

$$\nu_{4,5}^M = 0.089 \pm 0.014$$

The same values, but with the experimentally determined nuclear cascading correction, are

$$\nu_1^M = 0.081 \pm 0.016$$

$$\nu_4^M = 0.080 \pm 0.006$$

$$\nu_{4,5}^M = 0.075 \pm 0.012$$

The fact that the calculated nuclear cascading correction seems to be underestimated can again be observed from the mean values, although the two sets of results are in agreement within the two-sigma error limits.

Separate analysis of the $M_{1,2}$ x rays and the $L_1$-$L_3$ CK x rays is now possible due to better separation than in the neptunium spectra. Evalua-

tions of the net coincidence rates are given above in Table 9. By assuming again that the $M_2$-$N_1$ and $M_3$-O,P x-ray line intensities are equal, and by using efficiencies

$$\epsilon_{M_{1,2}} = (2.36 \pm 0.12) \times 10^{-3} \text{ at } 5.0 \text{ keV}$$

$$\epsilon_{L_1 L_3} = (2.70 \pm 0.13) \times 10^{-3} \text{ at } 5.55 \text{ keV}$$

one obtains for curium (Z=96)

$$\omega_1^M + f_{12}^M \omega_2^M = (7.5 \, {}^{+\,8.9}_{-\,7.5}) \times 10^{-3}$$

and

$$\omega_{13}^L = (2.8 \pm 2.0) \times 10^{-2}$$

3.6.4. Ge(Li)-Si(Li) Coincidence Measurements of Curium M X Rays Gated with K X Rays

A reasonable separation of the K-$M_2$ ($K_{\beta 3}$) and K-$M_3$ ($K_{\beta 1}$) x-ray lines in the Ge(Li) spectrum is illustrated in the large scale picture of the $K'_{\beta 1}$ group, as shown in Figure 21. The gate positions are also shown in this spectrum, and it is obvious that the lines do not overlap strongly within the gates (see Table 10). The presence of a previously unknown gamma ray at 122 keV under the K-$M_2$ x-ray line in $^{249}$Cf decay, contributes about five percent to the gross intensity of this x-ray peak according to Schmidt-Ott (48).

The coincidence spectra measured by the K-M x rays are free of the CK-type complications ($m_{ej}^K = 0$ in eq. 14) and, after correction for nuclear cascading, yield clean values for the quantities $\nu_2^M$ and

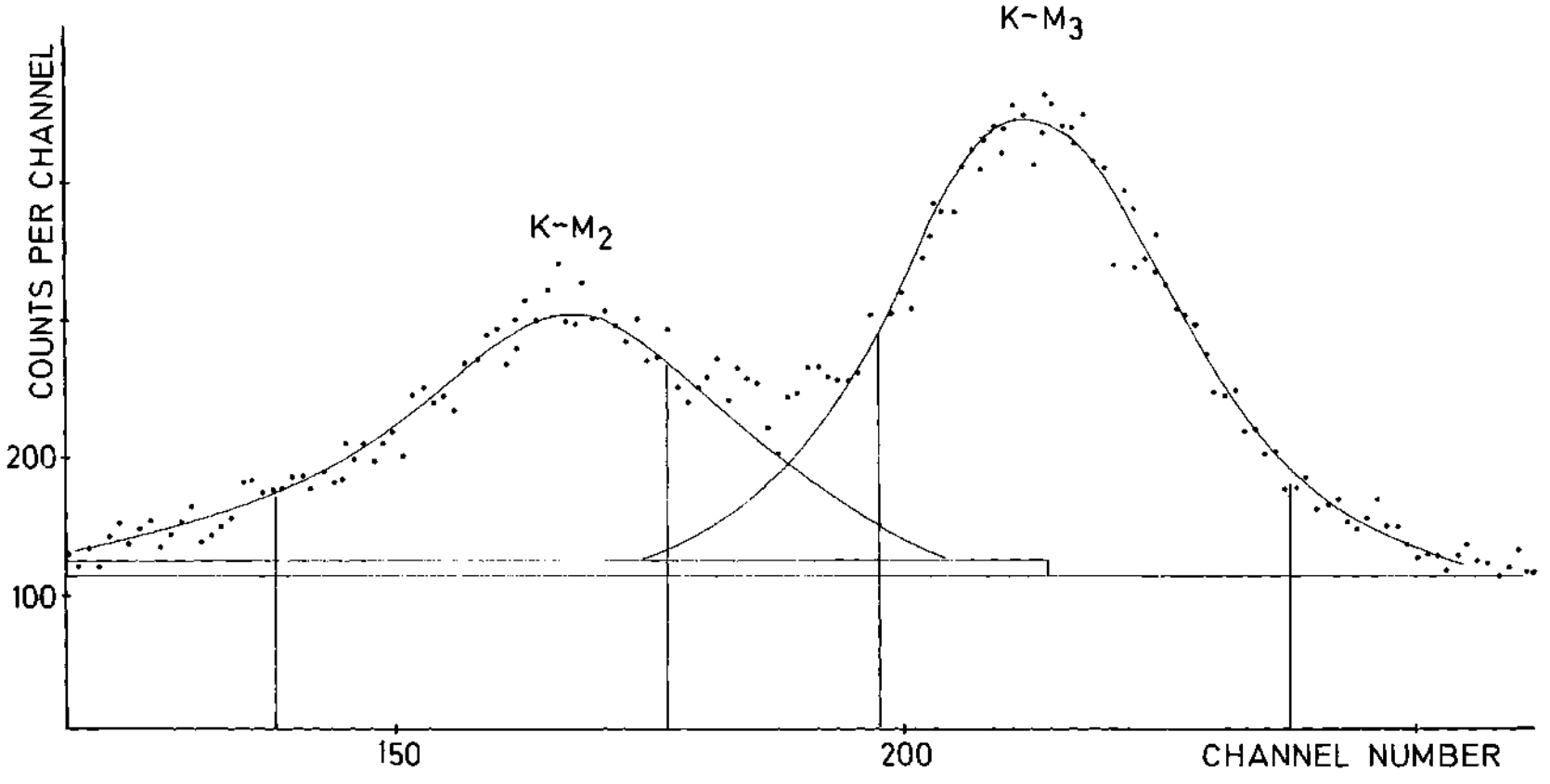


Figure 21. Gate Settings on the $K'_{\beta_1}$ Group in the Ge(Li)-Gated Measurements of K-M X-Ray Coincidences with $^{249}Cf$ Source. (Relatively High Continuum Level and Good Separation of the Peaks is Illustrated).

Table 10. Composition of the Four Coincidence Gates in the Ge(Li)-Si(Li) K-M X-Ray Coincidence Runs with a $^{249}Cf$ Source

| Gate | Contribution | Counting Rate counts/min |
|---|---|---|
| Continuum | | 1319.7 ± 1.3 |
| $K'_{\beta 2}$(K-N,O) | total | 1140.7 ± 0.7 |
| | continuum | 597.8 ± 0.7 |
| | net $K'_{\beta 2}$ | 542.9 ± 1.0 |
| $K\text{-}M_3$ | total | 1432.1 ± 0.5 |
| | continuum | 366.6 ± 9.2 |
| | $K'_{\beta 2}$ | 17.5 ± 1.5 |
| | $K\text{-}M_2$ | 8.6 ± 1.0 |
| | net $K\text{-}M_3$ | 1039.4 ± 9.5 |
| $K\text{-}M_2$ | total | 1002.7 ± 0.8 |
| | continuum | 345.9 ± 9.0 |
| | 122 keV gamma | 50.0 ± 10.0 |
| | $K'_{\beta 2}$ | 16.7 ± 1.7 |
| | $K\text{-}M_3$ | 53.2 ± 5.4 |
| | net $K\text{-}M_2$ | 536.9 ± 14.7 |

$\nu_3^M$, thus completing the series of mean subshell yields obtained from the L x-ray-gated measurements. The intensity of the $K_\beta$ lines is, however, small, which results in difficulties in obtaining adequate statistical accuracy.

An exact correction for the multiple M-shell vacancies due to nuclear cascading can, in principle, be measured by gating on the $K'_{\beta 2}$ group, which results from radiative transitions from the N shell and above. Because of the relatively high continuum level, an accurate determination of the continuum coincidence rate is of importance. For this purpose, a gate was set on the flat continuum above the K x-ray region. The analysis of the composition of the measured gate counting rates is given in Table 10.

One coincidence run and one chance coincidence run were measured with each gate. Although the duration of the coincidence measurement was 11 days, the statistics were still poor owing to the low efficiency of the gate detector at energies over 100 keV and to the small intensity of the K x rays. The coincidence spectra are shown in Figure 22. An expected small difference is observed in the energy region of the $M_{1,2}$ filling between the K-$M_2$ and K-$M_3$ gated spectra. This gives an opportunity to obtain an estimate of the clean subshell fluorescence yield $\omega_2^M$ from the former spectrum. The evaluation of the net coincidence rates is given in Table 11, both for the total M x-ray region and for the $M_{1,2}$-filling x rays in the K-$M_2$ gated spectrum. The error limits are determined by the counting statistics ($1\sigma$). By using the same efficiency values as in the L-M coincidence measurements above, the following mean subshell fluorescence yields are obtained from eq. (13) with calculated nuclear cascading

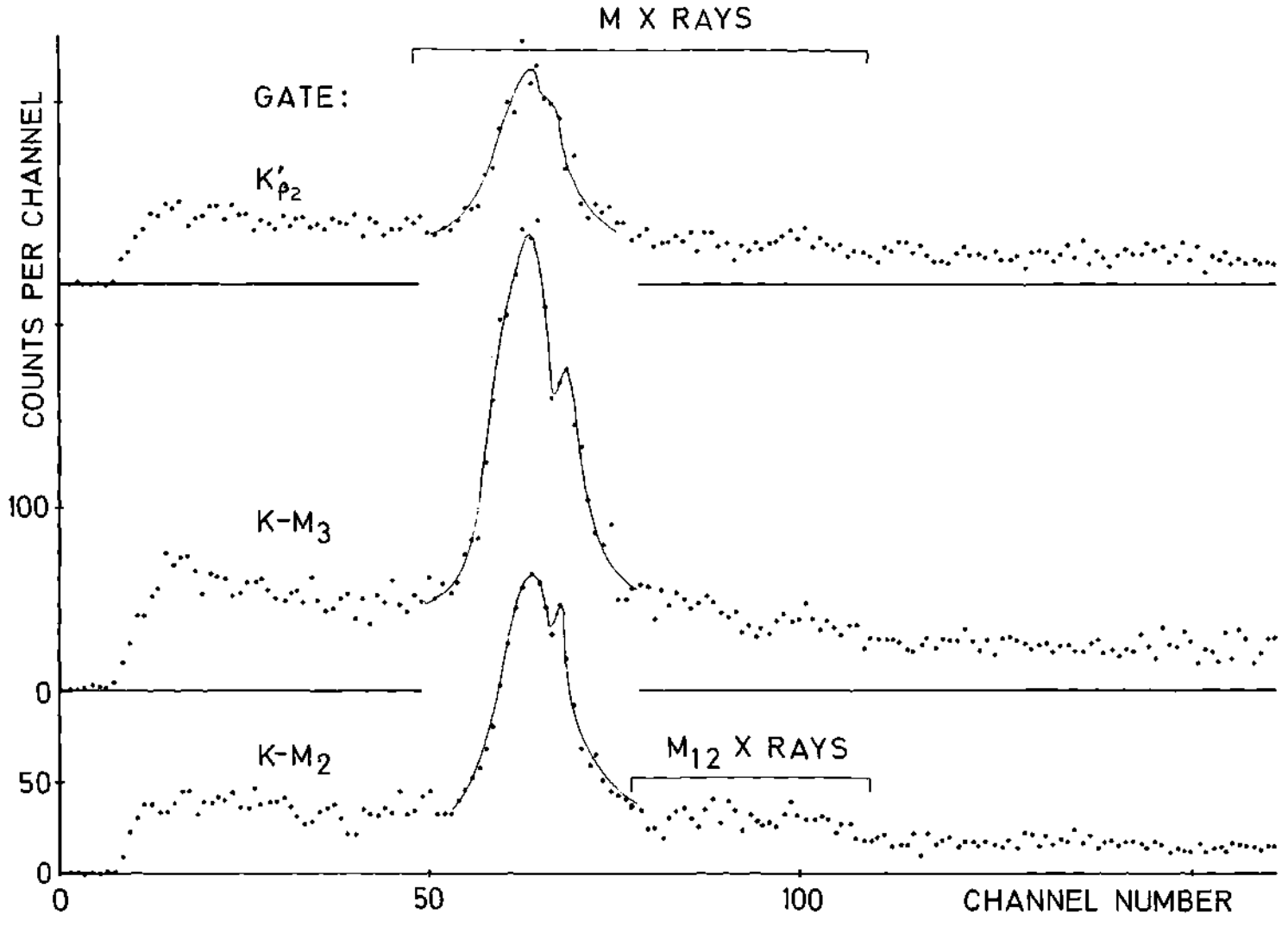


Figure 22. K X-Ray-Gated Coincidence Spectra of Cm M X Rays. (Low Intensity of the $M_2$ X-Ray Region Above the Main M X-Ray Peak in the K-$M_2$ Gated Spectrum Indicates a Small Value of $\omega_2^M$ .)

Table 11. Evaluation of Net Coincidence Counting Rates of M X Rays and $M_2$ X Rays in the Ge(Li)-Si(Li) Measurements of K-M Coincidences with a $^{249}Cf$ Source

| Gate | M or $M_2$ | Gross Counting Rate counts/min | Chance Coincidences | Gate Correction | $C'_{M(Gate)}$ [a] | Experimental Nuclear Cascading Correction | $C_{M(Gate)}$ [b] $C_{M_2(Gate)}$ |
|---|---|---|---|---|---|---|---|
| Continuum | M | 0.0854 ± 0.0145 | | | | | |
| K-N,O | M | 0.1019 ± 0.0047 | 0.0344 ± 0.0045 | 0.0302 ± 0.0034 | 0.0373 ± 0.0068 | | |
| K-$M_3$ | M | 0.2280 ± 0.0068 | 0.0307 ± 0.0031 | 0.0193 ± 0.0021 | 0.1780 ± 0.0078 | 0.0734 ± 0.0134 | 0.1046 ± 0.0155 |
| K-$M_2$ | M | 0.1551 ± 0.0054 | 0.0262 ± 0.0025 | 0.0226 ± 0.0023 | 0.1061 ± 0.0064 | 0.0449 ± 0.0082 | 0.0612 ± 0.0103 |
| K-$M_2$ | $M_2$ | 0.0069 ± 0.0033 | 0.0002 ± 0.0002 | 0.0008 ± 0.0006 | | 0.0004 ± 0.0003 | 0.0055 ± 0.0034 |

[a] Net rate without nuclear cascading correction.

[b] Net rate with experimental nuclear cascading correction.

correction (Appendix I, Table 23) at Z=96

$$\nu_2^M = 0.079 \pm 0.018$$

$$\nu_3^M = 0.072 \pm 0.015$$

The same results, but with the experimental nuclear cascading correction, are

$$\nu_2^M = 0.068 \pm 0.023$$

$$\nu_3^M = 0.062 \pm 0.019$$

With an assumption that the intensity of the $M_3$-O,P group is small compared to the total intensity of the $M_2$ x rays, one obtains for the $M_2$-subshell fluorescence yield of curium (Z=96)

$$\omega_2^M = (4.6 \begin{smallmatrix} + 5.1 \\ - 4.6 \end{smallmatrix}) \times 10^{-3}$$

A possible systematic error ($\lesssim$ 9 percent) in the detection efficiency due to the intensity measurement of the M x rays from $^{241}$Am is not included in any of the error limits given above, because it does not affect the reported values relative to each other.*

*Recent efficiency measurements (36) for a Si(Li) detector having an essentially constant intrinsic efficiency down to three keV indicate that this systematic error probably is less than five percent.

# CHAPTER IV

# DISCUSSION OF RESULTS

## 4.1. Mean M-Subshell Fluorescence Yields of Neptunium and Curium

The values obtained in the coincidence experiments for the mean M-subshell fluorescence yields of Np and Cm with radioactive sources of $^{241}Am$ and $^{249}Cf$ are summarized in Tables 12 and 13, respectively.

It can be observed from Table 12 that the accuracy of the results is essentially the same regardless of whether the M x rays are counted with a multiwire proportional counter (MWPC) or with a semiconductor x-ray spectrometer. The error is mainly due to uncertainties in the correction for multiple vacancies in coincidence with a gating x ray. The error limits are twice the statistical standard deviation ($2\sigma$), and do not include a possible systematic error in the efficiency calibration. This systematic error would be, however, the same ($\leq$ 9 percent) in all the results in Tables 12 and 13, owing to the fact that the efficiency calibration was made by determination of the absolute emission rate of the M x rays from the source.

The error limits in the results, obtained with either the experimental or the calculated nuclear cascading correction, are comparable. A calculation based on rather rough information on a complex decay scheme, (e.g. $^{249}Cf$) and on L-subshell quantities with large error bars, thus gave this correction with the same estimated accuracy as could be experimentally achieved. However, the absolute value calculated for the nuclear

Table 12. Summary of the Values of Mean M-Subshell Fluorescence Yields of Np (Z=93) Obtained from L-M X-Ray Coincidence Measurements with a $^{241}Am$ Source[a)]

| Mean M-Subshell Yield | MWPC-Ge(Li) | | Ge(Li)-Si(Li) | |
|---|---|---|---|---|
| | Calculated Nuclear Cascading | Experimental Nuclear Cascading | Calculated Nuclear Cascading | Experimental Nuclear Cascading |
| $\nu_1^{M}$ [b)] | 0.077 ± 0.030 | 0.056 ± 0.034 | | |
| $\nu_1^{M}$ [c)] | 0.089 ± 0.016 | 0.082 ± 0.018 | 0.072 ± 0.013 | 0.065 ± 0.014 |
| $\nu_2^{M}$ | 0.095 ± 0.027 | 0.080 ± 0.029 | | |
| $\nu_4^{M}$ | 0.080 ± 0.009 | 0.063 ± 0.012 | 0.070 ± 0.011 | 0.062 ± 0.005 |
| $\nu_{4,5}^{M}$ [d)] | 0.080 ± 0.011 | 0.069 ± 0.012 | 0.070 ± 0.012 | 0.065 ± 0.012 |

[a)] Error limits are the 2σ standard deviations and do not include a possible systematic error (≤ 9%) in efficiency.

[b)] From $L_2$-$M_1$ gating

[c)] From $L_3$-$M_1$ gating; 24% of the vacancies are in the $M_{3,4,5}$ subshells due to $L_{1,2}$-$L_3M$ CK transitions.

[d)] Mainly $\omega_5^{M}$; 24% of the vacancies are in the $M_{3,4,5}$ subshells due to $L_{1,2}$-$L_3M$ CK transitions.

Table 13. Summary of the Values of Mean M-Subshell Fluorescence Yields of Cm (Z=96) Obtained from L-M and K-M X-Ray Coincidence Measurements with a $^{249}Cf$ Source[a)]

| Mean Subshell Yield | Ge(Li)-Si(Li) | |
|---|---|---|
| | Calculated Nuclear Cascading | Experimental Nuclear Cascading |
| $\nu_1^{M}$[b)] | 0.091 ± 0.016 | 0.081 ± 0.016 |
| $\nu_2^{M}$ | 0.079 ± 0.018 | 0.068 ± 0.023 |
| $\nu_3^{M}$ | 0.072 ± 0.015 | 0.062 ± 0.019 |
| $\nu_4^{M}$ | 0.096 ± 0.014 | 0.080 ± 0.006 |
| $\nu_{4,5}^{M}$[b)] | 0.089 ± 0.014 | 0.075 ± 0.012 |

a) Error limits are 2σ standard deviations, and do not include a possible systematic error (≦ 9%) in efficiency.

b) Eighteen percent of the vacancies are in the $M_{3,4,5}$ subshells due to $L_{1,2}$-$L_3M$ CK transitions.

cascading correction factor $m_{nj}^{X}$ results in a correction which is lower by about 30 percent in the $^{241}Am$ decay, and by about 50 percent in the $^{249}Cf$ decay, than the correction observed experimentally. This is reflected in Tables 12 and 13, where the values of $\nu_i^M$ obtained with the calculated nuclear cascading correction are consistently higher than those obtained with the experimental correction. The results, however, agree within the ($2\sigma$) error limits. This fact indicates that the discrepancy in the magnitude of the correction may arise from the uncertainty in the basic information adopted in the calculation (Appendix I). The neglected nuclear cascades do not contribute more than five percent to the discrepancy, and the neglected K-Auger transitions not more than two percent (Appendix I) in $^{249}Cf$ decay. According to a published measurement by Rubinson (57) from $^{210}Po$ decay, $10^{-3}$ M x rays per alpha decay are emitted due to autoionization. Since the total number of the M x rays emitted by $^{241}Am$ (Section 3.4.) is $6.4 \times 10^{-2}$ per decay, autoionization results in only about 1.5 percent of M-shell vacancies and its contribution to multiple vacancies is negligible. The possible effect of vacancies in the shells below and above the M shell on the emission rate of the M x rays is discussed in Ref. (5) and deduced to be of the order of one percent, which is also negligible. The discrepancy between the calculated and the experimental correction for nuclear cascading is, therefore, probably due to the uncertainty in the values of the various subshell quantities and in the vacancy distribution. The results obtained with the experimental correction for nuclear cascading therefore are more likely to be correct.

The values obtained for the various mean M-subshell yields of Np and Cm are essentially identical within the experimental uncertainty.

Since the $M_{1,2}$-subshell fluorescence yields are low (Sections 3.6.2-4.), this requires that the CK transition probabilities to the outer subshells must be large. This is expected, because low transition energies make x-ray emission improbable and, on the other hand, the CK transitions resulting in the emission of a low-energy electron are favored over Auger transitions, whenever ionization of the adjacent higher shell in the CK process is energetically possible. For this reason it is expected that $f_{34}^M$ and $f_{35}^M$ are also high, while $f_{45}^M$ is probably small. The value of $\omega_4^M$ is, therefore, probably close to that of $\omega_5^M$. It should be noted that, for evaluation of the quantity $\nu_{4,5}^M$ ($\cong \omega_5^M$), the calculated correction for electronic vacancy multiplication is always applied. If this correction were too small, as probably is true of the calculated nuclear cascading correction, $\omega_4^M$ would be slightly higher than $\omega_5^M$.* The high probability of the M-shell CK transitions as compared to the Auger transitions has been directly observed at low Z by Mehlhorn (58) in electron spectra of krypton.

Owing to the existence of multiple M-shell vacancies, the values obtained for the mean M-subshell fluorescence yields are not completely pure, because a certain fraction of the original vacancies may be outside of the subshell signaled by the gate pulse. This tends to hide possible small differences between various mean M-subshell fluorescence yields. In order to be able to observe these differences, the effect of multiple vacancies must absolutely be minimized; i.e. only such radioactive sources may be used where vacancies are created only by electron capture to the ground state or by internal conversion of a single gamma ray.

---

*The radiative width of the $M_4$ subshell is larger than that of the $M_5$ subshell (see Figure 23).

As discussed above, essentially all of the inner M-subshell vacancies shift to the $M_4$ or $M_5$ subshell before the radiative filling occurs. Furthermore, since the quantities $\omega_4^M$ and $\omega_5^M$ are not very different, the mean M-fluorescence yield is insensitive to the vacancy distribution and the quantities $\bar{\omega}_M$ and $\omega_{LM}$ both are approximately equal to $\omega_5^M$. This explains the similarity of the values of $\bar{\omega}_M$ and $\omega_{LM}$ measured at Z=79, 82, and 83 (Table 1). This also gives a possibility of obtaining the Z-dependency of the subshell yield $\omega_5^M$ from present experimental information. In Figure 23 the measured values of $\bar{\omega}_M$, $\omega_{LM}$, and $\nu_{4,5}$ ($\approx \omega_5^M$) are plotted as a function of Z and compared with the calculated (11) radiative widths of the $M_4$ and $M_5$ subshells. It can be observed that the measured yield changes with Z in the same manner as the radiative width of the $M_5$ subshell [$\Gamma_r(M_5)$]. Since

$$\omega_5^M = \frac{\Gamma_r(M_5)}{\Gamma_{tot.}(M_5)} = \frac{\Gamma_r(M_5)}{\Gamma_r(M_5) + \Gamma_a(M_5)} \approx \frac{\Gamma_r(M_5)}{\Gamma_a(M_5)} ,$$

one concludes that the total width and the Auger width of the $M_5$ subshell [$\Gamma_a(M_5)$] are essentially constant with Z in the region from Z=76-96.

Figure 24 shows a comparison of the fluorescence yields of the $M_5$, $L_3$, and K shells, which are not affected by CK transitions, in the region where the main radiative transitions have comparable energies; i.e. where the $K_\alpha$ ($K\text{-}L_{2,3}$), $L_\alpha$ ($L_3\text{-}M_{4,5}$), and $M_\alpha$($M_5\text{-}N_{6,7}$) groups have an energy of one to four keV. Experimental values are taken from Ref. (5) and the theoretical curve of $\omega_3$ (23) is also included. Since no experimental values for $\omega_3$ are available in this region, the quantity $\omega_{KL}$, which arises mainly from the filling of $L_3$ vacancies is used in the comparison. In

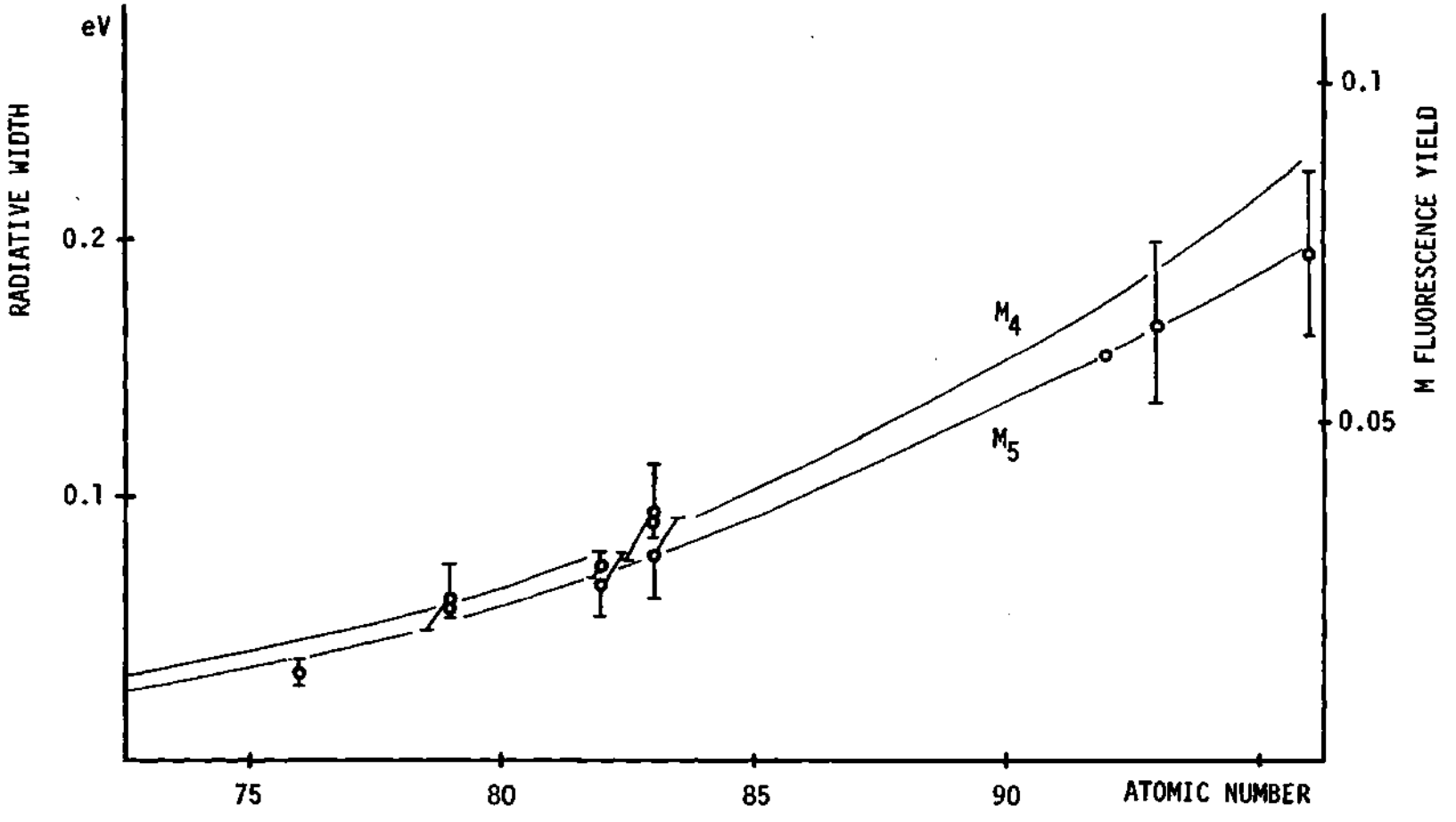


Figure 23. Experimental M-Shell Yields ($\bar{\omega}_M$, $\omega_{LM}$, $\omega_5^M$) as a Function of Atomic Number, and a Comparison with Theoretical Radiative Widths of $M_4$ and $M_5$ Subshells (11). (The M-shell fluorescence yield changes with atomic number similarly as $\Gamma_r$ (5).)

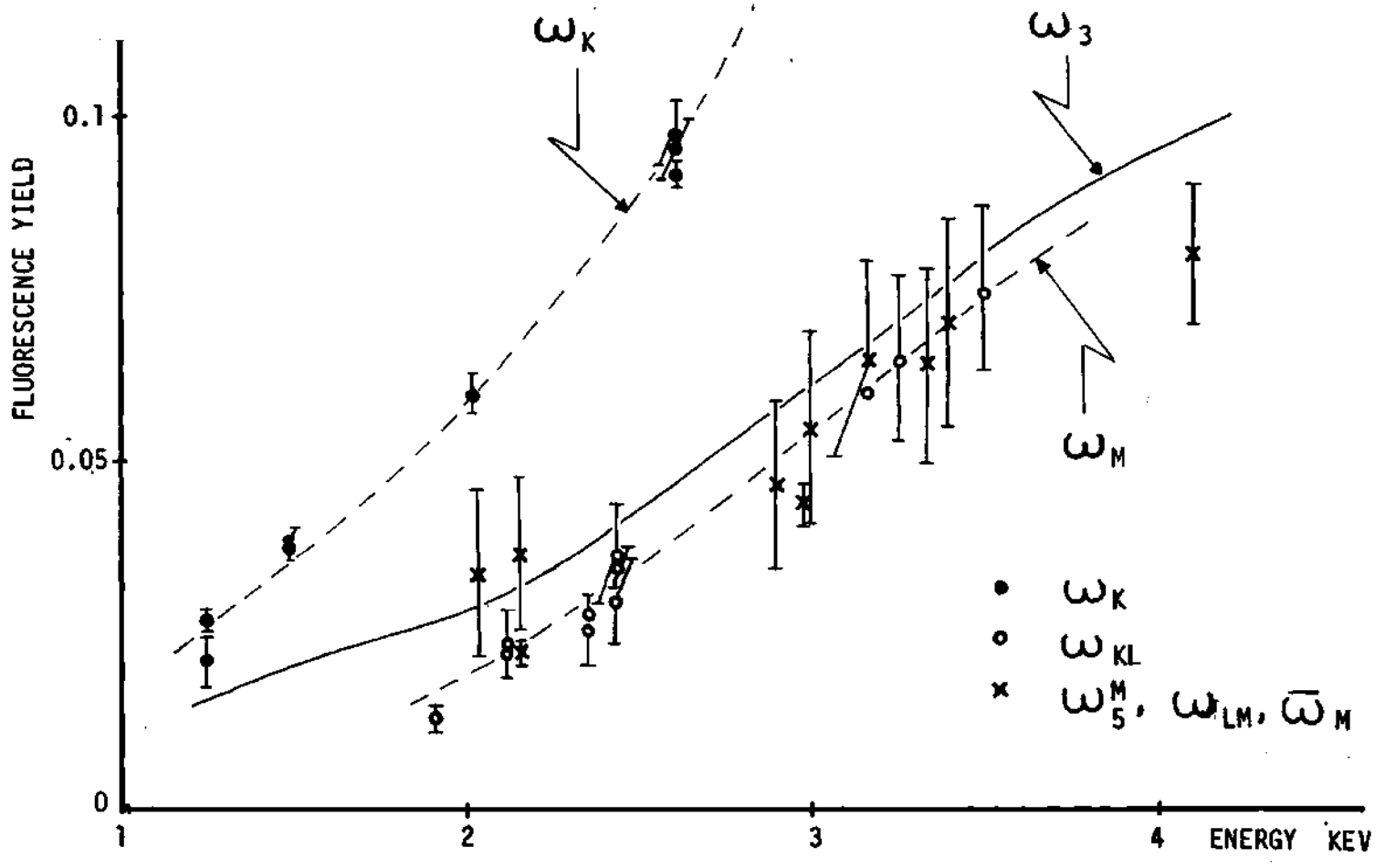


Figure 24. A Comparison of the K-Shell, Mean L- and M-Shell, and $L_3$-Subshell Fluorescence Yields as a Function of Transition Energy of the Main Radiative Component ($K_\alpha$, $L_\alpha$, $M_\alpha$). (The line representing $\omega_3$ is from theory (23), the points are from experiments. It is seen that $\omega_{KL}$ and any of the M-shell fluorescence yields are essentially equal at a fixed transition energy but $\omega_K$ is considerably larger.)

spite of the increase in the radiative width as one goes from K to $L_3$ and from $L_3$ to $M_5$ subshells at a fixed transition energy (10,11), the fluorescence yield tends to decrease, indicating that the Auger widths increase still faster with increasing angular momentum of the shell to be filled. This is clearly true between the K and $L_3$ shells, but less certain between the $L_3$ and $M_5$ subshells, where the experimental points essentially overlap, although the theoretical prediction of $\omega_3$ suggests this trend.

## 4.2. Radiative Filling of the $M_{1,2}$-Subshell Vacancies in Neptunium and Curium

The M x rays arising from radiative fillings of vacancies in the $M_1$ and $M_2$ subshells were analyzed in the various coincidence spectra measured with the Si(Li) detector. A value of the quantity ($\omega_1^M + f_{12}^M \times \omega_2^M$) of Np and Cm could thus be obtained from the $L_3$-$M_1$ x-ray-gated spectra, and a value of $\omega_2^M$ of Cm, from the K-$M_2$ x-ray-gated spectrum. A reasonable assumption was made that the intensity of the $M_2$-$N_1$ x ray which was not included in the integration of the $M_{1,2}$ x-ray peak (see Figures 15 and 18) is compensated by the unavoidable inclusion of the $M_3$-O,P x-ray group. A summary of the results is given in Table 14.

Because of poor counting statistics, only an upper limit for the $M_{1,2}$ quantities could be determined. The $M_2$-subshell yield is an order of magnitude smaller than the $M_5$-subshell yield, in contrast to the early calculation of Ramberg and Richtmeyer (28) for gold, which gave a difference of a factor of two, as shown in Section 1.3. However, this calculation can be expected to give only an order of magnitude estimate.

Table 14. A Summary of the Results on the Radiative Filling of $M_{1,2}$-Subshell Vacancies of Np (Z=93) and Cm (Z=96)

| | $\omega_1^M + f_{12}^M \cdot \omega_2^M$ | $\omega_2^M$ |
|---|---|---|
| Np | $(2.0 \begin{smallmatrix} + 3.1 \\ - 2.0 \end{smallmatrix}) \times 10^{-3}$ | |
| Cm | $(7.5 \begin{smallmatrix} + 8.9 \\ - 7.5 \end{smallmatrix}) \times 10^{-3}$ | $(4.6 \begin{smallmatrix} + 5.1 \\ - 4.6 \end{smallmatrix}) \times 10^{-3}$ |

Assuming that the Auger width for various M subshells is approximately the same--this is true for the L subshells according to calculation (23)--one concludes (Section 3.6.2.) that about 97 percent of the $M_{1,2}$ vacancies shift to higher subshells before the filling from higher major shells occurs. Therefore, in order to observe differences between the quantities $\nu_i^M$ (except probably between $\nu_4^M$ and $\nu_5^M$) from measurements with unresolved M x-ray spectra, accuracy to an order of one percent is required. This kind of experimental accuracy seems not to be feasible.

## 4.3. The Radiative $L_1$-$L_3$ Transition in Neptunium and Curium

The radiative $L_1$-$L_3$ transition was observed for the first time in the high-Z region in the course of this work and has been previously reported (59). This transition was identified both in the Np and Cm x-ray spectra according to the transition energy which accurately corresponds to the binding-energy difference (38,56) between the $L_1$ and $L_3$ subshells. The identification was confirmed in the coincidence measurements which

showed the transition to be in coincidence with $L_3$ x rays, but not with $L_2$ x rays. In low resolution measurements, the transition is hidden under the M x rays which probably explains why it has not been previously observed. In high resolution studies, it may incorrectly be interpreted to be an $M_{1,2}$ x ray in the same energy region. In the low-Z region (Z=11, 12,13,16) the radiative $L_1$-$L_3$ transition was identified previously by Tomboulian (60) with an optical spectrograph.

The intensity of the radiative $L_1$-$L_3$ transition compared to the $L_\alpha$ intensity can be obtained with good accuracy from the $L_\alpha$-gated coincidence measurements with the $^{241}$Am and $^{249}$Cf sources. It is, however, more meaningful to compare it with the intensity of other $L_1$ x rays, which is independent of the vacancy distribution. This comparison is given in Table 15, together with the theoretical prediction (10), as obtained by extrapolation from Z=92.

Table 15. Intensity of the Radiative $L_1$-$L_3$ Transition Compared to the Total Intensity of the $L_3$ and $L_1$ X Rays from Decay of $^{241}$Am and $^{249}$Cf, Together with the Theoretical Prediction (10)

| Intensity per | $^{241}$Am Decay | | $^{249}$Cf Decay | |
|---|---|---|---|---|
| | Experimental | Theory | Experimental | Theory |
| $L_3$ x ray | 0.0099 ± 0.0015 | | 0.0081 ± 0.0013 | |
| $L_1$ x ray[a] | 0.10 ± 0.07 | 0.060 | 0.083 ± 0.055 | 0.071 |
| $L_1$ x ray[b] | 0.029 ± 0.008 | | 0.048 ± 0.015 | |

[a] Deduced from intensity per $L_3$ x ray.

[b] Obtained from analysis of a singles spectrum.

The first value of the $L_1$-$L_3$ intensity per $L_1$ x ray in Table 15 is calculated from the intensity per $L_3$ x ray obtained from the $L_\alpha$-gated coincidence measurements, using information from Appendix I. The second value is based on a curve resolver analysis of a singles spectrum, from which the total $L_1$ x-ray intensity was obtained. This value which has smaller error limits disagrees with the theory. However, the systematic error introduced in a curve resolving process is very difficult to estimate.

A comparison of the number of $L_1$-$L_3$ x rays emitted to the number of $L_1$-subshell vacancies gives the following values for the radiative component of the CK yield $f_{13}$:

$$\omega_{13}\ (Z=93) = 0.030 \pm 0.014$$

$$\omega_{13}\ (Z=96) = 0.028 \pm 0.020$$

These are the first values ever reported for this quantity. It appears that approximately five percent of the total CK yield $f_{13}$ is radiative in the region Z=93-96.

# CHAPTER V

## CONCLUSIONS

1. The value of the mean M-subshell fluorescence yield is the same for all subshells of neptunium (Z=93) and all subshells of curium (Z=96) within the experimental accuracy obtained; i.e. within 15 percent for the $M_{1,2,4,5}$ subshells and about 35 percent for the $M_3$ subshell.

2. Only 6.5 and 7.5 percent of the $M_5$-subshell vacancies fill radiatively, respectively, in neptunium and curium.

3. From the $M_{1,2}$-subshell vacancies, about 97 percent shift to higher subshells through CK processes before the filling from higher shells occurs.

4. The subshell fluorescence yield for the $M_1$ and $M_2$ subshells is smaller than that for the $M_5$ subshell at least by a factor of five, more probably by a factor of ten.

5. The radiative $L_1$-$L_3$ transition occurs in the high-Z region approximately at the rate predicted theoretically.

6. Of the total L-shell CK yield $f_{13}$, five percent is radiative in the region Z=93-96.

7. The nonradiative width of the $M_5$ subshell is essentially constant from Z=76 to 96.

8. For a fixed energy of the main radiative component ($K_\alpha$, $L_\alpha$, $M_\alpha$) the value of $\omega_3^L$ is approximately the same as that of $\omega_5^M$, but $\omega_K$ is larger; thus the Auger width increases considerably more than the x-ray width with

increasing angular momentum from $s_{1/2}$ to $p_{3/2}$, while increasing only slightly more (if any) from $p_{3/2}$ to $d_{5/2}$.

9. The effect of multiple vacancies on L-M and K-M x-ray coincidence rates becomes large, especially when a radioactive source with complex decay scheme is used, and multiplication in the electronic shells alone can cause an increase of the $L_3$ x-ray-gated coincidence rates of M x rays by as much as 50 percent.

10. The accuracy of our knowledge of multiple vacancies is the major limiting factor in the total accuracy obtained in measurements of M-subshell yields with x-ray–x-ray coincidence techniques, especially when vacancies are created in cascading nuclear processes.

11. Owing to the strength of the CK process, an accuracy of the order of one percent is required in an experiment, in order to expose differences between various mean M-subshell fluorescence yields. Such an accuracy cannot presently be achieved.

The objective of this work was to explore possibilities of obtaining fundamental information on the radiative filling of M-subshell vacancies, as compared with the nonradiative modes of filling. Although the coincidence method fails to show differences between the various mean M-subshell fluorescence yields, determination of two subshell fluorescence yields, $\omega_2^M$ and $\omega_5^M$, is valuable when theoretical calculations of nonradiative transition probabilities are attempted.

# CHAPTER VI

## SUGGESTIONS FOR FUTURE WORK

For meaningful further investigation of the M-subshell yields, a better resolution in detection of M x rays is needed than was available for this study. Slight improvement in the resolution of semiconductor x-ray detectors may make possible the use of a stripping procedure, as described in Section 3.6.1., in order to separate the x rays filling vacancies in different subshells. Coincidence measurements between L-M x rays and M-Auger electrons, measured with a high-transmission spectrometer, should also be considered.

Accurate measurement of the probability of the radiative $L_1$-$L_3$ transition should be possible with coincidence techniques by gating on $L_1$ conversion electrons detected, e.g. with a windowless semiconductor detector.

Investigation of the possibility of two-electron transitions in doubly-ionized atoms would be of theoretical interest. This would require a comparison in a coincidence arrangement of x-ray or Auger-electron intensities, indicating, e.g. filling of $L_3$-subshell vacancies with K-$L_3L_3$ and K-$L_3$M gatings.

# APPENDIX I

## CALCULATION OF THE NUMBER OF M-SHELL VACANCIES COINCIDENT WITH K AND L X RAYS

### 1. Derivations

The existence of multiple M-shell vacancies at the moment of K-M or L-M x-ray emission may have two basically different origins: either starting from one original K- or L-shell vacancy and due to nonradiative transitions in the electronic shells; or arising from two or more original vacancies created simultaneously in cascading nuclear processes in the course of a radioactive decay. If $m_{ej}^{X}$ and $m_{nj}^{X}$ are the average numbers of M-shell vacancies per $X_j$-M x ray, due to vacancy multiplication in the electronic shells and due to multiple ionization in the nuclear cascades, respectively, the total average number of multiple M-shell vacancies per $X_j$-M x ray, denoted by $m_j^X$ is the sum

$$m_j^X = m_{ej}^X + m_{nj}^X \tag{14}$$

and the total average number of M-shell vacancies in coincidence with an $X_j$-M x ray is $(1+m_j^X)$. This number is important in the interpretation of the coincidence measurements involving x rays. The purpose of this section is the derivation of equations for the quantitative calculation of $m_j^X$.

The quantity $m_e^K$ is obviously zero. In the L shell $m_{ej}$ (the super-

script L is again consistently omitted) is proportional to that fraction of the final vacancy distribution $V_j$ that is created through M-shell ionizing electronic transitions, each weighted by the number of M-shell vacancies arising in this particular transition. By developing the earlier notation (5,33,34), let $n_{KL_jM}$ and $n_{L_iL_jM}$ mean the number of M-shell vacancies resulting from one initial vacancy in the K or $L_i$ shell, respectively, with consequent creation of an $L_j$ vacancy. One can then write the relationship

$$m_{ej} = \frac{1}{V_j}\left[(n_{L_1L_jM})\ N_1' + (n_{L_2L_jM})\ N_2' + (n_{KL_jM})\ N_K\right] \qquad (23)$$

where $V_j$ is the final number of vacancies in the $L_j$ subshell; and $N_1'$, $N_2'$, and $N_K$ are the numbers of vacancies directly produced in nuclear processes in the $L_1$, $L_2$, and K shell, respectively.

In the region of Z=93-96, which is of interest in this thesis, the only energetically-allowed L-LM CK transitions are $L_1$-$L_3M_{3,4,5}$ and $L_2$-$L_3M_{4,5}$, and therefore only the quantities $n_{L_1L_3M}$, $n_{L_2L_3M}$, and $n_{KL_jM}$ differ from zero and are given by

$$n_{L_1L_3M} = \frac{I(L_1\text{-}L_3M)}{I(L_1\text{-}L_3X)}\ f_{13} + \frac{I(L_2\text{-}L_3M)}{I(L_2\text{-}L_3X)}\ f_{12}\cdot f_{23} \qquad (24)$$

$$n_{L_2L_3M} = \frac{I(L_2\text{-}L_3M)}{I(L_2\text{-}L_3X)}\ f_{23}$$

$$n_{KL_jM} = \omega_K \frac{I(K\text{-}L_2)}{I(K\text{-}X)}\ \frac{I(L_2\text{-}L_3M)}{I(L_2\text{-}L_3X)} + a_K\ F_{KL_jM}\ .$$

Here I(X-YZ) is the intensity of the transition (X-YZ), and $F_{KL_jM}$ is the fraction of the K-Auger transitions which directly or through various transition sequences leads to consequent $L_j$-subshell and M-shell ionization, each transition or transition sequence of which is weighted by the number of M-shell vacancies produced. This quantity involves a large number of different processes (over 200 in $F_{KL_3M}$) which may give rise to as many as four M-shell vacancies in addition to an $L_j$ vacancy (e.g. the sequence K-$L_1L_1$, $L_1$-$L_3$M, $L_1$-$L_3$M, $L_3$-MM gives four M-shell vacancies in coincidence with one $L_3$ vacancy). In the high-Z region, $a_K$ is small (e.g. $\approx$ 0.025 at Z=96), so that generally the term $a_K F_{L_jM}$ is negligible in eq. (24)(see Section 2 in this Appendix). When this term is neglected and making use of the relationship

$$N_1 = N_1' \tag{25}$$

$$N_2 = N_2' + N_K \omega_K \frac{I(K\text{-}L_2)}{I(K\text{-}X)}$$

one obtains by inserting eqs. (24) into eq. (23)

$$m_{e1} = 0 \tag{15}$$

$$m_{e2} = 0$$

$$m_{e3} = \frac{1}{V_3}\left\{\left[\frac{I(L_1\text{-}L_3M)}{I(L_1\text{-}L_3X)} f_{13} + \frac{I(L_2\text{-}L_3M)}{I(L_2\text{-}L_3X)} f_{12} f_{23}\right] N_1 + \frac{I(L_2\text{-}L_3M)}{I(L_2\text{-}L_3X)} f_{23} N_2\right\}$$

from which the correction for the electronic M-vacancy multiplication can be calculated.

Several combinations of different processes occurring in the course of a radioactive decay can result in the direct creation of more than one electronic vacancy per decay; e.g. electron capture, internal conversion, autoionization in beta or alpha decay, and fluorescence self-excitation of the source. Here only the effect of simultaneous internal conversions in nuclear gamma cascades will be considered, since the nuclides in question are essentially pure alpha emitters, the probability of autoionization in alpha decay is small (57)(Section 4.1.), and since the fluorescent self-excitation is negligible when sources of high specific activity are used.

Assuming that the probability for a simultaneous conversion of three or more gamma rays is negligible, it is sufficient to develop expressions for the nuclear cascading correction term, $m_{nj}^{X}$, in the case of a simple cascade of two gamma transitions, labeled as gamma (1) and gamma (2).

Multiple M-shell vacancies, coincident with an $X_j$-M x ray, exist when an $X_j$ vacancy is created as a consequence of conversion of gamma (1), while the simultaneous conversion of gamma (2) ultimately produces an M-shell vacancy or vice versa. Let the intensity per decay of the transition (s) be $A_s$ where s refers to transitions (1) and (2), and let the total excitation per decay of the intermediate level between (1) and (2) be A. Further, let $V_j^X(s)$ be the final number of $X_j$-subshell vacancies per decay, created in conversion of gamma (s). Then a fraction $A_2/A$ of the transitions (1) is followed by a transition (2). This fraction creates $V_j^X(1)A_2/A$ vacancies in the $X_j$ subshell. Therefore, the number of $X_j$ vacancies in coincidence with transition (2) per total number of $X_j$ vacancies, and also the number of $X_j$ x rays in coincidence with transition (2) per

total number of $X_j$ x rays, is given by $V_j^X(1)A_2/V_j^X A$. On the other hand, if $N_j'^X(s)$ is the number of $X_j$-subshell vacancies per decay directly created in conversion of gamma ray (s), and since $n_{X_iM}$ is defined as the number of M-shell vacancies arising from one initial $X_i$ vacancy, the total number of M-shell vacancies per one decay, $b_2$, due to conversion of gamma (2) is

$$b_2 = N_M'(2) + N_K'(2)\ n_{KM} + N_1'(2)\ n_{L_1M} + N_2'(2)\ n_{L_2M} + N_3'(2)\ n_{L_3M}$$

The probability of obtaining an M-shell vacancy from conversion of gamma (2) is therefore $b_2/A_2$. The number of M-shell vacancies due to conversion of gamma (2) and in coincidence with $X_j$ x rays created due to conversion of gamma (1) is given by the product

$$\frac{V_j^X(1)}{V_j^X}\ \frac{A_2}{A}\ \frac{b_2}{A_1}$$

and the total number of M-shell vacancies in coincidence with $X_j$ x rays, $m_j^X$, is the sum

$$m_i^X = \frac{V_j^X(1)\ b_2 + V_j^X(2)\ b_1}{V_j^X\ A} \qquad (16)$$

The quantities $V_j^X(s)$ and $V_j^X$ can be calculated with the aid of eqs. (4) and (5) in 2.1 and

$$b_s = N_M'(s) + N_K'(s)\ n_{KM} + N_1'(s)\ n_{L_1M} + N_2'(s)\ n_{L_2M} + N_3'(s)\ n_{L_3M} \qquad (26)$$

where

$$n_{L_3M} = \omega_3 \frac{I(L_3\text{-}M)}{I(L_3\text{-}X)} + a_3 \frac{I(L_3\text{-}MN,O..)}{I(L_3\text{-}XY)} + a_3 \frac{2\ I(L_3\text{-}MN)}{I(L_3\text{-}XY)} \qquad (27)$$

$$n_{L_2M} = \omega_2 \frac{I(L_2\text{-}M)}{I(L_2\text{-}X)} + a_2 \frac{I(L_2\text{-}MN,O..) + 2\ I(L_2\text{-}MN)}{(L_2\text{-}XY)}$$

$$+ f_{23}\ n_{L_3M} + f_{23} \frac{I(L_2\text{-}L_3M)}{I(L_2\text{-}L_3X)}$$

$$n_{L_1M} = \omega_1 \frac{I(L_1\text{-}M)}{I(L_1\text{-}X)} + a_1 \frac{I(L_1\text{-}MN,O..) + 2\ I(L_1\text{-}MN)}{(I(L_1\text{-}XY)}$$

$$+ f_{12}\ n_{L_2M} + f_{13}\ n_{L_3M} + f_{13} \frac{I(L_1\text{-}L_3M)}{I(L_1\text{-}L_3X)}$$

$$n_{KM} = \omega_K \frac{I(K\text{-}M)}{I(K\text{-}X)} + \frac{I(K\text{-}L_3)}{I(K\text{-}X)}\ n_{L_2M} + \frac{I(K\text{-}L_3)}{I(K\text{-}X)}\ n_{L_3M} + F_{KM}\ a_K$$

The quantity $F_{KM}$ is the number of M-shell vacancies created through K-Auger transitions or through K-Auger initiated transition sequences, starting from one original K-shell vacancy. Because of the smallness of $a_K$ in the high-Z region, the term containing $F_{KM}$ can be neglected.

Examples of numerical calculations of M-shell multiple vacancies per K or L x ray are shown in the next section.

## 2. Numerical Evaluation of Multiple M-Shell Vacancies in the Decays of $^{241}Am$ and $^{249}Cf$

Numerical calculations of the vacancy distributions in the decay of $^{241}Am$ due to internal conversion of the individual gamma rays, the result of which is given in Table 16, are mainly based on photon intensities measured by Lederer et al. (40) and on conversion coefficient data from Yamazaki and Hollander (43). Where experimental information on the conversion coefficients is inadequate or is completely missing (i.e. for the 33.2, 43.4, and 55.6 keV M1+E2 transitions and the 26.4 keV E1 transition), theoretical values of Hager and Seltzer (55) and Dragoun, Pauli, and Schmutzler (61) were used. Because the multipole mixing ratios are well known, the theoretical values are expected to be rather accurate, except for the anomalous E1 transitions, for which they are too low. For the 59.5 keV E1 transition, the theoretical $L_1$-, $L_2$-, and $L_3$-conversion coefficients must be multiplied by factors 1.7, 3.0, and 1.1, respectively, to get agreement with experiment. These same factors were used to determine the L-subshell conversion coefficients for the anomalous 26.4 keV E1 transition from the theoretical values. Because the total excitation of the nuclear levels above 158.5 keV is less than 0.03 percent, transitions from these levels were neglected, as well as some very low intensity transitions ($<$ 0.02 percent) between lower levels.

Vacancy distributions arising in the decay of $^{249}Cf$ are given in Table 17. Calculation of the direct ionization ($N_i'$) is based on experimental work by Ahmad (47). Theoretical conversion coefficients from Refs. (55) and (61) were used when experimental information was missing. The total original distribution $\sum N_i$ (including vacancies shifted from the K

shell) was calculated using the measured $K_{\alpha_1}/K_{\alpha_2}$ x-ray intensity ratio by Hansen et al. (17), the Auger effect being neglected.

Table 16. Original ($N_j$) and Final ($V_j$) L-Shell Vacancy Distribution[a] and Direct M-Shell Ionization ($N'_M$)[a] Arising from Internal Conversion of Various Gamma Transitions in Decay of $^{241}Am$ (Vacancies/100 Decays)

| keV | $N_1$ | $N_2$ | $N_3$ | $V_2$ | $V_3$ | $N'_M$ |
|---|---|---|---|---|---|---|
| 59.5 | 8.62 | 16.80 | 4.70 | 17.66 | 14.74 | 8.10 |
| 43.4 | 2.64 | 5.01 | 2.76 | 5.27 | 5.79 | 2.30 |
| 55.6 | 0.33 | 0.46 | 0.26 | 0.49 | 0.59 | 0.25 |
| 99.0 | 0.01 | 0.29 | 0.16 | 0.29 | 0.27 | 0.14 |
| 26.4 | 1.03 | 13.30 | 3.70 | 13.40 | 8.30 | 3.96 |
| 33.2 | 1.30 | 0.57 | 0.22 | 0.70 | 1.14 | 0.46 |
| Total | 13.93 | 36.43 | 11.80 | 37.81 | 30.83 | 15.21 |

[a] Values in this table are accurate to about 10 percent.

Table 17. Directly-Produced ($N_j'$), Original ($N_j^X$), and Final ($V_j$) Vacancy Distributions in the K and L Shells Arising from Internal Conversion of Various Gamma Rays in Decay of $^{249}Cf$ (Vacancies/100 Decays)

| keV | $N_K$ | $N_1'$ | $N_2'$ | $N_3'$ | $N_M'$ | $N_2$ | $N_3$ | $V_2$ | $V_3$ |
|---|---|---|---|---|---|---|---|---|---|
| 43 | | 1.6 ± 0.5 | 1.0 ± 0.3 | 0.7 ± 0.2 | 0.83 | 1.0 ± 0.3 | 0.7 ± 0.2 | 1.1 ± 0.3 | 1.7 ± 0.3 |
| 55 | | 4.6 ± 1.0 | 6.6 ± 1.3 | 4.8 ± 1.0 | 4.1 | 6.6 ± 1.3 | 4.8 ± 1.0 | 6.8 ± 1.4 | 8.4 ± 1.3 |
| 241 | 0.51 ± 0.08 | 0.01 | | | | 0.14 | 0.23 | 0.14 | 0.17 |
| 253 | 4.3 ± 0.7 | 0.9 | 0.1 | | 0.18 | 1.26 | 1.93 ± 0.3 | 1.26 ± 0.2 | 2.63 ± 0.4 |
| 296 | 0.17 ± 0.03 | | | | | 0.05 | 0.07 | 0.05 | 0.08 |
| 333 | 0.7 | 0.09 | 0.07 | | 0.05 | 0.26 | 0.31 | 0.26 | 0.41 |
| 388 | 2.9 ± 0.4 | 0.38 | 0.25 | 0.03 | 0.25 | 1.02 | 1.36 | 1.04 | 1.74 |
| Sum | 8.6 ± 0.8 | 7.6 ± 1.1 | 8.0 ± 1.3 | 5.5 ± 1.0 | 5.4 | 10.3 ± 1.4 | 9.4 ± 1.3 | 10.5 ± 1.5 | 15.1 ± 1.7 |

For calculation of the final vacancy distribution from eqs. (5), and of the quantities $n_{X_jM}$ from eqs. (27), values of fluorescence, Auger, and CK yields for L subshells are needed. To obtain accurate values for these L-subshell quantities is difficult due to the lack of theoretical calculations and to the scarcity of good experimental points in the high-Z region. Experimental and theoretical values of the $L_1$-subshell quantities above Z=80 and on $L_2$- and $L_3$-subshell quantities above Z=90, are given in Tables 18 and 19, respectively. The values adopted for this work both at Z=93 and Z=96 are given at the bottom of these tables. The $L_1$ quantities for Np are essentially from Akalaev, Vartanov, and Samoilov (72), since they seem to fit into the general picture for this Z region. The value for $\omega_3$ was selected mainly on the basis of the accurate measurements at Z=92 (74) and Z=96 (80). The value of $f_{23}$ is a compromise between the high values at Z=92 and 94 by Byrne et al. (77) and the low values at Z=96, measured by McGeorge (80) and at Z=93, calculated nonrelativistically by Crasemann (78). The value adopted for $\omega_2$ covers both recent experimental results for neighboring elements (74,80) and the theoretical point calculated nonrelativistically for Np (78). The Auger yields are computed on the basis of eq. (1).

Numerical values for the x-ray intensity ratios needed in eqs. (27) and obtained from Ref. (10) by extrapolating from Z=92, are given in Table 20. These values are expected to be accurate within a few percent.

A nonrelativistic calculation of nonradiative transition rates by McGuire (23) was used to obtain the Auger intensity ratios for eq. (27). The magnitude of the error introduced by the nonrelativistic approach in

Table 18. Present Experimental and Calculated Information on $L_1$-Subshell Quantities above Z=80

| Z | $a_1$ | $\omega_1$ | $f_{12}$ | $f_{13}$ | Ref. |
|---|---|---|---|---|---|
| 81 | | 0.09 | | | (62) |
| | 0.16 | 0.11 ± 0.025 | 0.17 ± 0.05 | 0.56 ± 0.07 | (63) |
| | | | | 0.57 ± 0.10 | (64) |
| | | | | 0.76 ± 0.10 | (65) |
| | 0.27 | 0.07 ± 0.02 | 0.14 ± 0.03 | 0.56 ± 0.05 | (66) |
| 82 | | 0.09 ± 0.02 | 0.17 ± 0.05 | 0.61 ± 0.08 | (67) |
| | | | 0.16 | 0.60 | (62) |
| 83 | 0.11 | 0.11 | 0.16 | 0.62 | (68) |
| | 0.11 | 0.12 ± 0.01 | 0.19 ± 0.05 | 0.58 ± 0.05 | (69) |
| | | | 0.19 | 0.58 | (70) |
| | 0.133 ± 0.009 | 0.095 ± 0.005 | 0.18 ± 0.02 | 0.58 ± 0.02 | (71) |
| | 0.155 | 0.120 | 0.069 | 0.656 | (23)[a] |
| 90 | 0.159 | 0.197 | 0.069 | 0.575 | (23)[a] |
| 93 | 0.16 ± 0.03 | 0.19 ± 0.04 | 0.10[b] | 0.55 ± 0.09 | (72) |
| 93 | 0.16 ± 0.11 | 0.19 ± 0.04 | 0.10 ± 0.05 | 0.55 ± 0.09 | c |
| 96 | 0.24 ± 0.11 | 0.21 ± 0.04 | 0.05 ± 0.05 | 0.50 ± 0.09 | c |

[a] Theoretical calculation.

[b] Adopted for calculation of the other values.

[c] Value assumed for this work.

Table 19. Present Experimental and Calculated Information on $L_2$- and $L_3$-Subshell Quantities above Z=90

| Z | $a_2$ | $\omega_2$ | $f_{23}$ | $\omega_3$ | Ref. |
|---|---|---|---|---|---|
| 90 | | 0.56 | | 0.39 | (62) |
| | | | | 0.42 | (73) |
| | 0.397 | 0.473 ± 0.080 | 0.13 ± 0.13[b] | 0.517 ± 0.043 | (74) |
| | 0.369 | 0.529 | 0.102 | 0.461 | (23)[a] |
| 91 | 0.45 | 0.55 ± 0.06 | 0[b] | 0.46 ± 0.05 | (75) |
| 92 | | 0.59 | | 0.41 | (62) |
| | | | | 0.44 | (76) |
| | 0.325 | 0.545 ± 0.081 | 0.13 ± 0.13[b] | 0.500 ± 0.040 | (74) |
| | 0.08 ± 0.01 | 0.516 ± 0.040 | 0.40 ± 0.07 | | (77) |
| 93 | 0.20 ± 0.06 | 0.78 ± 0.19 | 0.02 ± 0.05 | 0.57 ± 0.18 | (72) |
| | 0.331 | 0.460 | 0.209 | | (78)[a] |
| 94 | | 0.413 ± 0.02 | | | (79) |
| | 0.11 ± 0.08 | 0.466 ± 0.023 | 0.42 ± 0.08 | | (77) |
| 96 | 0.23 ± 0.09 | 0.58 ± 0.06 | 0.19 ± 0.04 | 0.54 ± 0.05 | (80) |
| 93 | 0.20 ± 0.11 | 0.50 ± 0.04 | 0.30 ± 0.10 | 0.51 ± 0.05 | c |
| 96 | 0.23 ± 0.09 | 0.58 ± 0.06 | 0.19 ± 0.04 | 0.54 ± 0.05 | c |

[a]Theoretical calculation.

[b]Adopted value for calculation of $\omega_2$ from $\nu_2$.

[c]Value Assumed for this work.

Table 20. The Fractions of $L_3$, $L_2$, $L_1$, and K X Rays of Np and Cm Resulting in M-Shell Ionization and $L_3$- and $L_2$-Subshell Ionization (10)

| | Np | Cm |
|---|---|---|
| $\frac{I(L_3\text{-}M)}{I(L_3\text{-}X)}$ | 0.796 | 0.798 |
| $\frac{I(L_2\text{-}M)}{I(L_2\text{-}X)}$ | 0.782 | 0.777 |
| $\frac{I(L_1\text{-}M)}{I(L_1\text{-}X)}$ | 0.693 | 0.685 |
| $\frac{I(K\text{-}M)}{I(K\text{-}X)}$ | | 0.168 |
| $\frac{I(K\text{-}L_3)}{I(K\text{-}X)}$ | | 0.474 |
| $\frac{I(K\text{-}L_2)}{I(K\text{-}X)}$ | | 0.300 |

calculation is uncertain at high Z. However, a comparison of the ratios $I(L_3\text{-MX})/I(L_3\text{-XY})$ and $I(L_3\text{-MN})/I(L_3\text{-XY})$ calculated at Z=90 with those obtained from the measurements by Zender, Pou, and Aldridge (81) at Z=92 shows good agreement. The ratios of interest, as obtained from Ref. (23) at Z=90 are given in Table 21.

Table 21. The Fractions of $L_3$-, $L_2$-, and $L_1$-Auger Transition Rates Resulting in M-Shell Ionization[a)]

| | Z=90[b)] | Z=92[c)] |
|---|---|---|
| $\frac{I(L_3\text{-MM})}{I(L_3\text{-XY})}$ | 0.63 | 0.70 ± 0.6 |
| $\frac{I(L_3\text{-MX})}{I(L_3\text{-XY})}$ | 0.34 | 0.30 ± 0.5 |
| $\frac{I(L_2\text{-MM})}{I(L_2\text{-XY})}$ | 0.67 | |
| $\frac{I(L_2\text{-MX})}{I(L_2\text{-XY})}$ | 0.30 | |
| $\frac{I(L_1\text{-MM})}{I(L_1\text{-XY})}$ | 0.68 | |
| $\frac{I(L_1\text{-MX})}{I(L_1\text{-XY})}$ | 0.29 | |

a) Results for Z=90 are used for Np(Z=93) and Cm(Z=96).

b) Ref. (23).

c) Ref. (81).

It has been assumed that the small energy adjustment described in Ref. (23) affects only the L-MM transition rates. Since the ratios vary slowly with Z, the values obtained at Z=90 are used both for Np (Z=93) and Cm (Z=96).

It is expected that the transitions $L_1$-$L_3M$ and $L_2$-$L_3M$ are the dominant CK transitions when they are energetically allowed. Using the theoretically calculated curve (27) of $I(L_1\text{-}L_3X)$ versus Z as a guide, the following intensity ratios are estimated for Np and Cm

$$\frac{I(L_1\text{-}L_3M)}{I(L_1\text{-}L_3X)} = 0.8 \pm 0.1$$

$$\frac{I(L_2\text{-}L_3M)}{I(L_2\text{-}L_3X)} = 0.7 \pm 0.2$$

The latter ratio is smaller because the $L_2$-$L_3M_3$ transition is energetically forbidden, whereas the $L_1$-$L_3M_3$ transition is allowed.

Using information listed above, the quantities $n_{X_jM}$ can be calculated. The results are given in Table 22, together with theoretical values by McGuire (27) at Z=90. The agreement is seen to be excellent. For error analysis it has been assumed that the Auger-intensity ratios are accurate to within 10 percent.

It is now possible to evaluate the values of the quantities $m_{ej}^X$ and $m_{nj}^X$ from eqs. (15), (16), and (26). The following results for $m_{e3}$ in the decay of $^{241}$Am and $^{249}$Cf are obtained:

$$m_{e3}\ (^{241}\text{Am}) = 0.46 \pm 0.10$$

$$m_{e3}\ (^{249}\text{Cf}) = 0.29 \pm 0.08$$

Table 22. Values of Quantities $n_{X_jM}$ for Np (Z=93) and Cm (Z=96) Obtained Here, Compared to Theoretical Values at Z=90

| | Np | Cm | Z=90 |
|---|---|---|---|
| $n_{L_3M}$ | 1.19 ± 0.08 | 1.17 ± 0.08 | 1.23 |
| $n_{L_2M}$ | 1.29 ± 0.19 | 1.18 ± 0.19 | 1.22 |
| $n_{L_1M}$ | 1.62 ± 0.19 | 1.59 ± 0.19 | 1.61 |
| $n_{KM}$ | | 1.06 ± 0.06 | |

As a numerical example of the calculation of the quantity $m^X_{nj}$, the fraction of $m'_{nj}$ arising from the cascade 46.4 keV-(gamma 1)-59.5 keV (gamma 2) in $^{241}$Am decay is calculated below. Because essentially every decay feeds the 59.5 keV level, A in eq. (16) is unity. Using Tables (16) and (22), one obtains

$$b_2 = 49.3 \pm 4.6$$

$$b_1 = 16.3 \pm 1.4$$

and eq. (16) gives

$$m'_{n1} = 0.127 \pm 0.022$$

$$m'_{n2} = 0.145 \pm 0.025$$

$$m'_{n3} = 0.171 \pm 0.029$$

When all the contributions from different cascades are added, the values

of the quantity $m^X_{nj}$ given in Table 23 are obtained in the decays of $^{241}Am$ and $^{249}Cf$. This Table 23 also summarizes the results of this Appendix, giving the total, calculated number of M-shell vacancies in coincidence with K-M and L-M x rays, i.e. the factor $(1+m^X_j)$ to be applied in eq. (13).

Table 23. Total Number of M-Shell Vacancies in Coincidence with K-M and L-M X Rays Calculated for the Decays of $^{241}Am$ and $^{249}Cf$, and the Contributions due to Electronic and Nuclear Cascading

| | Gating x ray | $m_{ej}$ | $m^X_{nj}$ [a] | $1+m^X_j$ |
|---|---|---|---|---|
| $^{241}Am$ | $L_1$-M | | 0.41 ± 0.07 | 1.41 ± 0.13 |
| | $L_2$-M | | 0.45 ± 0.07 | 1.45 ± 0.07 |
| | $L_3$-M | 0.46 ± 0.10 | 0.48 ± 0.08 | 1.94 ± 0.13 |
| $^{249}Cf$ | K-M | | 0.49 ± 0.14 | 1.49 ± 0.14 |
| | $L_1$-M | | 0.30 ± 0.09 | 1.30 ± 0.09 |
| | $L_2$-M | | 0.29 ± 0.09 | 1.29 ± 0.09 |
| | $L_3$-M | 0.29 ± 0.06 | 0.32 ± 0.09 | 1.61 ± 0.12 |

[a] Relative accuracy of these numbers is about 10 percent for $^{241}Am$ and about 20 percent for $^{249}Cf$.

Because the factors $b_1$ and $b_2$ in eq. (16) are the same for all subshells and major shells, the accuracy of the quantities $n^X_{nj}$, relative to each other, is determined by the accuracy of the vacancy distribution $V^X_j$

which is known to 10 percent in the decay of $^{241}Am$ and to about 20 percent in the decay of $^{249}Cf$.

The maximum contribution of the K-Auger terms in eqs. (24) and (27) to the total vacancy multiplication in the M shell can be estimated by assuming that every K-Auger transition creates two L-shell vacancies. Because the K-Auger yield is about 0.025 at Z=96, the number of L-shell vacancies created is 0.4 per 100 decays. The highest number of multiple M-shell vacancies created in the K-Auger processes occurs in coincidence with $L_3$ x rays. The upper limit to this number is found by considering e.g. the sequence K-$L_1L_1$, $L_1$-$L_3M$, $L_1$-MM which gives four M-shell vacancies in coincidence with the $L_3$-M x ray filling this particular $L_3$ vacancy. Of 0.4 $L_1$-subshell vacancies due to the K-Auger effect, 0.1 can shift to the $L_3$ subshell, where they contribute 0.7 percent of the vacancies. Because a maximum of 2.6 $(1+n_{L_1M})$ M-shell vacancies are actually associated with them, a maximum of 0.02 M-shell vacancies due to the K-Auger effect are in coincidence with an average $L_3$ x ray. This contribution is, therefore, negligible.

# APPENDIX II

## "THE K-FLUORESCENCE YIELD OF Te AND THE TOTAL AND K-SHELL CONVERSION COEFFICIENTS OF THE 35.48 keV TRANSITION IN $^{125}$I DECAY"

3.B:3.C *Nuclear Physics* A131 (1969) 343—352; 

# THE K-FLUORESCENCE YIELD OF Te AND THE TOTAL AND K-SHELL CONVERSION COEFFICIENTS OF THE 35.48 keV TRANSITION IN $^{125}$I DECAY

E. KARTTUNEN †, H. U. FREUND and R. W. FINK
*School of Chemistry, Georgia Institute of Technology, Atlanta, Georgia, USA* ††

Received 17 March 1969

**Abstract:** High-resolution Ge(Li) X-ray spectrometers were used in the singles and coincidence modes to determine the K-fluorescence yield of Te from carrier-free sources of $^{125}$I. The same experiments give the total and K-shell conversion coefficients of the 35.48 keV transition in $^{125}$Te. The values found for $\omega_K$, $\alpha_T$ and $\alpha_K$ are $0.859\pm0.022$, $13.65\pm0.55$ and $12.01\pm0.36$, respectively, assuming that the K-capture probability in $^{125}$I decay is $P_K = 0.797\pm0.003$. The values of $\alpha_T$ and $\alpha_K$ agree with the theoretical prediction of Hager and Seltzer for an M1 transition with less than 0.4 % E2 admixture.

E RADIOACTIVITY $^{125}$I; measured $I_\gamma$, $I_K$, $x\gamma$-, xx-coin, cc. Ge(Li) detector.
ATOMIC PHYSICS Te; measured K-fluoresence yield.

## 1. Introduction

Critical review [1]) of K-fluorescence yield measurements reveals discrepancies between theoretical and experimental values of $\omega_K$ and among various experimental values. For $Z > 50$, the theoretical predictions are larger, and in the region of $20 < Z < 30$, smaller than the best available experimental values. Owing to the great practical importance of K-fluorescence yields and the scarcity of very accurate $\omega_K$ measurements above $Z = 30$, it is of interest to make additional measurements with high accuracy ($< 4\,\%$). In the present work, the value of $\omega_K$ at $Z = 52$ has been determined to better than 2.6 %.

## 2. Basis of the experiments

The nucleide $^{125}$I decays by electron capture with $60.25\pm0.06$ d half-life [2]) to the first excited state of $^{125}$Te. The decay scheme is shown in fig. 1. Together with table 1, it gives a summary of the known data on the decay of $^{125}$I.

The vacancies leading to K X-ray emission are created by K-capture and the K conversion of the prompt 35.48 keV transition following electron capture. Values of

† School of Nuclear Engineering.
†† Work supported in part by the US Atomic Energy Commission.

the K-conversion coefficient $\alpha_K$, the total conversion coefficient $\alpha_T$, the probability of K-capture $P_K$ and the K-fluorescence yield $\omega_K$ constitute therefore a set of interconnected data, and it is not possible to measure $\omega_K$ without adopting a value for at

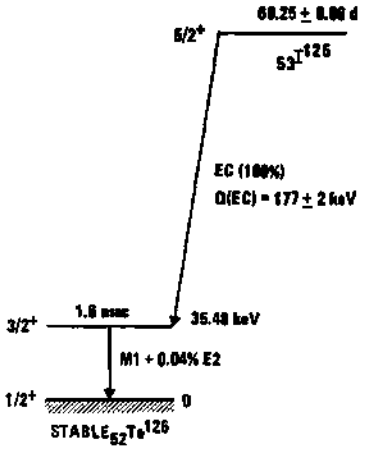


Fig. 1. Decay scheme of $^{125}$I.

TABLE 1

Known data on the decay of $^{125}$I

| Quantity | Value | Ref. | Method and remarks |
|---|---|---|---|
| $P_{(L+M+..)}/P_K$ | 0.2543±0.0027 | [2] | internal source in NaI(Tl) crystals |
| $P_{(L+M+..)}/P_K$ | 0.253 ±0.005 | [3] | internal source in NaI(Tl) crystals |
| $Q_{EC}$ | 177±2 keV | [7] | IB endpoint with Ge(Li) detector |
| $P_{(L+M+..)}/P_K$ | 0.238 ±0.014 | | calculated in present work from $Q_{EC}$ according to Behrens [8] |

| Conversion electron data | | Ref. | Method and remarks |
|---|---|---|---|
| K : L : M : N | (80±5) : (11±2) : (1.70±0.4) : (0.3±0.1) | [9, 10] | lens spectr., prop. counter coinc., mag. spectr. |
| K : L : M | 80 : 10.7 : 2.2 | | calcd. for pure M1 from Hager and Seltzer [5] |
| $L_1 : L_2 : L_3$ | 100 : 7.9 : 2.0 | | calcd. for pure M1 from Hager and Seltzer [5] |
| $L_1 : L_2 : L_3$ | 100 : (8.9±0.4) : (2.4±0.2) | [6] | mag. spectr. with momentum resolution 0.2 % |
| $\alpha_{K+L+M+N}$ | 13.3±1.8 | | calcd. from conv. ratio of refs. [9, 10] |
| $\alpha_{K+L+M}$ | 13.9 | | calcd. for pure M1 from Hager and Seltzer [5] |
| $\alpha_K$ | 11.4±2.5 | [9] | |
| $\alpha_K$ | 12.0 | | calcd. for pure M1 from Hager and Seltzer [5] |
| $\omega_K$(Te) | 0.872 | [11] | ioniz. chamber |

least one of the other quantities. It is essential, therefore, to have a consistent set of values for these quantities. By using the precisely known value of $P_K$ taken from the

accurate $(P_{L+M+\ldots})/P_K$ ratios of Leutz and Ziegler [2]) and Smith [3]) (see table 1), the other three quantities are obtained in this experiment in the following way.

(i) Comparing the intensities of the K X-rays and the 35.48 keV $\gamma$-ray, one can determine $\omega_K$ if $P_K$, $\alpha_K$ and $\alpha_T$ are known from the following equation:

$$\omega_K = \frac{\varepsilon_\gamma}{\varepsilon_K} \frac{C_K}{C_\gamma} \frac{1}{P_K(1+\alpha_T)+\alpha_K}. \tag{1}$$

The notation used here and in the following equations is $\varepsilon_\gamma$ and $\varepsilon_K$ are the detection probabilities for the $\gamma$-ray and K X-rays, respectively, $C_\gamma$ and $C_K$ the counting rates in the $\gamma$-peak and the $K_\alpha+K_\beta$ X-ray peaks, respectively, $C_{\gamma(K)}$, $C_{K(K)}$ and $C_{K(\gamma)}$ the coincidence counting rates for the peak of the first subscript where the second subscript in parentheses represents the peak taken in the coincidence gate; indices 1 and 2 refer to Ge(Li) detectors 1 and 2, respectively.

(ii) By measuring coincidences between K X-rays and the $\gamma$-ray, it is possible to eliminate the dependency of $\omega_K$ on the conversion coefficients, since no coincidences can occur with X-rays created by internal conversion. This method has been applied extensively to measure the product $P_K\omega_K$. Comparison of the coincidence rates $C_{K(\gamma)}$ and $C_{\gamma(K)}$ with the singles counting rates give the following equations:

$$P_K\omega_K = \frac{1}{\varepsilon_{K(2)}} \frac{C_{K(\gamma)(2)}}{C_{\gamma(1)}}, \tag{2}$$

$$P_K\omega_K = \frac{1}{\varepsilon_{K(1)}} \frac{C_{\gamma(K)(2)}}{C_{\gamma(2)}}. \tag{3}$$

(iii) The true coincidences between the K X-rays originating in radiative filling of two K-vacancies simultaneously created by K-capture and succeeding K-conversion can also be used advantageously. It is readily shown that the ratio of the two coincidence counting rates $C_{K(K)}$ and $C_{\gamma(K)}$ gives

$$\alpha_K\omega_K = \frac{1}{2} \frac{\varepsilon_{\gamma(2)}}{\varepsilon_{K(2)}} \frac{C_{K(K)(2)}}{C_{\gamma(K)(2)}}. \tag{4}$$

(iv) A fourth method depends on the summing in one detector of true coincident events which gives another independent equation. The sum spectrum $C_{K_\alpha+K_\alpha}$ together with the singles spectrum $C_{K_\alpha}$ in the same detector can be combined to give

$$\omega_K = \left[\frac{1+\alpha_T}{\alpha_K} + \frac{1}{P_K}\right] \frac{1}{2\varepsilon_K} \frac{[C_{(K_\alpha+K_\beta)}+2C_{(K_\alpha+K_\alpha)}]}{C_{K_\alpha}}. \tag{5}$$

If the value of $P_K$ is adopted from previous measurements [2,3]), then $\omega_K$ can be found from eqs. (2) and (3). Inserting this value of $\omega_K$ into eq. (4), the value of $\alpha_K$ can be determined, and eq. (1) can now be used to find the value of $\alpha_T$.

Eqs. (1)-(4) are rather convenient to use, because they contain only ratios of counting rates and, with the exception of eqs. (2) and (3), ratios of efficiencies, which are easier to measure accurately than are absolute counting rates and efficiencies. In fact only the absolute K X-ray efficiency of *one* detector is needed, since with the source in a fixed geometry, the singles spectra taken in each detector together with the coincidence spectra give the following ratio relationship:

$$\frac{\varepsilon_{K(1)}}{\varepsilon_{K(2)}} = \frac{C_{K(1)}}{C_{K(2)}}. \tag{6}$$

Eq. (6) together with eqs. (2) and (3) give an expression to prove consistency between the singles and the coincidence counting rates

$$\frac{C_{\gamma(2)}}{C_{\gamma(1)}} \frac{C_{K(1)}}{C_{K(2)}} \frac{C_{K(\gamma)(2)}}{C_{\gamma(K)(2)}} = 1. \tag{7}$$

## 3. Experimental procedure

### 3.1. RADIOACTIVE SOURCE

Sources were prepared from an aqueous solution of carrier-free $^{125}$I produced by means of the $^{124}$Xe(n, $\gamma$)$^{125}$Xe(EC)$^{125}$I reaction-decay sequence †. Several sources deposited on plastic backings had to be abandoned, since the $^{125}$I activity tends to oxidize to the free state and to migrate into and through the plastic backings. However, sources prepared on $HNO_3$ etched copper backings were found to be stable (probably due to formation of $Cu_2I_2$ compound which chemically fixes the iodine to the copper planchet). The source used throughout these measurements consisted of 0.45 $\mu$C of $^{125}$I deposited onto a 2.26 mg/cm$^2$ copper backing, and it was covered by about 400 $\mu$g/cm$^2$ krylon which was sprayed on. The source was 3-4 mm in diam. and invisible.

### 3.2. DETECTORS AND ELECTRONIC SYSTEM

Two very similar Ge(Li) X-ray detectors ( 8 mm diam. × 5 mm deep) †† were used to detect the $\gamma$-rays and K X-rays. The energy resolution in the region of 26 keV was 500 eV (detector 1) and 440 eV (detector 2) FWHM. A thin gold layer forms the $p^+$ surface barrier contact and together with a 0.25 mm beryllium window serves as an almost absorption-free detector window for energies above about 20 keV.

The block diagram for the coincidence setup is shown in fig. 2. The detector pulses were fed through highly stable low noise (10 $\mu$V at maximum gain and 0.07 % linearity) linear systems to meet the requirements for high-resolution Ge(Li) spectroscopy. The single-channel analysers (SCA) extracted a narrow pulse-height band with negligible drift (< 2 channels) over a period of 3 weeks. By using the routing facility

† Supplied by New England Nuclear Corp., Boston, Massachusetts.
†† Produced by ORTEC Inc., Models 8013 and 8113.

of the Nuclear Data 512-channel analyser, two coincidence spectra were stored simultaneously in the two halves of the memory gated by K- and γ-coincidence events, respectively. The two SCA output pulse rates were monitored with two timer-scaler-printer units using a time cycle of 40 min to check variations of geometry or the SCA

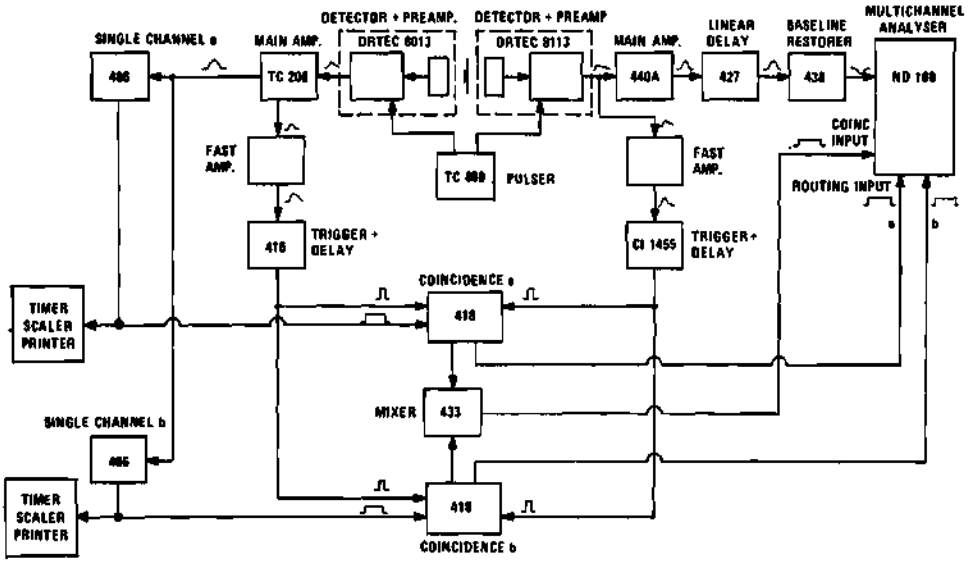


Fig. 2. Block diagram for the coincidence measurements. The detector systems ORTEC 8013 and 8113 are referred to by indices (1) and (2), respectively, in the text. Numbers in blocks are ORTEC module numbers.

window position stability. Two coincidence runs were made with resolving times of 1 μsec and 2 μsec, each followed by a chance coincidence run. The coincidence leading edge timing was set with pulses from a Tennelec TC-800 pulser (see fig. 2). Prompt resolution of the true pulses was measured by taking a time-to-pulse height converter spectrum. The latter showed a time distribution of 50 nsec and 110 nsec for the full width at half-maximum and tenth-maximum, respectively. Thus, the prompt coincidences are well enveloped by both coincidence resolving times † of 1 and 2 μsec. This was verified by the experimental results using eq. (7) which yields a ratio of $C_{\gamma(2)}/C_{\gamma(1)}$ of $1.020 \pm 0.012$ and $1.015 \pm 0.012$, respectively, for the two runs. The errors are the standard deviations. Singles and coincidence spectra are shown in fig. 3.

### 3.3. DETECTION EFFICIENCY

The coincidence measurements were carried out with source-to-detector surface distances of 14 and 16 mm, respectively. Absolute efficiency calibration was done at

† The coincidence resolving time was taken large compared to the prompt resolution of true coincidence pulses, in order to include all degraded pulses which are slower and result in a small tail in the time-to-pulse-height converter curve. This permits application of the same degradation corrections both to the singles and the coincidence spectra.

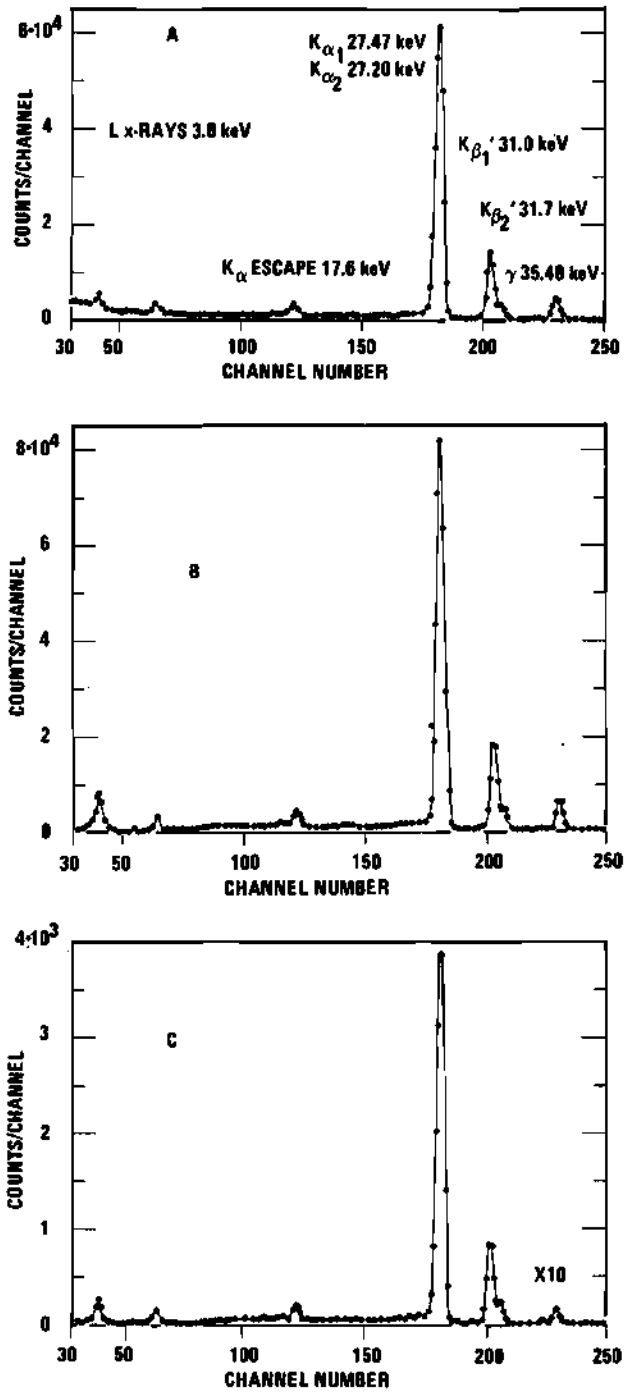


Fig. 3. The X-ray and $\gamma$-ray spectrum of the decay of $^{125}$I. a) Singles spectrum, b) spectrum in coincidence with $K_\alpha + K_\beta$ X-rays, c) spectrum in coincidence with 35.48 keV $\gamma$-rays.

41.8 mm, the larger distance being used to reduce geometry uncertainties. A set of standard sources † was used for calibration, the absolute $\gamma$-decay rates thereof in the energy region of interest being accurate to $\pm 1.8\,\%$ optimal ($^{57}$Co and $^{241}$Am). Detailed investigations have been made to fit a theoretical efficiency curve to the experimental values in the low-energy region [4]) for the two Ge(Li) detectors considering the 0.57 $\mu$m gold and $< 1$ $\mu$m germanium dead-layers on the detector surface and the germanium K X-ray escape from the detector. The mean efficiency for K X-rays was obtained by weighting the efficiencies of the $K_\alpha$ and $K_\beta$ X-rays with their intensities. For the coincidence geometry used, the mean efficiency thus was found to be $\varepsilon_{K(2)} = (9.40 \pm 0.19) \times 10^{-3}$.

The measured radiations are close in energy (27 to 36 keV), and the efficiency curve is essentially flat between 20 and 60 keV. Therefore, the systematic error for the calculated efficiency fitted to experimental points is regarded as negligible. The efficiencies obtained reflect mainly the uncertainty in the calibration sources themselves with a small contribution due to statistical fluctuation in the counting rates.

Care was taken to avoid systematic errors by evaluating the peak intensities in exactly the same manner for both calibration and $^{125}$I spectra. The spectral distribution for a discrete energy in the vicinity of the peak consists of a Gaussian distribution with a flat step-function-like tail which is smoothed by the detector resolution. Only the Gaussian peak was evaluated.

### 3.4. CORRECTIONS

The corrections that have been applied are listed in table 2, and a discussion of errors is given below.

3.4.1. *Background and degraded pulses.* The true background observed with the source removed was low and was subtracted from the spectra. A larger "background" arose from degraded pulses. As explained in the discussion of efficiencies (subsect. 3.3), only the Gaussian peak of the spectral response curve was counted. Therefore, the window intensity had to be corrected for the fraction of degraded true K- or $\gamma$-pulses falling into the window. Included also is a small number of Compton scattered events. These contributions are given in table 2.

3.4.2. *Sum peak losses.* Summing of true coincidence pulses in one detector occurred with about 1 % probability in each detector. The measured and calculated fractions are given in table 2.

3.4.3. *Chance coincidences.* The chance coincidence rates were measured after each coincidence run by inserting a 4 $\mu$sec delay into the logic and linear pulse procession of detector 2 (see fig. 2). The corrections thus obtained are given in table 2.

3.4.4. *Gamma escape peak contribution to the* K *X-ray peaks.* This correction was calculated from the measured escape peak to photopeak ratio for the Ge(Li) detector

† IAEA Standard Sources, Set. No. 31, dated to Jan. 1, 1969.

TABLE 2

Corrections (in percentage) applied to the measured counting rates

| Type of correction | Run no. | $C_{\gamma(1)}$ | $C_{\gamma(2)}$ | $C_{K(1)}$ | $C_{K(2)}$ | $C_{\gamma(K)}$ | $C_{K(K)}$ | $C_{K(\gamma)}$ | Footnote |
|---|---|---|---|---|---|---|---|---|---|
| background under Gaussian peaks | 1 | 3.81±0.19 | 3.51±0.17 | 5.33±0.26 | 5.25±0.26 | 2.32±0.12 | 5.15±0.26 | 4.75±0.24 | |
| | 2 | | | | | 2.28±0.11 | 5.05±0.25 | 4.64±0.23 | |
| chance coincidences | 1 | | | | | 2.19±0.09 | 1.98±0.04 | 2.29±0.09 | |
| | 2 | | | | | 3.52±0.14 | 3.38±0.07 | 3.05±0.12 | |
| sum correction | | 1.06±0.05 | 0.74±0.04 | 0.97±0.02 | 0.66±0.02 | | | | [a] |
| | | 1.01±0.05 | 0.70±0.04 | 1.06±0.05 | 0.69±0.03 | | | | [b] |
| gamma tail in gates | 1 | | | | | | 0.43±0.08 | 3.23±0.16 | [c] |
| | 2 | | | | | | 0.43±0.08 | 3.23±0.16 | [c] |
| K X-ray tail in gates | 1 | | | | | 9.81±0.49 | 9.81±0.49 | | [d] |
| | 2 | | | | | 9.81±0.49 | 9.81±0.49 | | [d] |
| gamma escape peak under $K_\alpha$ X-ray peak | 1 | | | | | | 0.13±0.005 | | |
| | 2 | | | | | | 0.13±0.005 | | |
| decay | 1 | 15.51±0.02 | 15.51±0.02 | 15.51±0.02 | | | | | [e] |
| | 2 | 6.69±0.01 | 6.69±0.01 | 6.69±0.01 | | | | | [e] |
| standard deviation (σ) in counting statistics | 1 | 0.17 | 0.18 | 0.04 | 0.04 | 0.64 | 0.14 | 0.67 | |
| | 2 | | | | | 0.72 | 0.16 | 0.75 | |

[a]) Calculated from sum rates (see subsect. 3.4.2).

[b]) Calculated from efficiency ratios and coincidence rates.

[c]) Contribution of degraded gamma pulses in the K X-ray gate and gamma gate.

[d]) Contribution of degraded K X-ray pulses in the K X-ray gate.

[e]) Correction for decay between the time of the coincidence measurements and the singles spectra runs.

as given in ref. [4]). It could also be estimated by comparing the K X-ray pulse shapes obtained in a singles run and in a $\gamma$-gated coincidence run. The correction found both ways is very small (see table 2).

3.4.5. *Countrate effects: pileup and deadtimes.* Pulse shaping times of 0.8 $\mu$sec (TC-200 amplifier) and 1 $\mu$sec (Ortec 440A amplifier) were used. Fast baseline recovery was obtained by pole-zero cancellation in the Tennelec amplifier and by baseline restoration following the ORTEC 440A amplifier (see fig. 2). The observed total counting rates were $< 250$/sec. Thus, the probability for accidental pulse pileup is $< 10^{-3}$. It is not further considered. Deadtime losses in the SCA and the coincidence logic circuits are $< 5 \times 10^{-4}$. The deadtime of the multi-channel analyser is compensated internally by operating in the "live mode" as was done. The error is $< 0.5\,\%$ at 5000/sec. Therefore, no correction was necessary at the counting rates used.

3.4.6. *Shifts of the SCA window and of geometry.* The window positions of the SCA were set wide enough to cover the Gaussian peak and a small fraction of the degraded pulses. Owing to the almost symmetric spectrum in the region of the $\gamma$-peak, the SCA counting rate shifts measured mainly any source-to-detector geometry changes, while the K X-ray SCA counting rate was sensitive to both SCA window stability and geometry changes. The counting rates were printed every 40 min, and no fluctuations larger than three times the standard deviation ($3\sigma$) occurred. In addition, the SCA window positions were tracked before and after every coincidence measurement. In one case only had the $\gamma$-window moved by as much as $1\frac{1}{2}$ channels giving a small correction to the fraction of the $\gamma$-ray tail included in the window.

3.4.7. *Further corrections.* The exponential decay of the $^{125}$I source gives corrections, which in view of the 0.1 % accuracy in the known half-life, were exact (see table 2).

The absorption in the 2.3 mg/cm$^2$ copper backing was measured. It need not be taken into account, however, since it cancels in all expressions used for evaluating $\omega_K$, $\alpha_K$ and $\alpha_T$.

## 4. Results and discussion

Table 3 gives a summary of the values obtained for $P_K\omega_K$, $\alpha_K\omega_K$ and $\omega_K[\alpha_K + P_K(1+\alpha_T)]$. The value obtained for $\omega_K$ from the sum spectrum it also given, but it is not included in the final result due to its comparatively large error. The final results for $\omega_K$, $\alpha_K$ and $\alpha_T$ are given with an error of twice the standard deviation ($2\sigma$).

The values for $\alpha_T$ and $\alpha_K$ are in agreement with the theoretical values for an M1 + $< 0.4\,\%$ E2 35.48 keV transition in $^{125}$Te obtained from the tables of Hager and Seltzer [5]) and with the much smaller limit of $< 0.03\,\%$ E2 admixture from the $L_1 : L_2 : L_3$ subshell conversion electron ratio measured by Geiger *et al.* [6]) using the same tables.

The value for $\omega_K$(Te) confirms a $1-1\frac{1}{2}\%$ lower $\omega_K$ experimental curve in this $Z$-region than has been predicted by the semi-theoretical calculations of Callan [1]).

TABLE 3
Results

| Measured quantity | Value | Standard deviation $\sigma$ | Standard deviation $2\sigma$ | Equation used | Run no. |
|---|---|---|---|---|---|
| $P_K\omega_K$ | 0.696 | 0.015 | | (2) | 1 |
| | 0.681 | 0.015 | | (2) | 2 |
| | 0.688 | 0.015 | | (3) | 1 |
| | 0.676 | 0.015 | | (3) | 2 |
| average | 0.685 | | ±0.018 | | |
| $\alpha_K\omega_K$ | 10.35 | 0.07 | | (4) | 1 |
| | 10.28 | 0.08 | | (4) | 2 |
| average | 10.31 | | ±0.15 | | |
| $\alpha_K\omega_K+P_K(1+\alpha_T)\omega_K$ | 20.38 | 0.08 | | (1) | (detector 1) |
| | 20.28 | 0.08 | | (1) | (detector 2) |
| average | 20.33 | | ±0.16 | | |
| $\omega_K$(Te) $Z=52$ | 0.805 | 0.055 | | (5) | (detector 1) |
| | 0.815 | 0.057 | | (5) | (detector 2) |
| $\omega_K$ | 0.859 | | ±0.022 | from $(P_K\omega_K)_{average}$ | |
| $\alpha_K$ | 12.01 | | ±0.36 | from $(\alpha_K\omega_K)_{average}$ | |
| $\alpha_T$ | 13.65 | | ±0.55 | from average of $[\alpha_K\omega_K+P_K\omega_K(1+\alpha_T)]$ | |

## References


1) R. W. Fink, R. C. Jopson, H. Mark and C. D. Swift, Revs. Mod. Phys. **38** (1966) 513;
W. Bambynek, B. Crasemann, R. W. Fink, H. U. Freund, H. Mark, R. E. Price, P. V. Rao and C. D. Swift, to be published
2) H. Leutz and K. Ziegler, Nucl. Phys. **50** (1964) 648
3) K. M. Smith and G. M. Lewis, Nucl. Phys. **89** (1966) 561
4) H. U. Freund and R. W. Fink, Phys. Rev., in press;
S. Hansen, H. U. Freund and R. W. Fink, to be published
5) S. Hager and E. C. Seltzer, Nucl. Data **A4** (1968) 1
6) J. S. Geiger, R. L. Graham, I. Bergström and F. Brown, Nucl. Phys. **68** (1965) 352
7) K. P. Gopinathan and W. Rubinson, Bull. Am. Phys. Soc. **13** (1968) 1452
8) H. Behrens and W. Buhring, Proc. Conf. on electron capture and higher order processes in nuclear decay, Debrecen, Hungary, Vol. 1 (Kultura Bookexport, Budapest, 1968) p. 61
9) J. C. Bowe and P. Axel, Phys. Rev. **85** (1952) 858
10) R. S. Narcisi, Harvard University Physics Report No. 2-9 (April, 1959) unpublished
11) I. Backhurst, Phil. Mag. **22** (1936) 757

## LITERATURE CITED*


1. A. H. Compton and S. K. Allison, X-Rays in Theory and Experiment, D. van Nostrand Co., Inc., New York, 1935.

2. E. H. S. Burhop, The Auger Effect and Other Radiationless Transitions, Cambridge University Press, London, 1952.

3. I. Bergstrom and C. Nordling, $\alpha$-, $\beta$-, $\gamma$-Ray Spectroscopy, Vol. 2, 1523 ff (editor: K. Siegbahn), North-Holland Publishing Co., Amsterdam, 1965.

4. W. Mehlhorn, Lectures on the Auger Effect, Behlen Laboratory of Physics, University of Nebraska Publication, 1970.

5. W. Bambynek, B. Crasemann, R. W. Fink, H. U. Freund, Hans Mark, R. E. Price, P. Venugopala Rao, and C. D. Swift, Rev. Mod. Phys. (to be published, 1971).

6. J. L. Powell and B. Crasemann, Quantum Mechanics, Addison-Wesley Publ. Co., Reading, Mass., 1961.

7. E. U. Condon and G. H. Shortley, The Theory of Atomic Spectra, Cambridge University Press, 1959.

8. V. O. Kostroun, M. H. Chen, and B. Crasemann, Phys. Rev. (in press).

9. R. W. Fink, R. C. Jopson, Hans Mark, and C. D. Swift, Rev. Mod. Phys., 38, 513 (1966).

10. J. H. Scofield, Phys. Rev., 179, 9 (1969).

11. H. R. Rosner and C. P. Bhalla, Z. Phys., 231, 347 (1969).

12. C. P. Bhalla, J. Phys., B (London) 3, 916 (1970).

13. D. J. Ramsdale, Thesis, Kansas State University (1969).

14. C. P. Bhalla, H. R. Rosner, and D. J. Ramsdale, J. Phys., B (London) 3, 1232 (1970).

15. D. R. Hartree, The Calculation of Atomic Structures, John Wiley, New York, 1957.


---

*Abbreviations used herein follow the form employed by Nuclear Science Abstracts. See NSA 25, Appendix 25 (January 15, 1971).

LITERATURE CITED (Continued)

16. C. P. Bhalla, Phys. Rev., A 2, 722 (1970).

17. J. S. Hansen, H. U. Freund, and R. W. Fink, Nucl. Phys., A 142, 604 (1970) and A 153, 465 (1970).

18. J. C. Nelson, S. I. Salem, and B. G. Saunders, At. Data (1971) (in press).

19. P. Venugopala Rao, J. M. Palms, and R. E. Wood (to be published).

20. C. P. Bhalla, D. J. Ramsdale, and H. R. Rosner, Phys. Lett., A 31, 122 (1970).

21. E. J. McGuire, Phys. Rev., 185, 1 (1969).

22. E. J. McGuire, Phys. Rev., A1, 8 (1971).

23. E. J. McGuire, Phys. Rev., A (1971) (in press).

24. V. O. Kostroun, M. H. Chen, and B. Crasemann (to be published).

25. B. Talukdar and D. Chattarji, Phys. Rev., A1, 33 (1970).

26. C. P. Bhalla, Phys. Rev., A2, 2575 (1970).

27. R. A. Rubenstein, Thesis, University of Illinois (1955) (unpublished).

28. E. G. Ramberg and F. K. Richtmeyer, Phys. Rev., 51, 913 (1937).

29. H. Lay, Z. Phys., 91, 533 (1934).

30. A. A. Jaffe, Bull. Res. Council (Israel) 3, 316 (1954); see Phys. Abstr., 58, 360, No. 2782 (1955).

31. A. A. Konstantinov and T. E. Sazanova, Bull. Acad. Sci. USSR, Phys., 32, 58 (1968).

32. R. C. Jopson, Hans Mark, C. D. Swift, and M. A. Williamson, Phys. Rev., 137, A1353 (1965).

33. B. L. Robinson and R. W. Fink, Rev. Mod. Phys., 27, 424 (1955) and 32, 117 (1960).

34. H. U. Freund and R. W. Fink, Phys. Rev., 183, 1055 (1969).

LITERATURE CITED (Continued)


35. H. U. Freund, J. S. Hansen, E. Karttunen, and R. W. Fink, Proceedings of the International Conference on Radioactivity in Nuclear Spectroscopy, Nashville, Tennessee, Aug. 11-15 (1969) (to be published).

36. D. Nix, J. C. McGeorge, and R. W. Fink (to be published).

37. H. Genz, J. P. Renier, and R. W. Fink (in Ref. 35).

38. C. M. Lederer, J. M. Hollander, and I. Perlman, Table of Isotopes, John Wiley & Sons, Inc., New York, 1967.

39. S. A. Baranov, V. M. Kulakov, and V. M. Shatinsky, Nucl. Phys., 56, 252 (1964).

40. C. M. Lederer, J. K. Poggenburg, F. Asaro, J. O. Rasmussen, and I. Perlman, Nucl. Phys., 84, 481 (1966).

41. W. Michaelis, Z. Phys., 194, 395 (1966).

42. C. Gunther and D. R. Parsignault, Nucl. Phys., A 104, 588 (1967).

43. T. Yamazaki and J. M. Hollander, Nucl. Phys., 84, 505 (1966).

44. J. L. Wolfson and J. J. H. Park, Can. J. Phys., 42, 1387 (1964).

45. S. A. Baranov, V. M. Shatinskii, and V. M. Kulakov, Sov. J. Nucl. Phys., 10, 513 (1969).

46. J. Kooi and A. H. Wapstra, J. Inorg. Nucl. Chem., 29, 293 (1967).

47. I. Ahmad, Ph.D. Thesis, University of California, Berkeley (1966).

48. W. D. Schmidt-Ott (private communication) (1971).

49. V. M. J. Veigele, E. Briggs, B. Bracewell, and M. Donaldson, X-Ray Cross Section Compilation, Report No. KN-798-69-2(R) (Kaman Nuclear Corporation)(1969)(unpublished).

50. H. U. Freund and J. C. McGeorge, Z. Phys., 238, 6 (1970).

51. R. A. Buckingham, Numerical Methods, 241 ff, Sir Isaac Pitman & Sons Ltd., London, 1962.

52. H. Genz, D. S. Harmer, and R. W. Fink, Nucl. Instrum. Methods, 60, 195 (1967).

LITERATURE CITED (Continued)


53. I. Backhurst, Phil. Mag., 22, 757 (1936).

54. J. C. Bowe and P. Axel, Phys. Rev., 85, 858 (1952).

55. S. Hager and E. C. Seltzer, Nucl. Data,Sect. A4, 1 (1968).

56. J. A. Bearden, Rev. Mod. Phys., 39, 78 (1967).

57. W. Rubinson, Phys. Rev., 130, 2011 (1963).

58. W. Mehlhorn, Z. Phys., 187, 21 (1965).

59. H. U. Freund, E. Karttunen, and R. W. Fink, Bull. Am. Phys. Soc., Ser. II, 15, 1305 (1970).

60. T. H. Tomboulian, Phys. Rev., 74, 1887 (1948).

61. O. Dragoun, H. C. Pauli, and F. Schmutzler, Nucl. Data, A6, 235 (1969).

62. B. B. Kinsey, Can. J. Res., A26, 404 and 421 (1948).

63. Z. Sujkowski and O. Melin, Ark. Fys., 20, 193 (1961).

64. L. Persson and Z. Sujkowski, Ark. Fys., 19, 309 (1961).

65. J. G. Ferreira, M. O. Costa, M. I. Goncalves, and L. Salgueiro, J. Phys. (Paris), 26, 5 (1965).

66. R. E. Wood, J. M. Palms, and P. V. Rao, Phys. Rev., 187, 1497 (1969).

67. P. V. Rao, J. M. Palms, and R. E. Wood (to be published).

68. J. Tousset and A. Moussa, J. Phys. Radium, 19, 39 (1958).

69. M. A. S. Ross, A. J. Cochran, J. Hughes, and N. Feather, Proc. Phys. Soc. (London), A68, 612 (1955).

70. K. Risch, Z. Phys., 150, 87 (1958).

71. H. U. Freund and R. W. Fink, Phys. Rev., 178, 1952 (1969).

72. G. G. Akalaev, N. A. Vartanov, and P. S. Samoilov, Izv. Akad. Nauk SSSR, Ser. Fiz., 28, 1158, and 1259 (1964); Bull. Acad. Sci. USSR, Phys. Columbia Tech. Transl., 28, 1260 (1964).

# VITA

Esko Ilmari Karttunen was born in Kuusjarvi, Finland on October 15, 1936. He received his M.S. degree in Physics in 1962 and his Licentiate of Philosophy degree in 1967 from the University of Helsinki.

From 1963 he worked as a laboratory engineer in the Department of Radiochemistry at the University of Helsinki. Since September 1968 he has been on leave of absence in order to attend the graduate studies at Georgia Institute of Technology. His publications include:

E. Karttunen, H. U. Freund, and R. W. Fink, "The K-Fluorescence Yield of Te and the Total and K-Shell Conversion Coefficients of the 35.48 keV Transition in $^{125}$I Decay," Nucl. Phys. A131, 343 (1969)

E. Karttunen and D. C. Gardner, "A Simplified Precision System for Oxygen Analysis by Fast Neutron Activation," J. Appl. Rad. Isot. 20, 801 (1969)

N. Ranakumar, E. Karttunen, and R. W. Fink, "Thermal and 14.4 MeV Neutron Activation Cross Sections of Argon," Nucl. Phys. A128, 333 (1969)

H. U. Freund, J. S. Hansen, E. Karttunen, and R. W. Fink, "Photon Spectrometry in the Low Energy Region of 500 eV to 100 keV," to be published in The Proceedings of the International Conference on Radioactivity in Nuclear Spectroscopy, Nashville, Tennessee, August 11-15, 1969.

Esko Karttunen is married to the former Marja-Liisa Kaaria and they have a daughter, Anu.